2021

Reverse Engineering of Short Circuit Analyses

Anurag Nagpure
Michigan Technological University, arnagpur@mtu.edu

REVERSE ENGINEERING OF SHORT CIRCUIT ANALYSES

By

Anurag Nagpure

A THESIS

Submitted in partial fulfillment of the requirements for the degree of

MASTER OF SCIENCE

In Electrical Engineering

MICHIGAN TECHNOLOGICAL UNIVERSITY

2021

This thesis has been approved in partial fulfillment of the requirements for the Degree of MASTER OF SCIENCE in Electrical Engineering.

Department of Electrical and Computer Engineering

Thesis Advisor:	*Dr. Chee-Wooi Ten*
Committee Member:	*Dr. Laura Brown*
Committee Member:	*Dr. Kuilin Zhang*
Department Chair:	*Dr. Glen Archer*

Dedication

This thesis work is dedicated to my advisor Prof. Chee-Wooi Ten who has been a constant source of support and encouragement during the challenges of graduate school. This work is also dedicated to my parents, Ravikiran and Jyoti Nagpure, whose good examples have taught me to work hard for the things that I aspire to achieve.

Contents

List of Figures

List of Tables

Preface

Over the past decades, an electrical distribution infrastructure has been built to connect the transmission network to the customers where residential, agricultural, and buildings are connected with overhead lines, electrically energized from the distribution substation. Power flow has gone from the transmission network through distribution feeders, then laterals, serving all connected utility's consumers one way. This is referred as a unidirectional direction of power flow. The characteristics of such a network are often operated in radial and unbalanced configuration. Since smart grid vision has been promoted under Obama administration, the distribution grid has undergone a significant transformation, such as the massive deployment of "smart" meters at each household, as well as the computerized automation to assist in locating the exact location of a fault. More importantly, the grid has also been connected with networked microgrid, distributed energy resources (DER), and electric vehicles. Hence, the power flow is bidirectional. The major contribution of this thesis is to provide the analytical method of extension by using "Backward/Forward Sweeping Techniques" (also known as Ladder technique), with equivalent impedance superposition model, to enhance the voltage-controlled DER. Such formulation also includes the algorithms of forming a larger impedance matrix, demonstrating the critical aspect of Thevenin circuits to initialize the currents across a feeder. This thesis emphasizes on homogeneous inference of a faulted location in latter chapters.

Acknowledgments

I would like to thank all those who have helped me learn, understand and appreciate this subject

My advisor, Prof. Chee-Wooi Ten

My father, Prof. Ravikiran N. Nagpure

List of Abbreviations

ACL	Access Control List
CIS	Customer Information System
DA	Distribution Automation
DDC	Distribution Dispatching Center
DG	Distributed Generation
DMS	Distribution Management System
FI	Fault Indicators
IED	Intelligent electronic devices
OMS	Outage Management System
PFL	Possible Fault Location
MV	Medium Voltage of Electrical Network
LV	Low Voltage of Electrical Network

Abstract

The electrical distribution system has evolved with embedded computer systems that can better manage the electrical fault that occurred around the feeders. Such random events can affect the reliability indices of overall systems. Computerized management system for distribution operation has been improving with the advanced sensing technologies. The general research question is here to articulate is the responsiveness for utility crew to pinpoint the exact location of a fault based on the SCADA fault indicators from pole-mounted feeder remote terminal units (FRTUs). This has been a tricky question because it relies on the information received from the sensors that can conclude fault with logic's of over currents. The merit of this work can benefit at large the grid reliability because of time-saving in searching the exact location of a fault. The main contribution of this thesis is to utilize the 3-phase unbalanced power flow method to incrementally search for narrowing the localization of electrical short circuits. This is known as the reversal of the typical short circuit approach where a location of the fault is presumed. The 3 topological configurations of simulation studied in this thesis exhibit the typical radial configuration of a distribution feeder have been researched based on unidirectional and bidirectional power flow simulation. The exact fault location is carried in two steps. Firstly, a bisection search algorithm has been employed. Secondly, an incremental adjustment to match the simulated currents of fault with the measurements is conducted. Finally, the sensitivity analysis

of a search can be improved with the proposed algorithm that leads to matching of telemetered and calculated values. The analysis of exact fault location is carried in unidirectional and bidirectional flow of power. Distributed energy resources (DER) such as residential PV at a household level as well the wind energy changes affect the protective relaying within a feeder as well as the reconfigurability of the switching sequences. Furthermost, the bidirectionality of power flow in an unbalanced manner would also be a challenging issue to deal with the power quality in automation. Finally, the simulation results based on unidirectional and bidirectional power flow are extensively discussed along with the future scope.

Chapter 1

Directionality of Power Flow

1.1 Introduction

Over the past decades, the top-down power transfer from the bulk generation to end-user consumers has been the salient part of power engineering and system design. This forms a unidirectional sense of power flow from distribution substations to consumers. However, due to the massive deployment of renewable distributed energy resources in medium-voltage (MV) and low-voltage (LV) distribution networks, it implicates overall system design in analytical methods as well as the protective relaying. Both unidirectionality and bidirectionality of power flow have implicated the search of fault. This chapter provides an overview of state-of-the-art technologies and development,

exploring these major two directions of power flow and potential application in outage management systems (OMS) in distribution dispatching center (DDC).

1.2 Unidirectional Direction of Power Flow

A power system is a non-linear system where the voltages and currents are state variables to be identified using the iterative numerical methods. This steady-state analysis is what has been used in power engineers in operation or planning to get a sense of system condition whether or not if a feeder is overloaded or any violation of voltage along the feeders and laterals. The approach employed would provide a global view of system states where the guarantee of solutions is defined by the convergence of solutions. Hence, it is imperative that the analytical methods addressing the balanced nature of distribution feeders. For the remainder of this section, operation and planning of distribution feeders, fault identification methods, and the new sensing technologies are introduced and elaborated in the distribution system.

1.2.1 Steady-State Approach

Load flow or the power flow is defined as the solution for the static operating condition of an electric-power transmission system, and is the most frequently performed

of routine digital-computer power network calculations. Preceding to and some time after the emergence of the digital computers, network analyzers were used to obtained the load-flow solutions. The first practical automatic digital solution methods was first cited in the literature in the year 1956. As the first generation computers required minimal storage for data so Y matrix iterative methods were best suited for these computers. The main disadvantage of these Y matrix iterative methods was that they perform satisfactory operation on some problems where they perform solve convergence but sometimes not at all. This disadvantage was overcomed by the Z-matrix which converge very efficiently but requires large storage and fast speed when dealing with large power systems. At the same time the method that shown powerful convergence properties was Newton-Raphson method but the computational speed of this speed was slow as compared to other methods. Many methods for power system network computation was invented in the mid - 1960's and also some best methods was invented by Tinney and others which were very effective. During these years the success was in rigorous improvement in computing speed as well as the storage requirements of the Newton-Raphson method which is now regraded as the most efficient method in the calculation of the load flow approach and widely used in many industries. When the increasing complexity of the power system , different online applications and optimizing the power system, new methods are been developed which are expected to find wide range of applications. Load flow calculations are used in

power system planning, power system operations and control and also used to multiple cases such as outage security assessment and complicated calculations involved in power system optimization and stability [1].

Due to the such appealing properties such as linear, non-complex, bilateral and state-independent, DC-type of power flow model can be helpful during analytical and computational calculation in the power system. The use of linear MW-only DC network power flow models are extensively use in congestion-constrained market applications. They are also used where the network voltage and VAr conditions are effects are very minimal. But they have better advantages over AC power flow model. As compared the solution of the DC power flow models are non-iterative, reliable and unique, and the methods and softwares the DC power flow models used are relatively simple. The usage of the network data is minimal and its very easily obtained. The linearity graph of DC power flow models matches with the economic theory which is based on transmission oriented market design [2]. The main disadvantage of DC power flow is that its linear approximation model is not suitable if the distribution systems have high R/X ratio and also performing unbalanced operation. But the linear approximation can be used on a complex not with radial topology and PV nodes but by considering distribution generators with the unity power factor [3].

1.2.2 Unbalanced 3-Phase Circuits

Many of the new and existing approaches assumes that the for designing the distribution network reconfiguration the distribution system is three phase balanced as well as single phase equivalent. But due to the enormous number of single phase loads, non symmetrical conductor spacing as well as three phase line topology the distribution feeders are considered as unbalanced network. But still various distributed generation (DG) can be integrated into the system so that bidirectional flow of power is possible. Using the sensitivity analysis and nonlinear programming the locations of three-phase bus as well as the sizes of distributed generation are determined and the distribution feeders are reconfigured every hour depending on the variation of the loads and output power given by the DG and at the same time the faults that are occurring on the system. This is done in accordance that the system losses will be less and minimal operating costs of the DG. Due to the implementation of this method computational efficiency and the effectiveness of the system is improved.[4].

1.2.3 Distribution Feeder Reconfiguration

Due to the increased generation and the capital costs in the distribution systems motivated the distribution engineers to apply knowledge to improve the operation of

the distribution systems.Feeder reconfiguration is defined as altering the topological structures of distribution feeders by altering the open/closed states of the tie switches as well as sectionalizing [5]. By applying the feeder reconfiguration technique, the switches are designed in such a way that they are allowed to change the status(either ON/OFF) to improve the power flow in the distribution system in time varying location as well as time varying distribution loads. The end result of this technique is that by switching to the better distribution loads resulted in better efficiency and system I-squared-R losses decreases. The feeder reconfiguration in integrated with three-phase feeder sectionalizing devices, three-phase capacitor banks and a proper operation scheduling which will dynamically reconfigure the system in order to optimise the loads variations on daily, weekly and seasonal load variations by reducing the system losses and increasing the efficiency [6]. In addition to changing the switching sequences of the switches, a load balance index is defined which will approximate the load balancing. Estimation methods and the search method are two different power flow approximation methods which are used to calculate the new power flow in the distribution systems after a branch-exchange and by using the power flow equations which are developed for radial distribution systems. The advantage of this estimation method is that it take into account the active and the reactive power flows for computational calculations and give very conservative results.The end result is improved performance of the system [7].

Due to the various switching options, results into voltage problems, overloads and

other operating constraints that are associated with the power system protection. So in order to eliminate these problems as soon as possible in distribution systems, a heuristic search strategies are adopted which evaluate the best first tree and also helps in reduction of the search space [8]. It is approximated that the about 5% to 13% of the total generated power is lost in the form of the I-squared-R losses. These losses can be reduced and can result in substantial savings for the electric utilities by implementing the loss minimization techniques which is of one of the best features of the Distribution Automation (DA). The loss minimization technique is a combination of linear programming method which uses the transportation technique and new Heuristic Search method. While the linear programming method in the form of transportation algorithms is nit suited for the real time monitoring of the feeder configuration but the Heuristic approaches which is not optimal helps in substantial savings of losses if it formulated properly and is used for real time monitoring of the feeder reconfiguration [9].

Due to the radial configuration, only unidirectional flow of power is possible except for some short duration of time. But in complex feeder structures like distribution systems integrated with Distribution Management Systems (DMS) it is required to model bidirectional feeder models which helps in system-reconfiguration or service restoration functions. This paper describes three bidirectional feeder models in order to simplify distributed system calculations. The bidirectional voltage drop model is the first model used to simulate the total series voltage drop at the extreme end of

the feeder. The second model is bidirectional line-loss model which represents the total copper loss of the feeder and the third model which is a hybrid model is called the bidirectional hybrid model which is used to model both the total voltage drop and feeder loss. This models are used to reduce some complex feeders into equivalent simple models for the study of voltage profile and losses with very minimal error even if the power feed to these feeders change dynamically [10].

The extended fast decoupled Newton-Raphson method which helps in reconfiguration of modern distribution networks uses information from the network switching equipment status (either ON/OFF). The advantage of this method is this method can be applicable to distribution networks which have high R/X ratio lines. The power flow calculation by the fast decoupled approach becomes possible due to complex per unit normalisation technique. The simulation results proved that this method qualifies as the most relevant computational tool for network reconfiguration which involves emergent distribution systems [11].

In the modern grid due to the cyber physical nature it is possible for the active power entities to exchange information signals between one another in order to take intelligent local actuation decisions. It is becoming common in today's electric grid to have effective coordination between these cyber enabled entities with high fluctuating power components such photovoltaics, wind energy and electric vehicles with the help of signal exchanges. A decentralized topology reconfiguration algorithm is adopted

for the distribution network that will adapt itself in real time with the unexpected perturbations and congestion's to restore back the balance in the loads and improve the voltage profile. With the help of individual agents that are available in the distribution network continuously exchange signal with the neighboring nodes and make use of their information for taking decisions regarding switching of local line. This algorithm works best for power system where bidirectional flow of power is adopted. [12].

1.2.4 Fault Location and Diagnosis

Distribution feeders of the electric power system are prone to faults which occurs due to various situations such as accidents, unfavourable weather conditions, equipment's failure, etc. These faults results in into the problems related to reliability of the service as well as customer power quality. In the earlier days, due to the recloser lockout or the blown fuse results in the interruption of customer supply was the key for factor for determination of of service reliability. But with the advancements in the technology sensitive customer loads such as power electronics devices and adjustable-speed motor drives which are very sensitive to the voltage sag are introduced in the distribution system. Due to these devices temporary self-clearing faults become difficult. Power utilities perform the task of fault location as well as fault diagnosis depending on the outage reports by the customers. When trouble calls are received from the customer,

then the dispatchers checks the configuration map and the protection design manual in order to determine the outage area. The outage area is patrolled by the crew to locate and diagnose the fault which can be time consuming and rigorous task. Also temporary faults are hard to detect because these types of faults are not caused because of blown fuse and evidence of the fault cause and location is not available. Around in late 2000, an automated distribution system was proposed which is used for fault location and diagnosis. The information is collected from the substation digital transient recording device along with the knowledge of the feeder configuration and protective coordination which is contained in the distribution database. Such system will benefit in speed up the restoration service because it give more accurate fault location indication [13]. Due to automation in the distribution systems of the electric utilities, there has been an increased focus on the automated remote control of the distribution feeder sectionalizing and deployment in order to improve the time required for the service restoration on the unfaulted feeder and also for load transfer between the feeders. Digital processor algorithms are used for the determination of the fault location and then switching instructions are generated which is based on tree searching techniques[14].

The distribution systems has an unbalanced nature because of single phase laterals and loads which give rise to difficulty in finding fault location. In order to overcome this problem, an direct circuit analysis based fault location algorithm is developed for unbalanced distribution systems [15]. One of the most interesting features of the

smart grids is realization of self healing networks. Fault location is considered as the most important application between intelligent monitoring and outage management tasks. Various intelligent electronic devices(IED) are installed throughout the power system in order to gather accurate data which in turn use smart approaches to detect faults in distribution system [16]. Traditional impedance based fault location consider that the all the feeders in the distribution systems will have the same impedance characteristics. If the feeders have branches and other line sections consisting of various types of conductor and tower configurations then it will introduces errors on the feeders. A new impedance based method uses a detailed feeder model along with fault event reports and in addition with the information from the intelligent field devices for the estimations of all fault locations. This method determine the fault location within a minute after the fault occurs [17].

In order to improve the reliability and outage duration reduction fault indicators (FIs) which are fault indicating devices are widely used in the distribution systems. FIs are equipped with communication interfaces and then are integrated into distribution system to reduce the fault timing by reporting the status to control center. Whenever the fault occurs, the system operators receives the information from Outage Management System (OMS), Trouble Call System (TCS) and Customer Information System (CIS). Due to this, identification of faults on line in vast distribution system becomes difficult when n number of faults occurs at the same time and distributed generators (DGs) are connected. The line sections neighbouring to the FIs are considered as

possible fault location (PFL) and line current (LC) is the fault current detected by the FIs. A relationship matrix is developed between the possible fault location (PFL) and line current (LC) and is adopted to detect the fault in very effective and efficient way. This method can be used in distribution systems where bidirectional flow of power is required as this method used distributed generation (DGs) to detect the fault in the lines [18].

1.2.5 Smart IP-Based Meters in LV Network

With the recent advances in the measurement and the communication systems, the power utilities are exploring new efficient and solutions to improve the automation as well as the monitoring of the distribution systems. The advancement provides a two way communication of the meter, real time monitoring of the information such as power outages, voltage sags and consumption. Due to this advancement the smart meter have achieved the potential applications well beyond of just meter reading for monthly consumer billing purposes. One of the application of the smart meter is regrading the fault management, because faults creates problems such as power outages, power quality and power interruptions problems, voltage sags and heavy operational costs. In order to estimate the fault location in the distribution systems, voltage measurements are taken from the smart meters which are installed at different locations on different buses. The fault current which is calculated on the

basis of the bus impedance is related to the voltage deviation of depicted by each meter. To improve the precision of the method, the loads are considered to have constant impedance [19].

With the growing improvement in the smart meters technology smart meters can be used for outage management. To improve the service restoration in the distribution systems, the voltage monitoring capabilities is combined with the impedance based fault location method. With the application of the impedance based method the fault location is roughly estimated. Since the result of this application is the estimated distance from the fault and as the distribution system network is complicated which involves multiple nodes and multiple branches it is very challenging to detect the exact fault location. The voltage monitoring capability of the smart meter is used to build the low voltage zones (LVZs).This capability will helps to decrease the number of multiple estimations carried out by the impedance based methods and designed a systematic approach to build the low voltage zones which increases the efficiency of the time required to clear the fault [20].

Power Flow (PF) and power system state estimation (PSSE) are the important components of planning, monitoring and control of electricity networks.These problems were previously studied for transmission networks and but there is growing interest for using novel methods in distribution systems. Due to shortcomings in the

instrumentation, the challenges the distribution grids is facing are observability issues. The electric utility operators monitor the distribution system by monitoring current,voltage and load magnitude measurements at some buses. With the increase use of renewable energy resources (DERs) there is a utmost need of grid obervability both in space as well as time so that objectives of the grid dispatch such as power loss minimization and the voltage regulation can be achieved. This can be achieved with the help of smart meter data which is readily available as well as with the help of smart inverters installed in solar panels and electric vehicles which can be controlled within fraction of seconds. Both these technologies can be integrated into the system in order to enhance the observability in distribution systems. [21].

1.2.6 Optimal Power Flow

Feeder reconfiguration involves changing the topology or the structure of the distribution systems by altering the open/close status of the switches that will occur during both normal and abnormal conditions. Algorithms were developed for the two purposes mainly service restoration as well as load balancing with the combination of optimization techniques with the help of heuristic rules and fuzzy logic which increases efficiency and the robust performance of the distribution system. service restoration can be achieved by isolating the faulted area and at the same time supplying power to the unfaulted out of service area and minimizing the problem of load shedding.

Load balancing will helps to distribute the load in the distribution system evenly due to which optimal power will flow. The algorithms solves the concerns regarding operating constraints, optimize selection of switching operation as well as system coordination along with many other distribution automation functions [22]. In addition to these functions, the benefits of above configuration includes power restoration in the outage portion of the distribution system in a timely manner which reduces the average outage time and reduces overloads on feeders by shifting it to the adjacent feeders in real time which will reduce capital expansion projects costs, reduces resistive line losses which in turn reduces the operating cost of the distribution system [23].

In the past, service restoration was carried using heuristic approach and expert systems which were developed to determine the restoration plans and building look up tables for the distribution system personnel. Also fuzzy set theory and network reduction methods were applied to reduce the outage time. For large scale radial distribution system, a quick and effective service restoration algorithm which allows multi-tier or system-wide switching as well as capacitor control actions is developed which is constrained on multiple objective optimization problem. In this method manual switches are used from the information received by the three-phase power flow analysis which will optimise the system the total load depending on the priority with the help of minimum number of control actions as well as the geographic distance. This method avoides multi-tier switching [24].

In an automated distribution network, feeder reconfiguration is necessary so that the distribution system can operate in an optimum performance. Considering that optimum performance of the distribution system includes no overloading of cables and transformers, optimum voltage profile, minimum losses, absence of imbalances in phase voltage and phase current, only performing network reconfiguration alone is not sufficient. In addition, techniques for rearrangement of the phase between the specific primary feeder as well as distribution transformer banks is required. Also there is a need of dynamic phase and load balancing for a feeder with radial structure.To accomplish this, a neural network in addition with the heuristic approach will enables variety of reconfiguration switches which are to be either turn ON or OFF which will switched between different phases in order to keep the phase balanced [25].

The functions which are carried out by an Advanced Distribution Management System (DMS) are monitoring each and every component and using dynamic state estimation performing protection. Synthesizing the real time model of the entire feeder after the information about the estimated states are received by the DMS. Performing upper level optimization i.e. operations planning and real time control that's comes under lower level optimization by using the real time model and finally applying the proper control, so that the system will operate optimally. These functions are extremely necessary in the distribution feeder where bidirectional flow of power takes place so that the power in the distribution system will be reliable and used optimally [26].

1.2.7 Distribution System Planning

Distribution system planning includes developing a efficient and static optimization model for the network expansion. This efficient model can be used to find the most optimal design for a particular distribution system or optimal design for the previous distribution system in order to meet the load demand. The optimization variables consists of rating and location of the new substations that need to be installed, number of the substations, sharing of load between the substations as well as the topology of the feeder and the feeder cross-sectional area. The design will reduced the variable as well as annualized fixed costs and at the same time satisfying the system's operational constraints [27].

Feeder reconfiguration in the distribution system is related to the closing and the opening of the switches in order to satisfy the objective and at the same time following the operating constraints. For normal operation, the constraints are to avoid feeder thermal overloads, abnormal voltages and transformer overloads and at the same time minimizing the power losses. For the emergency cases, the system needs to be arranged in such a way that maximum customers can have electrical supply in case of fault or outage. Feeder reconfiguration program is considered as real time control tool which proves to be helpful in power system planning. Along with the planning, it is also helpful to predict the configuration of the distribution systems for different cases.

In Distribution system power flow planning improves the operating condition of the system and allows the full utilization of the preset system hardware capabilities. The end result is reduced capital cost as well as reduced operating cost [8].

1.2.8 Protective Relaying

Distribution system protection includes recloser or circuit breakers. These are the two most important components of the distribution networks which is used to achieve the basic requirements of the power supply such as reliability, safety and quality. The system protection is used to clear faults and limit the damage caused to the equipment's. The protection system must provide reliability, speed and selectivity to the power system on which it is installed. Reliability of the protection systems depends on two factor namely dependability and security. These factors will guaranteed that the protection system will behave properly when the fault occurs on the distribution networks. An excellent coordinated protection system has sensitivity which will disconnect the minimum section of the network during fault isolation. Variety of protective devices such as over-current relays, reclosers and fuses are used in distribution systems [28].

During the normal operation of the distribution system, the feeders are reconfigured by changing the states of the switches either open or closed in order to achieve load

balancing and loss reduction. So far the switches switching operation was determined by considering constant load conditions. As the loads are always changing and due to the limitations that are imposed on the life expectancy of the switches, feeder configuration remains in a service for a certain period of the time. So a heuristic search approach has been developed to determine better feeder configuration which will adapt to the changing load conditions. Using this approach the appropriate location of the fuses are determined in the distribution systems. A region in which the switch operations are allowed in the feeder reconfiguration are identified. Due to this approach, efficiency of the switching operations for loss reduction or for load balancing have increased significantly [29].

Protection systems includes a Distribution Automation System (DAS) which is an automatic system used for power distribution systems which carries out remote monitoring as well as control of Automatic Switches (ASs) from the central server. A DAS consists of both manual as well as automatic switches. The manual switches are controlled by the humans as they are installed at the location of operation while the automatic switches which is an important element of DAS is controlled by a DAS server. A DAS server sends the command to the FRTU or a recloser which then sends the control signal to the automatic switches and circuit breaker. The advantages of a DAS are voltage profile improvement and power factor management, loss minimization, fault section minimization and restoration. The composition and placement of the automatic switches leads to the better operation of the DAS and they play

a critical role when they are installed in power system with number of distributed generation. But at the same time if the number of automatic switches increases it also increases the cost and the maintenance of the distribution system. Therefore an algorithm should be used for optimal composition as well as placement of automatic switches in distribution automation system [30].

1.3 Bidirectional Power Flow

Distributed generation is the new key elements that has been introduced feeders where networked microgrids are the collective elements that may introduced net-zero or net-negative loads. New addition includes battery, plug-in electric vehicles (PHEVs), Photovoltaic (PV) panel that can play the crucial role in introducing the reconfigurability of the interconnected feeders that are radially energized with tie switches. This section revisits some of the already deployed new additions in the distribution system.

1.3.1 Advanced Metering Reading

Meter reading technology has been evolving because of the advances in the technology in computerized technology as well as power electronics. Nowadays electric utilities

are deploying more and more automatic meter reading (AMR) in the distribution system.With the help of radio networks and telecommunication networks the billing process has become automated resulting in the savings for the utility as well as for the consumers also. In addition to this these meters enables a real time communication between the consumers and the electric utility. AMR consists of communication modules which transmits data to an intermediate gateway device via a radio frequency. This data is sent to the central computer where it populates a database. The database gives the information regarding real time usage, total usage as well as daily usage to the electric utilities. The functions performed by the AMR are on demand meter reading, theft or tamper detection, easy access to the outages which significantly reduced the fault location time and fault resolution time. The utilities don't have to rely on the customers call for the outage information. The customers call regrading outages are reduced where AMR are deployed [31].

1.3.2 New Addition in Distribution Network

In the modern distribution system which consists of distribution generation (DG) and renewable energy sources (RES) bidirectional flow of power is possible. The asset which includes in these distribution systems are battery, photovoltaics (PV) and plug-in hybrid electric vehicles (PHEVs) and electric vehicles (EVs).

1.3.2.1 Lithium-ion Battery as Energy Storage

Distributed Generation (DG) and Renewable Energy Sources (RESs) are growing exponentially which are moving towards smartgrids because of design change and operation in distribution systems. With the development of microgrid which is the another form of smartgrids the role of energy storage system(ESS) or battery is becoming important. The ESS helps in not only solving the randomness as well as uncertainty in RESs but also play a significant role in power flow control, energy management and reliable electric supply to the customers. The technical as well as the environmental benefits of the distribution network operators (DNOs) are enhanced due to the economic dispatch of the ESS.There is need to enhance the present ESS technologies in microgrids and also appropriate treatment for uncertainty handling and various other ESS technologies. ESS includes different technical as well as economical aspects such as lowering the cost while supplying the power in the microgrids, improvising the battery life and emission reduction, risks minimization, demand and generation balance, reduction in the cost of energy purchased from the grid and lastly increasing the reliability of the supply. But due to high price of the battery, it not currently used widely in microgrids system.[32].

The over-voltage problem in microgrids can be reduce with the help of integrating the energy storage systems to store excessive energy rather than curtailing it. The

ESS are very compact and helps in maintaining the voltage profile of the residential distribution system in terms of Time Shift which means storage charging energy during off peak hours and discharging the energy stored during peak hours. For high power and small duration applications, low energy density and deep discharging of non battery-type ESS like the electro-chemical capacitors are used. For residential distribution systems which comes under high energy and long duration applications, ESS is widely used [33].

1.3.2.2 Plug-in Hybrid Electric Vehicles (PHEVs)

The traditional view of industrial systems are reshaped due to the economics and environmental incentives and advances in the technology. The future presence of electric vehicles in personal transportation sector have held together because of decreasing the dependency on fossil fuels and also reducing emissions [34]. The introduction of enormous number of plug in hybrid electric vehicles (PHEV) and plug in hybrid vehicles (PEV) into the automotive market which increases the technical problems which are related to the industrial information technologies in next ten years. So, there is an immediate need of in-depth knowledge regarding to the electrification of the transportation in the growing industrial environment. In order to support the emerging electric vehicles technologies it is very important to collaborate the partial and the conceptual knowledge of industrial informatics [35].

Due to the stochastic charging behaviour in plug in hybrid vehicles (PHEV) which occurs in various charging strategies arises new challenges such as feeder overloading and loss increase in distribution networks. In this way, the larger penetration of these vehicles makes it compulsory to employ new operative tools which will inspect the impact of these vehicles on electrical grids. Therefore, the krill herd optimization algorithms which is one of the novel optimal stochastic reconfiguration methodology is used to moderate the charging effect of plug in hybrid electric vehicles (PHEV) which changes the topology of grid by using some remote controlled switches. Various uncertainties that are associated with network demand, energy price and charging behaviour of plug in hybrid vehicles (PHEV) in different frameworks are handled using Monte Carlo simulation. Numerical studies on distribution systems shows that the reconfiguration improves the system performance when plug in hybrid electric vehicles (PHEV) charging loads are considered [34].

In addition to this, a novel stochastic dynamic programming technique is used to study the optimal topology and the maximum capacity of the distribution systems in order to accommodate the charging demands of the electric vehicles (EV). This method finds the optimal feeders tie switch locations and also their associated on/off schedule which will minimize the operation costs and also satisfies the constraints of the system operation [36]. Also a self-adaptive evolutionary algorithm which is based on symbiotic organism search (SOS) is adopted to as a reliability-enhancing strategy which helps in coordination of vehicle-to-grid (V2G) plug in hybrid electric vehicles

(PHEV) in a stochastic framework [37].

1.3.2.3 Residential Photovoltaic (PV) Solar Panels

Due to the favorable technical, economical and environmental factors, the energy sector has entered into an era where the energy demand is partially ,met by the renewable energy resources like photovoltaics. Every year the energy production of rooftop photovoltaics is increasing by around 16-20%. Due to these renewable energy resources bidirectional flow of power is possible in distribution systems. But excess penetration of photovoltaics in distribution systems leads to many technical problems such as over-voltages issues at the end of the feeder in the distribution networks particularly in the overhead transmission lines. By conducting the instantaneous demand forecasting and power measurements injected by the distributed generations (DGs), the on-load tap changer (OLTC) settings can be changed to enable high generation from the DGs as well as without violating any voltage levels. A complex algorithm is required which will allows a reliable communication regrading data exchange between the DGs and the loads [33].

1.3.3 Redefining Grid Resiliency

Resiliency in power system is defined as the ability of the network to minimize the negative impacts of infrequently occurring adverse events. Low frequency and high impact events are termed as unfavourable events. Analytical hierarchical process and the percolation process methods are used to quantify and enable the resiliency of a power distribution system. This method can be used to carry out quantitative analysis to analyze the impact due to the possible control decisions taken in order to proactively activate the resilient operation of the distribution system by integrating other resources and multiple microgrids. The short term distribution system planning used developed resiliency metric. This is very helpful to distribution planning engineers and operators to take certain control actions, with a detailed comparison for using different reconfiguration algorithms and develop proactive control actions to prevent power system outages due to the catastrophic situations or adverse conditions. This method improves the resiliency of the system using multiple microgrids along with two stage reconfiguration algorithms [38].

Microgrids with distributed generation (DGs) is a resilient solution if the major faults occurs on the distribution systems due to to natural disasters. A novel distribution system operational approach is formed by integrating multiple microgrids energized

and de-energized with distribution generators (DGs) from the radial distribution systems which will help to restore the critical loads when the power outage occurs.A mixed integer linear program is executed in such a way that it will maximize the critical loads along the following the criteria for self-adequacy and operation required for the microgrids formulation problem by controlling the ON/OFF function status of the controlled switch devices which are operated remotely and the distributed generation (DG). The formed microgrid is used for power quality problems and it is then connected to the larger microgrid before the main grids restoration is complete [39].

Smartgrids technologies can decrease the number of consumers affected by the long power outages which increases the system reliability through automation switches in order to restore the supply. Such technologies are reactive in nature i.e. they will carry out their function only when the fault or power outages occurs. Due to this function, it is assumed that unfaulted phase are healthy and capable of power flow. A automated as well sophisticated real-time analysis of electrical waveforms of the feeder are used for prediction of the failures and determine the health of line apparatus as well as distribution lines. Intelligent systems for improved reliability and failure diagnosis in distribution systems. Due to this reliability of the system will increase because the fault will be detected, located and repaired before the catastrophic event or outage occurs. The failured are detected using intelligent distribution fault automation (DFA) algorithms [40].

Due to the scarcity of the power generation resources the continuous operating time (COT) is used to determine the accessibility of the microgrids for restoration of the critical load as well the for accessing the service time by taking into account the uncertainties which occurs due to the intermittency of renewable energy resources and the load. To overcome this problem a two stage heuristic approach is developed. In the first stage, a strategy table is prepared which contains the information of all possible restoration paths and in the second stage a linear integer program is used to obtain the strategy for critical load restoration [41].

In distribution systems when multiple microgrids are integrated with distributed generation serves as a resilient solution for the critical load to restore from natural disasters. As the number of microgrids increases, continuous variables and dummy variables also increases which increases the complexity of the model. By using sectionalizing switches, the distribution system forms a different network in such a way that one DG is associated with one microgrid in order to make the system adequate enough. Due to this configuration, number of binary and continuous variables are reduced thereby increasing the computational performance [42].

1.3.4 Extensive Planning Against Natural Disasters

Today, for the whole society the fundamental issue has been the improvement required for resiliency of power grids against natural disasters. Due to the hurricanes and extreme weather conditions resulted in human casualties and enormous economic losses. The propaganda of the electric utilities is to supply continuous and reliable power it is extremely important to to upgrade the technologies in order to increase the resiliency of the existing power system or grids against the natural disasters. For a resilient distribution network planning problem (RDNP) a robust optimization based decision support tool is used which minimizes the system damage by coordinating both hardening and the distributed generation resource allocation. The effective tool reveals that the distributed generation (DGs) plays an important role in increasing the resiliency of the distribution network in terms of microgrids against the natural disasters. Distributed Generation (DGs) also plays a critical load in bidirectional flow of power and also improve the power quality, reduces the system losses and helps in enhancement of the reliability of the supply. When the main supply interruption occurs during any natural disasters DG are served as backup generation [43].

1.3.5 Outage Coordination and Management

The critical performance index of a power system is the reliability. According to the report by customer outage statistics 80% of the service interruptions occurs due to fault or the failure of the components in power distribution systems. The reliability of the distribution system is enhanced because of use of the advanced technologies such as remote controlled switches which are adopted to detect faster detection of the fault and also helps in faster system restoration. Distribution automation consists of Supervisory Control and Data Acquisition (SCADA), outage management systems (OMS) and Distribution Management Systems (DMS) which are deployed in distribution operating centers. Quick fault location identification and activation of the protective devices by the fault is the most critical function in outage management. With the ongoing research in smart grid development, various smart meters and the fault indicators equipped with communication capabilities provides accurate and efficient data to the outage management [44].

Due to the bidirectional flow of power, distributed generation will be installed in the system and this will increase the cases of service interruptions. So Automatic Meter Reading (AMR) data can be used by the electric utilities to detect the fault and provide an additional information for the outage detection and along with the restoration phases of outage management. By developing an intelligent information

filter will prevent false outage notifications and will also improve the quality of the outage data [31].

1.3.6 Knowledge-Based System in Distribution Automation

Electric power system consists of three operating states such as preventive state, emergency state and restorative state. For the most period of the time the power system is in preventive state. Emergency state occurs when a large disturbance occurs on the power system. The system enters into the restorative state if the disturbance is large. After the restorative state the system goes in blackout. If the partial power outage occurs it is termed as brownouts. Once this condition occurs the system dispatchers re-energize the area where the power is down. System restoration is defined as the control to re-energize the system. At the present time, the system restoration is performed by manual operation which takes a longer time. Nowadays as the distribution system has been bidirectional, there is a need of an automatic system for restorative control. Therefore a knowledge based system has been developed for automatic control in the restorative state of the power system. During the system restoration the system operator's heuristics plays a critical role. The heuristics are represented by a set of knowledge in which the ultimate goal is to restore the power supply of the system without overloading the transmission lines.

The overload checking is based on the numerical computation whereas the knowledge based system is the symbolic computation. The KB system proved to be the effective method of writing the physical and the artificial laws of the power system which is needed to evaluate the restorative control problem.The knowledge based system will help to manage the large power system in the restorative state [45].

Also a knowledge based system (KBS) is used to locate outages in distribution system bu using comprehensive data provided from the customer trouble calls, wireless automated meter reading (AMR) system and distribution supervisory control and data acquisition (SCADA). The two major parts of the algorithm of the developed KBS are an outage escalation procedure and the meter-polling procedure. The wireless AMR system has the on demand read capability which allows the electric utilities to directly communicate with the meter controllers. In respect to the comprehensive outage information, the escalation procedure includes searching for the outage region. The meter polling procedure consists of confirming the outage locations and designing the meter-polling schema. The algorithm has the ability to handle the single outage and multiple outage situations [46].

1.4 Conclusion

This chapter provides an overview of system directionality and potential implication of system design, ranging from one direction to both directions due to the geographically scattered distributed energy resources within a distribution network. Such overview would provide a broader understanding of grid survivability in reconfiguration possibilities. The following chapters of this thesis will provide specific modeling and extension to the reserve engineering of a presumed short circuit analyses.

Chapter 2

Modeling of Distribution Feeders

2.1 Introduction

This chapter deals with the distribution feeder analysis under normal steady-state operating conditions (also called as power-flow analysis) and under short-circuit conditions (also called as short-circuit analysis). In addition to this an analytical method is derived with the help of Backward/Forward Sweeping Techniques also called as Ladder technique with inclusion of equivalent impedance superposition model to improve the voltage controlled Distributed Energy Resources (DER).

2.2 Power Flow Analysis

The power-flow analysis carried out in distributed feeder is same as an interconnected transmission systems. In this analysis the three-phase voltages at the substation are known and complex power of every load and load models which includes constant impedance, constant current and constant complex power or the combination of the any one of the above. In addition to these, input complex power from the substation that is supplied to the feeder is known [47].

The following quantities in terms of total single phase as well as total three-phase of the distributed feeders are calculated with the help of the power-flow analysis.

1. All nodes voltage magnitudes and the angles connected to the feeder
2. Active power and reactive power, current and power factor in each line section
3. Each line section power losses
4. Total input active power and reactive power of the feeder
5. Total power losses of the feeder
6. Depending on the specified model for the load calculate load active power and reactive power

2.2.1 Ladder Iterative Techniques

The iterative techniques used in the power-flow studies of the transmission systems cannot be directly applied here in electrical distribution system due to the unbalanced and radial topology of the network. Therefore, ladder iterative technique is specifically implemented that navigates the parent-children fashion within a graph [47] [48]. Such process is referred as a combination of backward and forward steps that constitutes an iteration. A flowchart shown in Fig. 2.1 provides the flow of information to be computed iteratively for a non-linear system. Such flow provides steps that enables information, such as 3-phase voltages and 3-phase currents to be computed. The termination of iteration relies on the error constant to be defined by users. The following two subsection will illustrate the major differences between linearized and preserved non-linear systems.

2.2.1.1 Linear Distribution Feeder

This section provides a direct method to solve a linear ladder network, which is presumed to be 100% constant impedance loads. While this assumption may be not accurately characterized in the real-world electrical load scenarios, this section exhibits a simple step to determine voltages of a given example. Because the nature of

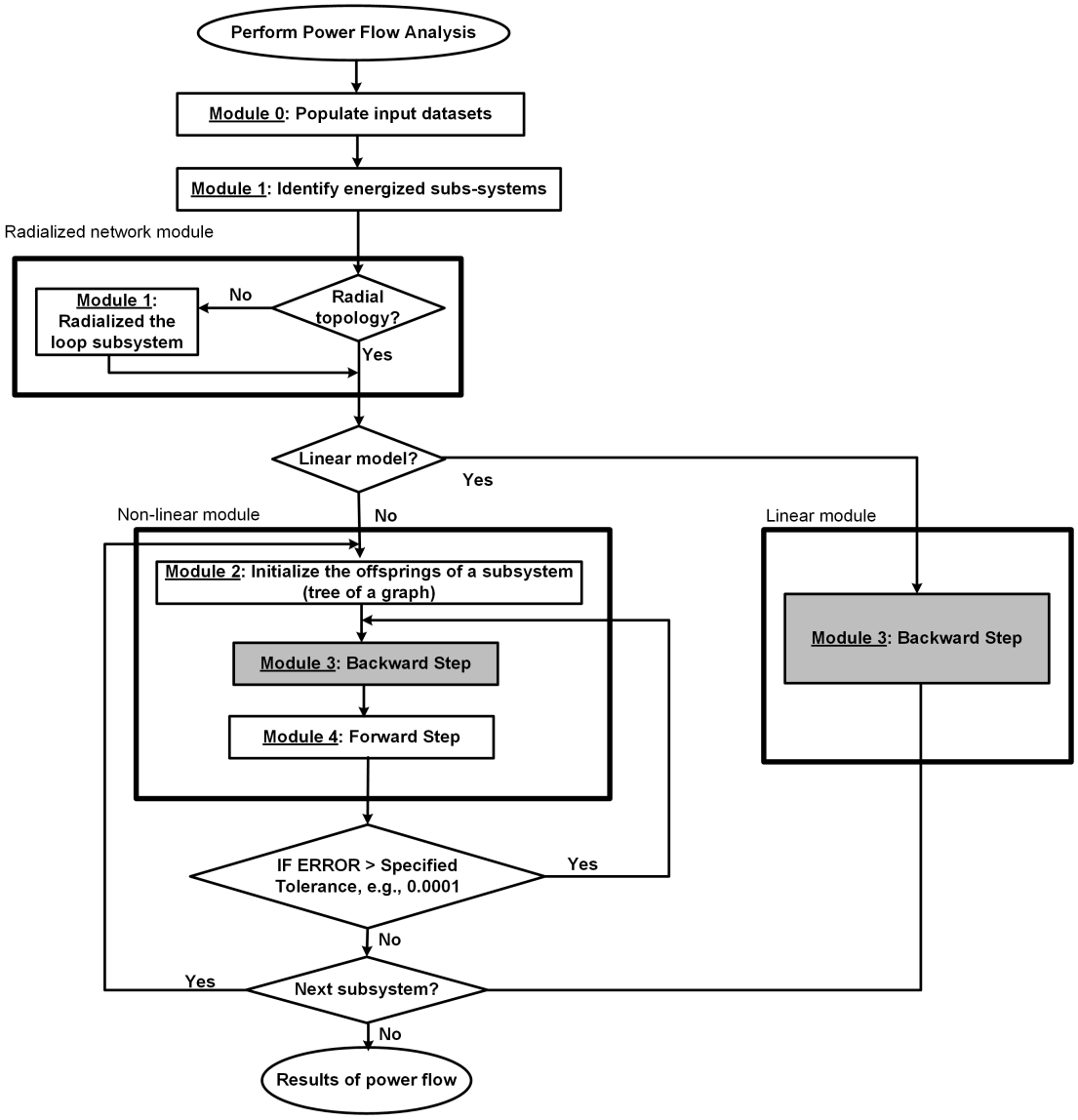

Figure 2.1: Flowchart of generalized 3-phase power flow analysis

this formulation is linear, this example shows it takes one single forward step update to determine the voltage for all fictive buses in a distribution feeder.

Since this is a linear system (constant impedance), the initialization of currents using backward step is needed where all voltages for each node is presumed to be nominal values, e.g., 12.47kV rated line voltage would be $\frac{12.47}{\sqrt{3}}$ with zero angle in a basic circuit

topology. The linear ladder network is depicted in Fig. 2.2.

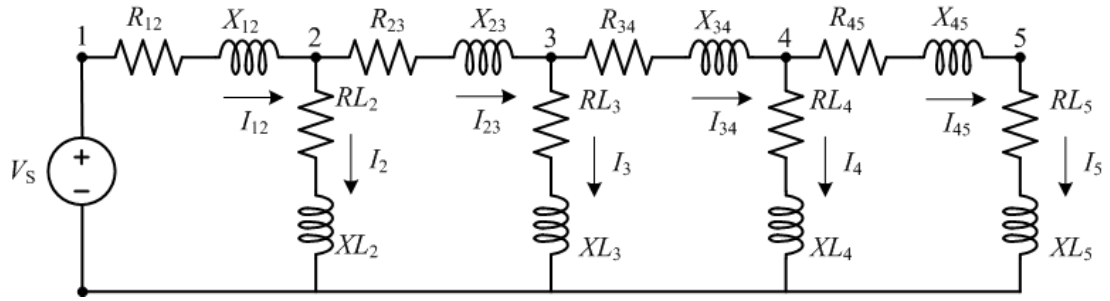

Figure 2.2: Linear Ladder Network

In this method it is assumed that the line impedances and load impedances at the source voltage (V_s). Forward sweep method is used to find the solution of this network. The voltage at node 5 i.e V_5 is calculated at no-load condition. As the network has no line currents as well as load currents, the voltage at node 5 will be equal to the source voltage. The load current at node 5 is calculated by backward sweep method. The load current I_5 is calculated as:

$$I_5 = \frac{V_5}{R_{L,5} + X_{L,5}} \tag{2.1}$$

In this case load current I_5 is equal to the line current I_{45}.By applying Kirchhoff's Voltage Law (KVL), the voltage at node 4 is given by:

$$V_4 = \frac{V_5}{(R_{L,4-5} + X_{L,4-5}) \times I_{4-5}} \tag{2.2}$$

After calculating load current I_4, applying Kirchhoff's Current Law (KCL) for determination of line current I_{34}:

$$I_{3-4} = I_{4-5} + I_4 \tag{2.3}$$

This process continues till the voltage (V_1) is calculated at the source. The calculated voltage (V_1) is compared with the source voltage (V_S). The ratio of the source voltage (V_s) to the computed voltage (V_1) is determined as:

$$\text{Ratio } \gamma = \frac{V_s}{V_1} \tag{2.4}$$

2.2.1.2 Non-Linear Distribution Feeder

The non-linear network is obtained by replacing constant load impedances in linear ladder network by constant complex power loads as depicted in Fig. 2.2. The voltage at node 5 is calculated by forward sweep method in the similar manner as calculated in the linear ladder network. The load current at every node node is calculated as:

$$I_N = \left(\frac{S_N}{V_N}\right)^* \tag{2.5}$$

The source voltage V_S is calculated with the help of backward sweep method. Due to non-linear nature of the distribution loads, forward sweep method is used. The

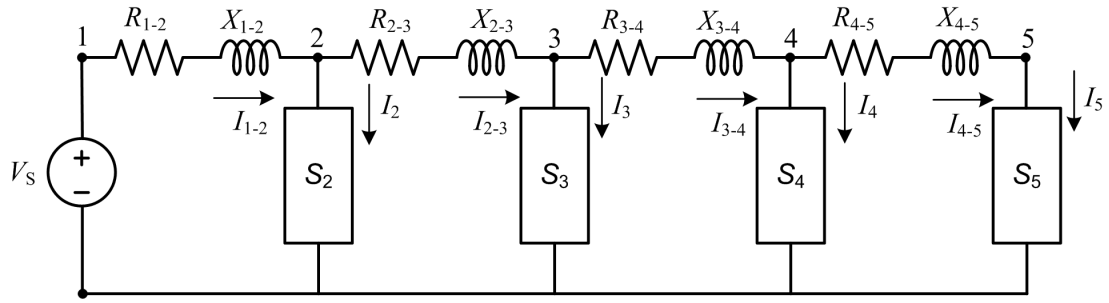

Figure 2.3: Non-Linear Ladder Network

forward sweep method starts by considering the source voltage as well as the line currents calculated in the case of the backward sweep method.

In general, the backward step consists of the following:

$$V_n^{\text{abc}} = [a]V_m^{\text{abc}} - [b]I_m \tag{2.6}$$

$$I_n^{\text{abc}} = [c]V_m^{\text{abc}} - [d]I_m \tag{2.7}$$

The forward step generally uses the voltage update from the backward step to predict the voltage as follows:

$$V_n^{\text{abc}} = [a]V_m^{\text{abc}} - [b]I_m \tag{2.8}$$

$$I_n^{\text{abc}} = [c]V_m^{\text{abc}} - [d]I_m \tag{2.9}$$

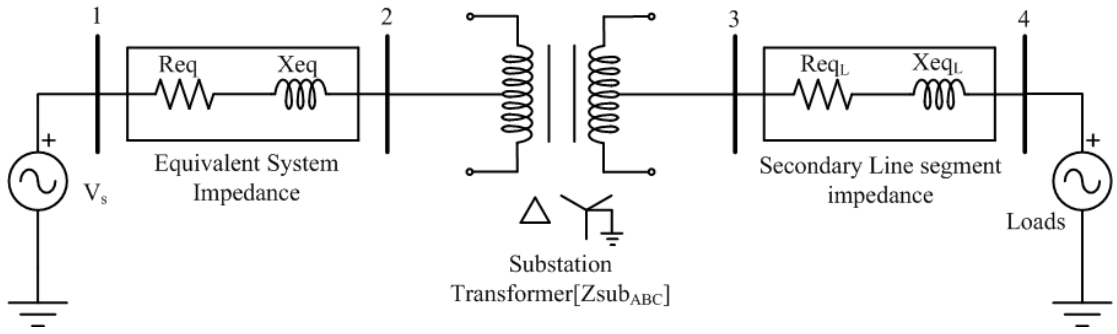

Figure 2.4: IEEE 4 Bus Test Feeder

2.2.2 Example IEEE 4-Node Feeder

For the analysis purpose the IEEE 4 bus test feeder is developed. This 4 bus test feeder is used to demonstrate the analysis of power with and without distributed energy resources (DER), loop flow analysis as well as formation of **Z** - impedance matrix and short circuit studies. The adjustment or addition in terms loads or line impedances or generating sources will be carried out depending on the analysis method which is discussed in the further section. A single-line diagram of the IEEE 4 bus test feeder is illustrated in Fig. . The system source voltage is considered to be 12.47 kV line-to line. The equivalent system impedance segment from bus 1 to bus 2 is 2000 ft long and secondary line segment impedance from bus 3 to bus 4 is 2500 ft respectively. The single phase transformer is connected in delta grounded wye with kVA rating = 6000, primary and secondary voltage as 12.47kV and 4.16kV respectively and the per unit impedance of the transformer is assumed as $\mathbf{Z_{pu}} = 0.01 + j0.06$.

2.2.3 Analysis of Power Flow with and without DER

This section deals with the analysis of power flow in distribution feeders with and without injection of distributed energy resources (DERs). The analysis shows that the injection of distributed energy resources results in increase in the node voltages and requires less number of iterations to converge for a given distribution feeders. In this analysis, total 4 nodes are considered including the source voltages and 3 loads respectively. Depending upon the requirements, the position of the voltage as well as the nature of the loads are changed accordingly.

2.2.3.1 Case 1: Analysis of Power Flow Without DER

In this case the voltage source is connected at node 1 which is considered as 7200 $\angle^{\circ}0$ and the loads are connected to the nodes 2, 3 and 4 respectively. The initial conditions are I_{1-2}, I_{2-3} and I_{3-4} equal to 0 and the convergence is 0.0001 and initial source voltage is assumed to be zero.

The impedance between nodes 1-2, 2-3 and 3-4 are respectively: $Z_{1-2} = 0.1414 + j0.5353\ \Omega$, $Z_{2-3} = 0.0288 + j0.1728\ \Omega$ and $Z_{3-4} = 0.1907 + j0.5035\ \Omega$. The loads S_2, S_3 and S_4 respectively are: $S_2 = 1500 + j750$ kVA, $S_3 = 1045 + j344$ kVA and $S_4 = 900 + j500$ kVA.

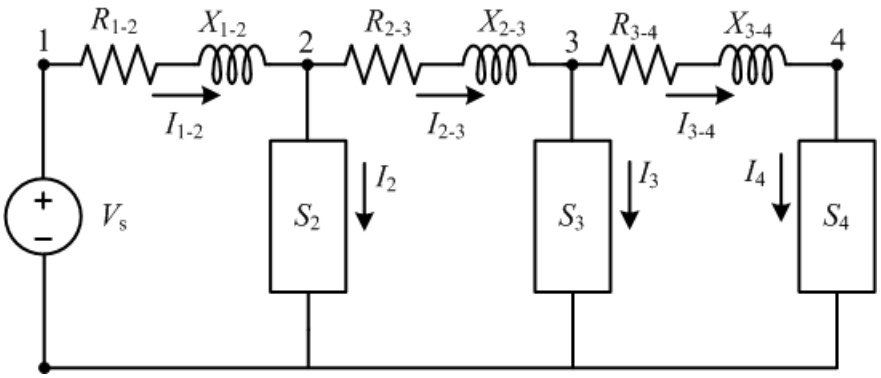

Figure 2.5: Single-phase distribution feeder without DER

A complete iteration consists of a backward step and a forward step. Each iteration will perform a first a backward step in which the currents between the nodes as well the loads currents are calculated. Then a forward step is performed where the voltage of each nodes are determined.

Applying the **first backward step**: In this step, the currents values between the nodes as well as the current through the loads are considered to be zero.

The **first forward step** is applied here: $V_2 = V_S - Z_{1-2} \cdot I_{1-2} = 7200\angle 0°$ V, $V_3 = V_2 - Z_{2-3} \cdot I_{2-3} = 7200\angle 0°$ V and $V_4 = V_3 - Z_{3-4} \cdot I_{3-4} = 7200\angle 0°$ V. Notice that the current values are zeros. To perform an error calculation, the difference between the source and the node 4 is $\text{Err}(\beta) = \frac{V_4 - V_S}{V_{nominal}} = 1$.

The **second backward step** is applied here in order to determine the current flowing in nodes 4-3, 3-2 and 2-1 respectively. Also the currents through loads S_2, S_3 and S_4 are calculated. So, the current flowing between nodes 4 and 3 (I_{3-4}) is : $I_4 =$

$I_{3-4} = \left(\frac{(900+j500)\cdot 1000}{7200\angle 0^\circ}\right)^* = 142.9948\angle -29.0546^\circ$ A. Current flowing at node 3: $I_3 = \left(\frac{(1045+j344)\cdot 1000}{7200\angle 0^\circ}\right)^* = 152.8005\angle -18.2208^\circ$ A. Current flowing between nodes 2 and 3 (I_{2-3}): $I_{2-3} = I_3 + I_{3-4} = 152.8005\angle -18.2208^\circ + 142.9948\angle -29.0546^\circ = 294.4757\angle -23.4575^\circ$ A. Current flowing through node 2 $I_2 = \left(\frac{(1500+j750)\cdot 1000}{7200\angle 0^\circ}\right)^* = 232.9237\angle -26.5650^\circ$ A. Current flowing between nodes 1 and 2 (I_{1-2}) is : $I_{1-2} = I_2 + I_{2-3} = 232.9237\angle -26.5650^\circ + 294.4757\angle -23.4575^\circ = 527.2081\angle -24.8298^\circ$ A. It is observed that the current decreases as we move away from the generating source.

To complete the second iteration, the **second forward step** is applied here: $V_2 = V_S - Z_{1-2} \cdot I_{1-2} = 7017.4376\angle -1.8359^\circ\ V$ $V_3 = V_2 - Z_{2-3} \cdot I_{2-3} = 6990.9430\angle -2.1979^\circ\ V$ *and* $V_4 = V_3 - Z_{3-4} \cdot I_{3-4} = 6934.2836\angle -2.6268^\circ$ V . From the results, it is seen that the voltage at node 4 is less than nodes 1, 2 and 3 respectively. This means as number of nodes are increased then the voltage at extreme end of the feeder will have lowest voltage as compared to previous node voltages. Calculating the error for the second iteration: $\text{Err}(\beta) = \frac{V_4 - V_{4old}}{V_{nominal}} = 0.0369$. As the error is more than the specified tolerance (i.e. 0.0001), it is required to carry out further iterations.

Applying the **third backward step** the current flowing between nodes 4 and 3 (I_{3-4}) is : $I_4 = I_{3-4} = \left(\frac{(900+j500)\cdot 1000}{6934.2836\angle -2.6268^\circ}\right)^* = 148.4743\angle -31.6814^\circ$ A. Current flowing at node 3: $I_3 = \left(\frac{(1045+j344)\cdot 1000}{6990.9430\angle -2.1979^\circ}\right)^* = 157.3699\angle -20.4187^\circ$ A. Current flowing between nodes 2 and 3 (I_{2-3}): $I_{2-3} = I_3 + I_{3-4} = 157.3699\angle -20.4187^\circ + 148.4743\angle -31.6814^\circ = 304.3694\angle -25.8857^\circ$ A. Current flowing through node 2 $I_2 = \left(\frac{(1500+j750)\cdot 1000}{7017.4376\angle -1.8359^\circ}\right)^* =$

$238.9833\angle -28.4009°$ A. Current flowing between nodes 1 and 2 (I_{1-2}) is : $I_{1-2} = I_2 + I_{2-3} = 238.9833\angle -28.4009° + 304.3694\angle -25.8857° = 543.2237\angle -26.9919°$ A.

To complete the third iteration, the **third forward step** is applied here: $V_2 = V_S - Z_{1-2} \cdot I_{1-2} = 7003.1683\angle -1.8349°\ V$ $V_3 = V_2 - Z_{2-3} \cdot I_{2-3} = 6973.8702\angle -2.2001°\ V$ *and* $V_4 = V_3 - Z_{3-4} \cdot I_{3-4} = 6912.6207\angle -2.6240°$ V . From the results, it is seen that the voltage at node 4 is less than nodes 1, 2 and 3 respectively. This means as number of nodes are increased then the voltage at extreme end of the feeder will have lowest voltage as compared to previous node voltages. Calculating the error for the second iteration: $\text{Err}(\beta) = \frac{V_4 - V_{4old}}{V_{nominal}} = 0.0030$. As the error is more than the specified tolerance (i.e. 0.0001), it is required to carry out further iterations.

Applying the **fourth backward step** the current flowing between nodes 4 and 3 (I_{3-4}) is : $I_4 = I_{3-4} = \left(\frac{(900+j500)\cdot 1000}{6912.6207\angle -2.6240°}\right)^* = 148.9396\angle -31.6786°$ A. Current flowing at node 3: $I_3 = \left(\frac{(1045+j344)\cdot 1000}{6973.8702\angle -2.2001°}\right)^* = 157.7551\angle -20.4209°$ A. Current flowing between nodes 2 and 3 (I_{2-3}): $I_{2-3} = I_3 + I_{3-4} = 157.7551\angle -20.4209° + 148.9396\angle -31.6786° = 305.2170\angle -25.8874°$ A. Current flowing through node 2 $I_2 = \left(\frac{(1500+j750)\cdot 1000}{7003.1683\angle -1.8349°}\right)^* = 239.4703\angle -28.3999°$ A. Current flowing between nodes 1 and 2 (I_{1-2}) is : $I_{1-2} = I_2 + I_{2-3} = 239.4703\angle -28.3999° + 305.2170\angle -25.8874° = 544.5582\angle -26.9919°$ A.

For the fourth iteration, the **fourth forward step** is applied here: $V_2 = V_S - Z_{1-2} \cdot I_{1-2} = 7002.6938\angle -1.8396°\ V$ $V_3 = V_2 - Z_{2-3} \cdot I_{2-3} = 6973.3169\angle -$

2.2059° V *and* $V_4 = V_3 - Z_{3-4} \cdot I_{3-4} = 6911.8839\angle - 2.6312°$ V . Calculation of the error for fourth iteration $\text{Err}(\beta) = \frac{V_4 - V_{4old}}{V_{nominal}} = 0.00010$. The above voltages and currents are converged to an error of 0.000010. For this particular case, the system required fourth iterations to get converged. The summary of the above iteration process is illustrated in table 2.1.

Table 2.1
Summary of Iteration Process for Case 1

Parameters	First Iteration	Second Iteration	Third Iteration	Fourth Iteration
Current (I_{12})	0	527.2081∠-24.8298° A	543.2237∠-26.9919° A	544.5582∠-26.9919° A
Current (I_2)	0	232.9237∠-26.5650° A	238.9833∠-28.4009° A	239.4703∠-28.3999° A
Current (I_{23})	0	294.4757∠-23.4575° A	304.3694∠-25.8857° A	305.2170∠-25.8874° A
Current (I_3)	0	152.8005∠-18.2208° A	157.3699∠-20.4187° A	157.7551∠-20.4209° A
Current (I_{34})	0	142.9948∠-29.0546° A	148.4743∠-31.6814° A	148.9396∠-31.6786° A
Current (I_4)	0	142.9948∠-29.0546° A	148.4743∠-31.6814° A	148.9396∠-31.6786° A
Voltage (V_2)	7200∠0° V	7017.4376∠-1.8359° V	7003.1683∠-1.8349° V	7002.6938∠-1.8396° V
Voltage (V_3)	7200∠0° V	6990.9430∠-2.1979° V	6973.8702∠-2.2001° V	6973.3169∠-2.2059° V
Voltage (V_4)	7200∠0° V	6934.2836∠-2.6268° V	6912.6207∠-2.6240° V	6911.8839∠-2.6312° V
Error (β)	1.0000	0.0369	0.0030	0.0001

2.2.3.2 Case 2: Analysis of Power Flow with DER

In this case a voltage source V_S which is considered as 7200 ∠0° V is connected to node 1. A distributed energy resources (V_{DER}) is connected to node 3 and as well as node 4 and the voltages on all nodes are considered equal to the source voltage and the branch currents in every transmission line as zero. The internal impedance of the DER source are represented as R_{DER} and X_{DER} respectively which are calculated

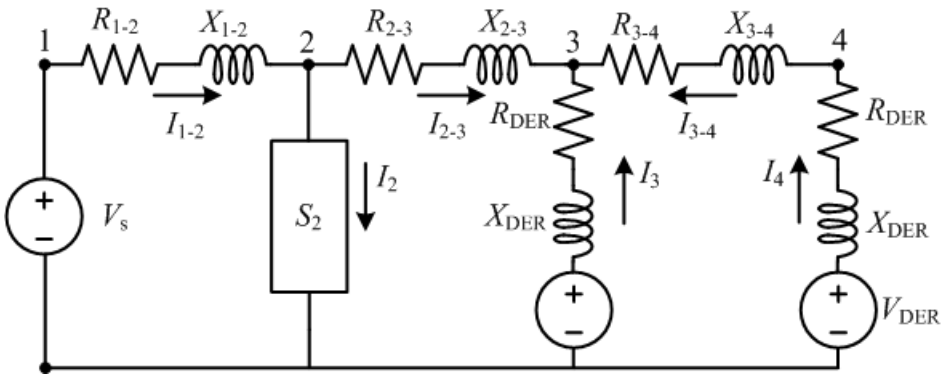

Figure 2.6: Single-phase distribution feeder with DER

using the loads, voltage of the DER source and the current through the node 3 and node 4 respectively. To determine the node voltages and currents backward and forward step are applied. The same procedure as carried out in case 1 is followed for the case 2. The calculated voltages at each node and the currents in each branch during three iterations is are summarized in the table 2.2.

Table 2.2
Summary of Iteration for Case 2

Parameters	First Iteration	Second Iteration	Third Iteration
Current (I_{12})	0	485.5324∠-9.7829° A	484.4124∠-10.7885° A
Current (I_2)	0	232.9237∠-26.5650° A	236.4575∠-28.5402° A
Current (I_{23})	0	271.0062∠-4.5856° A	269.0522∠-4.7540° A
Current (I_3)	0	152.8005∠161.7791° A	155.1679∠159.4208° A
Current (I_{34})	0	142.9948∠29.0546° A	144.9107∠32.0230° A
Current (I_4)	0	142.9948∠150.9453° A	144.9107∠147.9769° A
Voltage (V_2)	7200∠0° V	7092.3963∠-1.9752° V	7088.3056∠-1.9557° V
Voltage (V_3)	7200∠0° V	7090.1516∠-2.3583° V	7086.1984∠-2.3363° V
Voltage (V_4)	7200∠0° V	7104.8075∠-2.9684° V	7104.9690∠-2.9478° V
Error (β)	1.0000	0.0132	0.000022

2.2.3.3 Case 3: Analysis with Node 4 as the DER Reference

In this case source voltage is considered as 7200 ∠0° V is connected to node 1. The node 4 is considered as the reference node and the reference voltage is 7200 ∠0° V. The DER is connected to the node 3 and node 4 respectively. The load currents, branch currents and the voltage at every node is calculated using backward forward sweep method. The procedure demonstrated in case 1 and case 2 is carried out in case 3 also and the summary of the iteration of voltages and currents are summarized in the table 2.3.

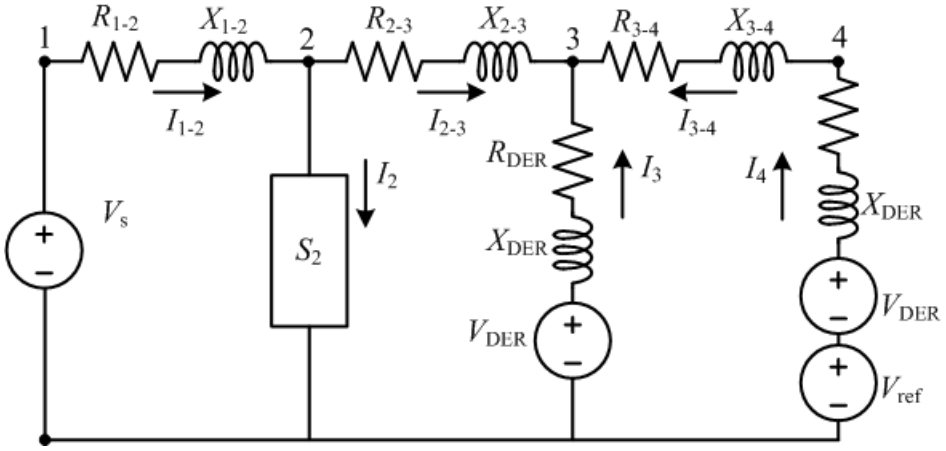

Figure 2.7: Single-phase distribution feeder with DER and Node 4 Referenced

Table 2.3
Summary of Iteration for Case 3

Parameters	First Iteration	Second Iteration	Third Iteration
Current (I_{12})	0	485.5324∠-9.7829° A	494.7995∠-14.9775° A
Current (I_2)	0	232.9237∠-26.5650° A	236.4575∠-28.5402° A
Current (I_{23})	0	271.0062∠4.5856° A	270.6767∠3.1561° A
Current (I_3)	0	152.8005∠161.7791° A	155.1679∠159.4208° A
Current (I_{34})	0	142.9948∠29.0546° A	142.9948∠29.0546° A
Current (I_4)	0	142.9948∠150.9453° A	142.9948∠150.9453° A
Voltage (V_2)	7200∠0° V	7092.3963∠-1.9752° V	7206.0733∠-2.1787° V
Voltage (V_3)	7200∠0° V	7090.1516∠-2.3583° V	7202.8155∠-2.5549° V
Voltage (V_4)	7200∠0° V	7200∠0° V	7200∠0° V
Error (β)	1.0000	0.0000	0.0000

2.3 Constructing an Impedance matrix

In transmission network, the Y admittance matrix has often been utilized because of the direct relationship between nodes and provides easy determination of admittance by inferring from the off-diagonal matrices. It is considered as the most powerful matrices used for analysis of the power system. The less popular approach, which will employ significant computational complexity (full rank matrix) as the result it is not well implemented in power control centers. The following equation shows the inverse relationship between the impedance $\mathbf{Z}$ and admittance $\mathbf{Y}$ matrices where N is the size of a feeder. Under unbalanced condition, the constants of 3 indicates three

times the original nodes for each phase of the feeder circuits.

$$\mathbf{Z}_{(3\times N)} = \mathbf{Y}^{-1}_{(3\times N)} \tag{2.10}$$

This subject is being brought up here in this section and it is timely right after the discussion of backward and forward sweeping technique because of the necessity in determining the initial current values for each node. It could also help in convergence of 3-phase power flow analysis with appropriate values that can improve quality of measurement data to the entire distribution feeder. The impedance **Z** matrix is full rank.

The relationship between the voltage of the bus as well as the injected currents in the bus in the **Z** is:

$$\mathbf{Z}_{matrix} = \mathbf{IC_b}^{-1} \times V_b \tag{2.11}$$

The off-diagonal elements of the impedance-matrix **Z** are called transfer impedance:

$$\mathbf{Z}_{xy} = \mathbf{IC_y}^{-1} \times V_x \tag{2.12}$$

The diagonal elements of the impedance-matrix **Z** are called the driving-point

impedance or the Thevenin Impedance:

$$\mathbf{Z}_{xx} = \mathbf{IC_x}^{-1} \times V_x \tag{2.13}$$

2.3.1 Algorithmic Construction of Impedance Matrix

Unlike construction of Y matrix, it can be built by inspection. The connectivity between nodes can be directly related from and to nodes. The Z-impedance matrix Z can be constructed in following 4-major steps using direct **Z**-Matrix building algorithm.

Case 1: Add a new node i to the reference node, which is the feeder head in distribution substation. In this case, it virtually establishes a connection from the new node for the reference node known as swing bus. Later in case 4, as the feeder has grown out to complete a topology construction, a Kron reduction will be performed. This means that the reference node 0 will be incorporated together with all nodes created in this process.

Case 2: Add another virtual node $i + 1$ connecting the node i. This continues for the rest of the feeder nodes. If a network is completely radial, then case 2 will be utilized before case 4 in the final step. If there is a weakly meshed network within a feeder, then case 3 will be processed, i.e., $\mathbf{Z}^{\text{new}}_{(i+1,i+1)}$ where i is initiated with integers

$1, 2, \cdots N$, which constitutes the following:

$$\mathbf{Z}^{\text{new}}_{(i+1,i+1)} = \begin{bmatrix} z_i & z_i \\ \\ z_i & z_i + z_{i+1} \end{bmatrix} \tag{2.14}$$

If N = 2 where it is connected in radial fashion. The following equation is as follows:

$$\mathbf{Z}^{\text{new}}_{(i+1,i+1)} = \begin{bmatrix} z_i & z_i & z_i \\ \\ z_i & z_i + z_{i+1} & z_i + z_{i+1} \\ \\ z_i & z_i + z_{i+1} & z_i + z_{i+1} + z_{i+2} \end{bmatrix} \tag{2.15}$$

Case 3: If there is a weakly mesh network, connect the existing two nodes and form the mesh network. Apply the Kron reduction process to calculate the impedance matrix.

Case 4: Addition of the distribution feeder from the existing bus (b) to the reference node. Formulate the impedance matrix and apply the Kron reduction process to calculate the final impedance matrix of the network.

2.3.2 Flowchart in Constructing Impedance Matrix

Fig. 2.8 depicts the flowchart for the construction of the impedance matrix. In the first step, the node i is connected to the reference node and the impedance matrix is computed. Further, node i+1 is connected to node i and the impedance matrix is computed. In the next step, the size of the impedance matrix is compared with the number of nodes including the reference node. If the size of the impedance matrix is greater than the number of the nodes, Kron reduction is applied. If the matrix size is not greater then another condition i.e. whether i+n node is connected to the reference node. If it is connected then compute the final impedance matrix and if not continue the process of addition of the new node to the previous node.

2.3.3 Example Construction of Impedance Method

Establishing connection from new node to the reference node thus forming a 1×1 bus impedance matrix

$$\mathbf{Z}_{\text{bus-1}} = \Big[0.0192 + j0.0575\Big]\ \Omega$$

Add another virtual node 2 connecting the node 1. Elements $\mathbf{Z_{12}}$ and $\mathbf{Z_{21}}$ are equal to the $\mathbf{Z_{11}}$. The elements $\mathbf{Z_{22}}$ is the sum of the $\mathbf{Z_{11}} = 0.0192 + j0.0575\ \Omega$ and the value of the impedance $\mathbf{Z_a} = 0.1414 + j0.5353\ \Omega$ which is connected between nodes 1

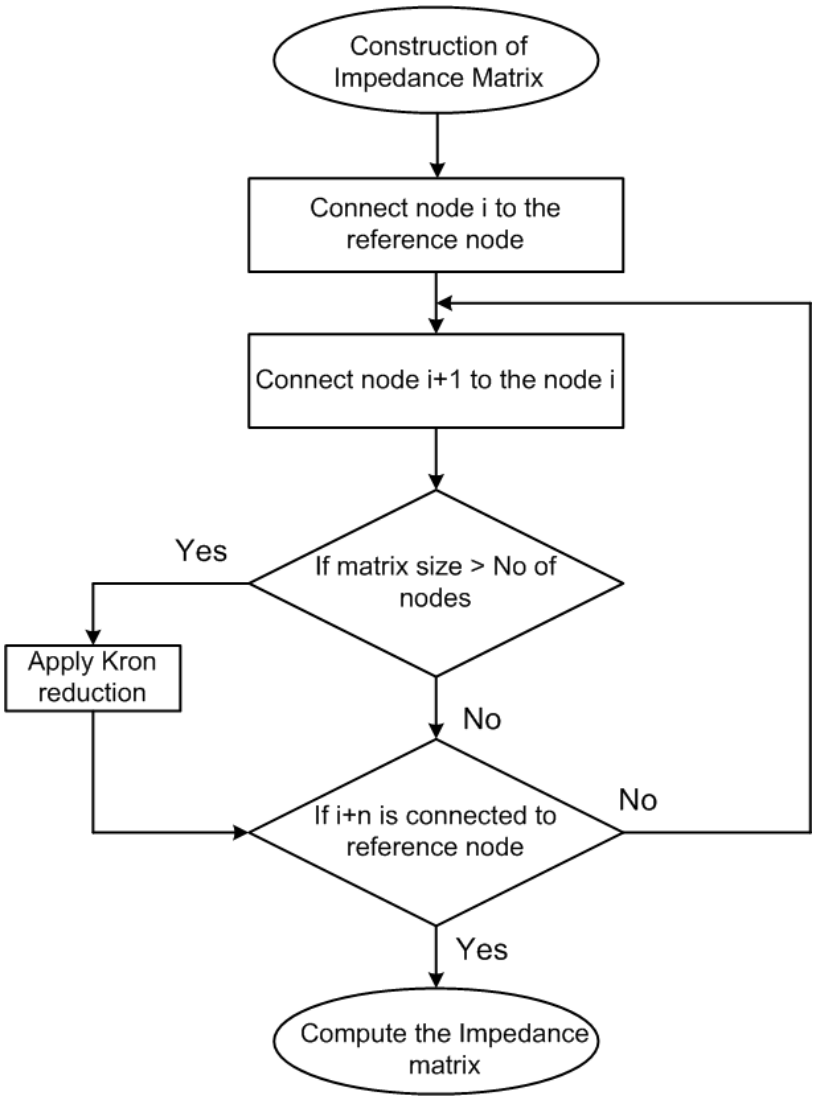

Figure 2.8: Flowchart for the construction of impedance matrix

and 2

$$\mathbf{Z}_{\text{bus-2}} = \begin{bmatrix} 0.0192 + j0.0575 & 0.0192 + j0.0575 \\ 0.0192 + j0.0575 & 0.1606 + j0.5928 \end{bmatrix} \Omega$$

The elements in the new row and new column will be same as the elements in the row 2 and column 2 because the new node is connected to node 2. The elements $\mathbf{Z_{33}}$ is the sum of the of $\mathbf{Z_{22}} = 0.1606 + j0.5928\ \Omega$ and the impedance $\mathbf{Z_a} = 0.0288 + j0.1728\ \Omega$

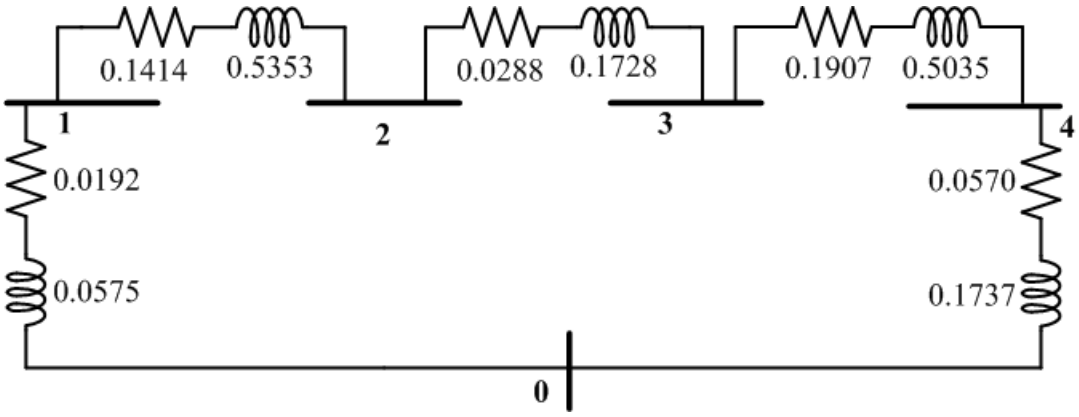

Figure 2.9: Network for determination of **Z**-Impedance matrix

which is connected between the nodes 2 and 3 respectively

$$\mathbf{Z}_{\text{bus-3}} = \begin{bmatrix} 0.0192 + j0.0575 & 0.0192 + j0.0575 & 0.0192 + j0.0575 \\ 0.0192 + j0.0575 & 0.1606 + j0.5928 & 0.1606 + j0.5928 \\ 0.0192 + j0.0575 & 0.1606 + j0.5928 & 0.1894 + j0.7656 \end{bmatrix} \Omega$$

The elements in the new row and new column will be same as the elements in the row 3 and column 3 because the new node is connected to node 3. The elements $\mathbf{Z_{33}}$ is the sum of the of $\mathbf{Z_{33}} = 0.1894 + j0.7656\ \Omega$ and the impedance $\mathbf{Z_a} = 0.1907 + j0.5035\ \Omega$ which is connected between the nodes 3 and 4 respectively

$$\mathbf{Z}_{\text{bus-4}} = \left[\begin{array}{ccc|c} 0.0192 + j0.0575 & 0.0192 + j0.0575 & 0.0192 + j0.0575 & 0.0192 + j0.0575 \\ 0.0192 + j0.0575 & 0.1606 + j0.5928 & 0.1606 + j0.5928 & 0.1606 + j0.5928 \\ 0.0192 + j0.0575 & 0.1606 + j0.5928 & 0.1894 + j0.7656 & 0.1894 + j0.7656 \\ \hline 0.0192 + j0.0575 & 0.1606 + j0.5928 & 0.1894 + j0.7656 & 0.3801 + j1.2691 \end{array}\right] \Omega$$

Applying Kron reduction to eliminate final row and final column,the generalized equation require to calculate the new elements of the **Z**-impedance matrix is given as:

$$\mathbf{Z}_{\mathrm{ij}(new)} = \mathbf{Z}_{\mathrm{ij}(old)} - \frac{\mathbf{Z}_{\mathrm{iN}(old)} \cdot \mathbf{Z}_{\mathrm{Nj}(old)}}{\mathbf{Z}_{\mathrm{NN}(old)}} \tag{2.16}$$

where $\mathbf{Z_{ij(old)}}$ represents the particular element of the previous matrix, Using the above equation to calculate the new elements of the matrix, the modified **Z**-impedance matrix is:

$$\mathbf{Z}_{\text{bus-5}} = \begin{bmatrix} 0.0164 + j0.0502 & 0.0099 + j0.0267 & 0.0080 + j0.0219 \\ 0.0099 + j0.0267 & 0.0339 + j0.1131 & 0.0275 + j0.0928 \\ 0.0080 + j0.0219 & 0.0275 + j0.0928 & 0.0330 + j0.1073 \end{bmatrix} \Omega$$

Now connect bus 3 with the reference node, the elements $\mathbf{Z_{44}}$ is the sum of the $\mathbf{Z_{33}} = 0.0776 + j0.2806\ \Omega$ and the impedance $\mathbf{Z_a} = 0.0570 + j0.1737\ \Omega$ which is connected between node 3 as well the as the reference bus, the resultant $\mathbf{Z_{bus-4}}$ will be:

$$\mathbf{Z}_{\text{bus-4}} = \left[\begin{array}{ccc|c} 0.0192 + j0.0575 & 0.0192 + j0.0575 & 0.0192 + j0.0575 & 0.0192 + j0.0575 \\ 0.0192 + j0.0575 & 0.0644 + j0.2427 & 0.0644 + j0.2427 & 0.0644 + j0.2427 \\ 0.0192 + j0.0575 & 0.0644 + j0.2427 & 0.0776 + j0.2806 & 0.0776 + j0.2806 \\ \hline 0.0192 + j0.0575 & 0.0644 + j0.2427 & 0.0776 + j0.2806 & 0.1346 + j0.4543 \end{array}\right] \Omega$$

Applying Kron reduction to eliminate final row and final column,the generalized equation require to calculate the new elements of the **Z**-impedance matrix is given as:

$$\mathbf{Z}_{\mathrm{ij}(new)} = \mathbf{Z}_{\mathrm{ij}(old)} - \frac{\mathbf{Z}_{\mathrm{iN}(old)} \cdot \mathbf{Z}_{\mathrm{Nj}(old)}}{\mathbf{Z}_{\mathrm{NN}(old)}} \tag{2.17}$$

where $\mathbf{Z_{ij(old)}}$ represents the particular element of the previous matrix, Using the above equation to calculate the new elements of the matrix, the modified **Z**-impedance matrix is:

$$\mathbf{Z}_{\text{bus-5}} = \begin{bmatrix} 0.0164 + j0.0502 & 0.0099 + j0.0267 & 0.0080 + j0.0219 \\ 0.0099 + j0.0267 & 0.0339 + j0.1131 & 0.0275 + j0.0928 \\ 0.0080 + j0.0219 & 0.0275 + j0.0928 & 0.0330 + j0.1073 \end{bmatrix} \Omega$$

The new bus 4 is connected to bus 3 with impedance of $\mathbf{Z_a} = 0.0119 + j0.0414\ \Omega$. The off-diagonal elements of the matrix $\mathbf{Z_{bus-6}}$ will be same as the elements in row 3 and column 3 respectively. The diagonal element $\mathbf{Z_{44}}$ is, sum of the element $\mathbf{Z_{33}} = 0.0330 + j0.1073\ \Omega$ and the impedance $0.0119 + j0.0414\ \Omega$.

$$\mathbf{Z}_{\text{bus-6}} = \begin{bmatrix} 0.0164 + j0.0502 & 0.0099 + j0.0267 & 0.0080 + j0.0219 & 0.0080 + j0.0219 \\ 0.0099 + j0.0267 & 0.0339 + j0.1131 & 0.0275 + j0.0928 & 0.0275 + j0.0928 \\ 0.0080 + j0.0219 & 0.0275 + j0.0928 & 0.0330 + j0.1073 & 0.0330 + j0.1073 \\ 0.0080 + j0.0219 & 0.0275 + j0.0928 & 0.0330 + j0.1073 & 0.0449 + j0.1487 \end{bmatrix} \Omega$$

Finally, adding the new line having impedance $\mathbf{Z_a} = 0.0581 + j0.1763\ \Omega$ between the buses 2 and 4 respectively. The new elements are calculated by subtracting the

elements connected between these buses. The diagonal element is calculated by using the following equation:

$$\mathbf{Z}_{\mathrm{NN}} = \mathbf{Z}_{\mathrm{ii}} + \mathbf{Z}_{\mathrm{jj}} - 2 \cdot \mathbf{Z}_{\mathrm{ij}} + \mathbf{Z}_{\mathrm{a}} \tag{2.18}$$

After calculating all the elements, the $\mathbf{Z}_{bus-7}$ matrix can we written as:

$$\mathbf{z}_{\text{bus-7}} = \left[\begin{array}{ccccc|c} 0.0164+j0.0502 & 0.0099+j0.0267 & 0.0080+j0.0219 & 0.0080+j0.0219 & | & 0.0019+j0.0048 \\ 0.0099+j0.0267 & 0.0339+j0.1131 & 0.0275+j0.0928 & 0.0275+j0.0928 & | & 0.0064+j0.0203 \\ 0.0080+j0.0219 & 0.0275+j0.0928 & 0.0330+j0.1073 & 0.0330+j0.1073 & | & -0.0055-j0.0145 \\ 0.0080+j0.0219 & 0.0275+j0.0928 & 0.0330+j0.1073 & 0.0449+j0.1487 & | & -0.0174-j0.0559 \\ \hline 0.0019+j0.0048 & 0.0064+j0.0203 & -0.0055-j0.0145 & -0.0174-j0.0559 & | & 0.0819+j0.2525 \end{array}\right] \Omega$$

Applying Kron reduction to the above matrix in order to calculate the final $\mathbf{Z}_{bus}$:

$$\mathbf{Z}_{\mathrm{bus}} = \begin{bmatrix} 0.0163+j0.0501 & 0.0097+j0.0263 & 0.0081+j0.0221 & 0.0084+j0.0229 \\ 0.0097+j0.0263 & 0.0334+j0.1114 & 0.0279+j0.0939 & 0.0288+j0.0972 \\ 0.0081+j0.0221 & 0.0279+j0.0939 & 0.0326+j0.1064 & 0.0318+j0.1454 \\ 0.0084+j0.0229 & 0.0288+j0.0972 & 0.0318+j0.1454 & 0.0412+j0.1363 \end{bmatrix} \Omega$$

2.4 General Short-Circuit Analysis

The calculation of the short-circuit currents in the unbalanced faults in a balanced three phase system is achieved with the help of application of symmetrical components. However, if the distribution feeder is unbalanced then this is not suitable for calculation of short circuit currents. If an unequal mutual coupling is present between any of the phases, this will eventually leads to the mutual coupling within sequence

networks. Another shortcomings of this method is, it is restricted to number of the phases in which the faults occur means that in case of single line to ground faults the short circuit currents are calculated in phase a with respect to ground. In this section, for analyzing such shortcomings a method is developed using phase frame which will analyzed the short-circuit currents in an unbalanced three-phase distribution feeder. Fig. 2.10 shows the model for the unbalanced feeder used for the short

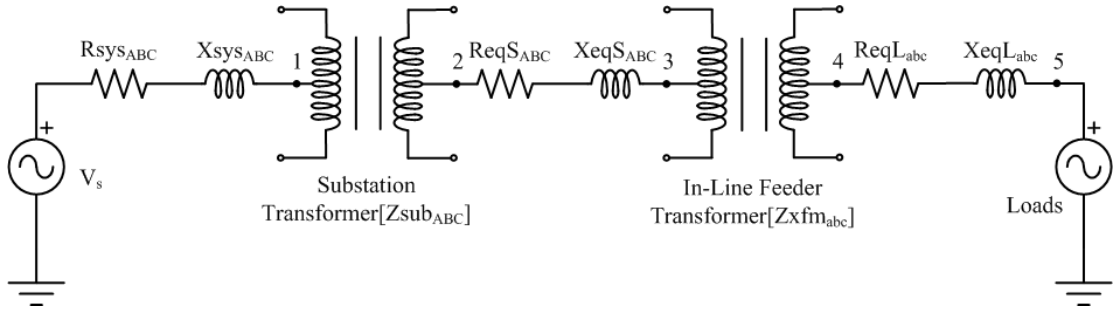

Figure 2.10: Short-circuit analysis model for unbalanced feeder

circuit calculations. The model is divided into five different sections and the short circuit can occur on any of these five sections. The transmission system short circuit study is used to determine the values of the short circuit currents at point 1 as shown in Fig. 2.11. The results of the short circuit study of the transmission system are computed in terms of single phase and three phase short circuit Mega-Volt-Amperes (MVAs) and using these MVAs the equivalent system's positive sequence as well as zero sequence are calculated. The positive and the negative sequences impedances are calculated from the 3ø MVA magnitude as well as angle while the zero sequences is calculated from 1ø MVA magnitude as well as angle. Equations for the determinations

of positive and the zero sequences impedances are:

$$\mathbf{Z}_1 = \mathbf{Z}_2 = \frac{KV^2_{nomL-L}}{(MVA_{3\emptyset})^*}\ \Omega \tag{2.19}$$

$$\mathbf{Z}_0 = \frac{KV^2_{nomL-L}}{(MVA_{1\emptyset})^*} - 2 \cdot \mathbf{Z}_1\ \Omega \tag{2.20}$$

Using the symmetrical component transformation matrix, the positive sequence impedance as well as the zero sequence impedance are converted into phase sequence impedance.

$$[\mathbf{Z_{abc}}] = [\mathbf{A_s}] \cdot [\mathbf{Z_{012}}] \cdot [\mathbf{A_s}]^{-\mathbf{1}}$$

$$[\mathbf{Z_{abc}}] = \frac{1}{3}\begin{bmatrix} 1 & 1 & 1 \\ 1 & a_s^2 & a_s \\ 1 & a_s & a_s^2 \end{bmatrix} \cdot \begin{bmatrix} Z_0 & 0 & 0 \\ 0 & Z_1 & 0 \\ 0 & 0 & Z_2 \end{bmatrix} \cdot \begin{bmatrix} 1 & 1 & 1 \\ 1 & a_s & a_s^2 \\ 1 & a_s^2 & a_s \end{bmatrix}$$

The Thevenin equivalent three phase circuit is required to calculate the short circuit currents at points 2, 3, 4 and 5 respectively. At points 2 and 3 respectively, the equivalent Thevenin voltages are calculated by taking the product of the generalised transformer matrix $[\mathbf{A_t}]$ which is obtained from the substation transformer and the system voltages. Also, the Thevenin equivalent voltages at point 4 and 5 are calculated by multiplying the voltages at node 3 and the generalized transformer matrix $[\mathbf{A_t}]$ obtained from the in-line feeder transformer. The sum of Thevenin phase impedance matrix obtained from each device which is connected between the voltage source and the point at which the fault occur is termed as Thevenin equivalent

phase impedance matrix. During the calculation, if the three phase transformer is present, the total phase impedance matrix on the primary side must be referred to the secondary side of the transformer.

$$[\mathbf{VLL_{abc}}] = [\mathbf{BV}] \cdot [\mathbf{VLL_{ABC}}] - [\mathbf{Zt_{abc}}] \cdot [\mathbf{I_{abc}}] \tag{2.21}$$

Equation 2.21 is the forward step equation in terms of line-to-line voltages. $[\mathbf{VLL_{ABC}}]$ is the line-to-line voltages from the substation transformer, $[\mathbf{Zt_{abc}}]$ is the impdeances of three-phase transformer and $[\mathbf{I_{abc}}]$ is the secondary line currents.

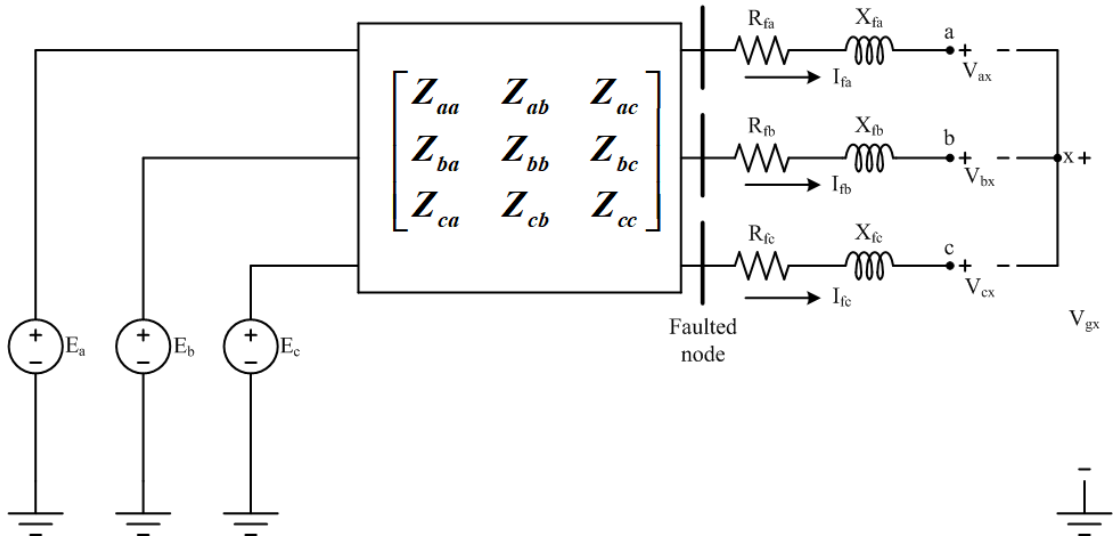

Figure 2.11: Thevenin Equivalent circuit for short circuit calculation

In figure 2.11 the Thevenin equivalent line to line voltages with respect to ground at the faulted node are represented by $\mathbf{E_a}$, $\mathbf{E_b}$ and $\mathbf{E_c}$ respectively. The Thevenin equivalent phase impedance matrix at the faulted node is represented by $[\mathbf{Z_{Total}}]$ and fault impedance in phase a is the combination of fault resistance $\mathbf{R_{fa}}$ and fault

reactance $\mathbf{X_{fa}}$. By applying KVL in figure 2.11 the Thevenin voltages obtained in the matrix form is:

$$\begin{bmatrix} E_a \\ E_b \\ E_c \end{bmatrix} = \begin{bmatrix} Z_{aa} & Z_{ab} & Z_{ac} \\ Z_{ba} & Z_{bb} & Z_{bc} \\ Z_{ca} & Z_{cb} & Z_{cc} \end{bmatrix} \cdot \begin{bmatrix} I_{fa} \\ I_{fb} \\ I_{fc} \end{bmatrix} + \begin{bmatrix} R_{fa} + jX_{fa} & 0 & 0 \\ 0 & R_{fb} + jX_{fb} & 0 \\ 0 & 0 & R_{fc} + jX_{fc} \end{bmatrix} \begin{bmatrix} I_{fa} \\ I_{fb} \\ I_{fc} \end{bmatrix} + \begin{bmatrix} V_{ax} \\ V_{bx} \\ V_{cx} \end{bmatrix} + \begin{bmatrix} V_{xg} \\ V_{xg} \\ V_{xg} \end{bmatrix} \tag{2.22}$$

Equation 2.22 can re-written as:

$$[\mathbf{E_{abc}}] = [\mathbf{Z_{Total}}] \cdot [\mathbf{I_{fabc}}] + [\mathbf{R_f} + \mathbf{jX_f}] \cdot [\mathbf{I_{fabc}}] + [\mathbf{V_{abcx}}] + [\mathbf{V_{xg}}] \tag{2.23}$$

Adding all the impedance in the circuit, the equivalent impedance $[\mathbf{Z_{Equi}}]$ which is the summation of $[\mathbf{Z_{Total}}]$ and $[\mathbf{R_f} + \mathbf{jX_f}]$, equation 2.23 in compressed form is given as:

$$[\mathbf{E_{abc}}] = [\mathbf{Z_{Equi}}] \cdot [\mathbf{I_{fabc}}] + [\mathbf{V_{abcx}}] + [\mathbf{V_{xg}}] \tag{2.24}$$

Admittance is the reciprocal of impedance, therefore the $[\mathbf{Z_{Equi}}]^{-1}$ - impedance matrix can be replaced by $[\mathbf{Y_{Equi}}]$, the equation in terms of fault currents is given as:

$$[\mathbf{I_{fabc}}] = [\mathbf{Y_{Equi}}] \cdot [\mathbf{E_{abc}}] + [\mathbf{Y_{Equi}}] \cdot [\mathbf{V_{abcx}}] + [\mathbf{Y_{Equi}}][\mathbf{V_{xg}}] \tag{2.25}$$

In equation 2.25, the values of $[\mathbf{Y_{Equi}}]$ and $[\mathbf{E_{abc}}]$ are known, therefore defining a new term $[\mathbf{IX_{abc}}]$ for the product of these two parameters and rearranging the hand calculated results, equation 2.25 can we written as:

$$\begin{bmatrix} IX_a \\ IX_b \\ IX_c \end{bmatrix} = \begin{bmatrix} I_{fa} \\ I_{fb} \\ I_{fc} \end{bmatrix} + \begin{bmatrix} Y_{aa} & Y_{ab} & Y_{ac} \\ Y_{ba} & Y_{bb} & Y_{bc} \\ Y_{ca} & Y_{cb} & Y_{cc} \end{bmatrix} \cdot \begin{bmatrix} V_{ax} \\ V_{bx} \\ V_{cx} \end{bmatrix} + \begin{bmatrix} Y_{aa} & Y_{ab} & Y_{ac} \\ Y_{ba} & Y_{bb} & Y_{bc} \\ Y_{ca} & Y_{cb} & Y_{cc} \end{bmatrix} \cdot \begin{bmatrix} V_{xg} \\ V_{xg} \\ V_{xg} \end{bmatrix} \tag{2.26}$$

Expanding equation 2.26 by performing multiplication and addition respectively,

$$\begin{aligned} \mathbf{IX_a} &= \mathbf{I_{fa}} + (\mathbf{Y_{aa}} \cdot \mathbf{V_{ax}} + \mathbf{Y_{ab}} \cdot \mathbf{V_{bx}} + \mathbf{Y_{ac}} \cdot \mathbf{V_{cx}}) + (\mathbf{Y_{aa}} + \mathbf{Y_{ab}} + \mathbf{Y_{ac}}) \cdot \mathbf{V_{xg}} \\ \mathbf{IX_b} &= \mathbf{I_{fb}} + (\mathbf{Y_{ba}} \cdot \mathbf{V_{ax}} + \mathbf{Y_{bb}} \cdot \mathbf{V_{bx}} + \mathbf{Y_{bc}} \cdot \mathbf{V_{cx}}) + (\mathbf{Y_{ba}} + \mathbf{Y_{bb}} + \mathbf{Y_{bc}}) \cdot \mathbf{V_{xg}} \\ \mathbf{IX_c} &= \mathbf{I_{fc}} + (\mathbf{Y_{ca}} \cdot \mathbf{V_{ax}} + \mathbf{Y_{cb}} \cdot \mathbf{V_{bx}} + \mathbf{Y_{cc}} \cdot \mathbf{V_{cx}}) + (\mathbf{Y_{ca}} + \mathbf{Y_{cb}} + \mathbf{Y_{cc}}) \cdot \mathbf{V_{xg}} \end{aligned} \tag{2.27}$$

Equation 2.27 are the generalized equations used for calculation of all types of faults.There are seven unknown variables and other three variables such as $\mathbf{IX_a}$, $\mathbf{IX_b}$ and $\mathbf{IX_c}$ are known because they are the functions of total impedance as well as the Thevenin voltages. Depending on the type of the fault, the above equations are modified to determine three phase faults, three-phase to ground faults, line to line faults, Line to line to ground faults and line to ground faults respectively.

2.5 Conclusion

This chapter illustrates various implementation of element models used for short circuit analysis as well as power flow analysis of a distribution feeders. For power flow analysis, backward/forward sweep also known as modified ladder iterative technique

was used. The backward forward sweep were interchanged by the addition of voltage and current equations for simple radial systems. In case of short circuit analysis of a distribution feeder using the symmetrical component analysis cannot be implemented because it is not possible to modeled every short circuit. In contrast, phase domain method was developed as well as demonstrated for computational purpose for any type of short circuits. These methods equipped with computer program provides a powerful tool for executing present day problems and long term power system studies planning.

Chapter 3

Fault Localization Under Unidirectional Flow Conditions

3.1 Reverse Engineering of Short Circuit Process

This chapter deals with the analysis of the distribution feeders using fault analysis methods. As discussed in chapter 2 regarding the short circuit studies in which the faults can occur at any of the five locations in a power system. The disadvantage of this method is the crew members have to detect the exact fault location which requires ample amount of time and reduces the power supply reliability as well as power quality. This chapter will discuss about various modern fault diagnosis algorithm

which is helpful in unbalanced distribution feeders in order to reduce the time for detecting the exact fault location as well as increasing the reliability of the system and power quality. Also impact of fault in the distribution feeders will be studied depending on unidirectional and bidirectional flow of power.

3.2 Definition of "Segment" and Concluding a Faulted Segment

The distribution feeder in the power system is radial network consisting of n number of line segments as shown in 3.1. Due to the radial network, the measured values of the voltages and the currents are available at the substation. Therefore, an estimation procedure is required to calculate the voltage as well as the currents at the beginning of the faulted line segment depending on the loading condition of the customer and the pre-fault and the post fault measurements of the voltages and the currents at the substation. It is observed that same voltages and currents will be measured at various fault locations as the distribution feeder in a large power system is radial in nature and number of laterals are connected to the main feeder.The first step is to find the possible fault locations which can be determined by scanning the network and the applying algorithm for the fault distance on a section by section basis.

Assumptions include:

1. The radial distribution feeder system is considered to be ideal.

2. The fault occurred is within the segment circled in Fig. 3.1.

3. Only symmetrical or unsymmetrical fault occurred on the distribution feeders.

4. Incremental change in the distance will be equal.

5. Fault location is between Yes and No.

6. The breaker was tripped from SCADA network.

7. Capture the status of fault indicators from the remote controlled switches information before occurrence of the fault.

8. Single-event fault with potential multiple fault types that does not disrupt the majority of the electrical overhead lines. It is rather a localized fault that is generally deemed an "abnormal" condition, not the extreme scenarios like those incurred by hurricanes nor tornadoes.

3.3 Searching for Exact Fault Location(s)

The flowchart shown in Fig. 3.2 and Fig. 3.1 gives the information to be computed to determine the exact fault location. In order to determine the exact fault location

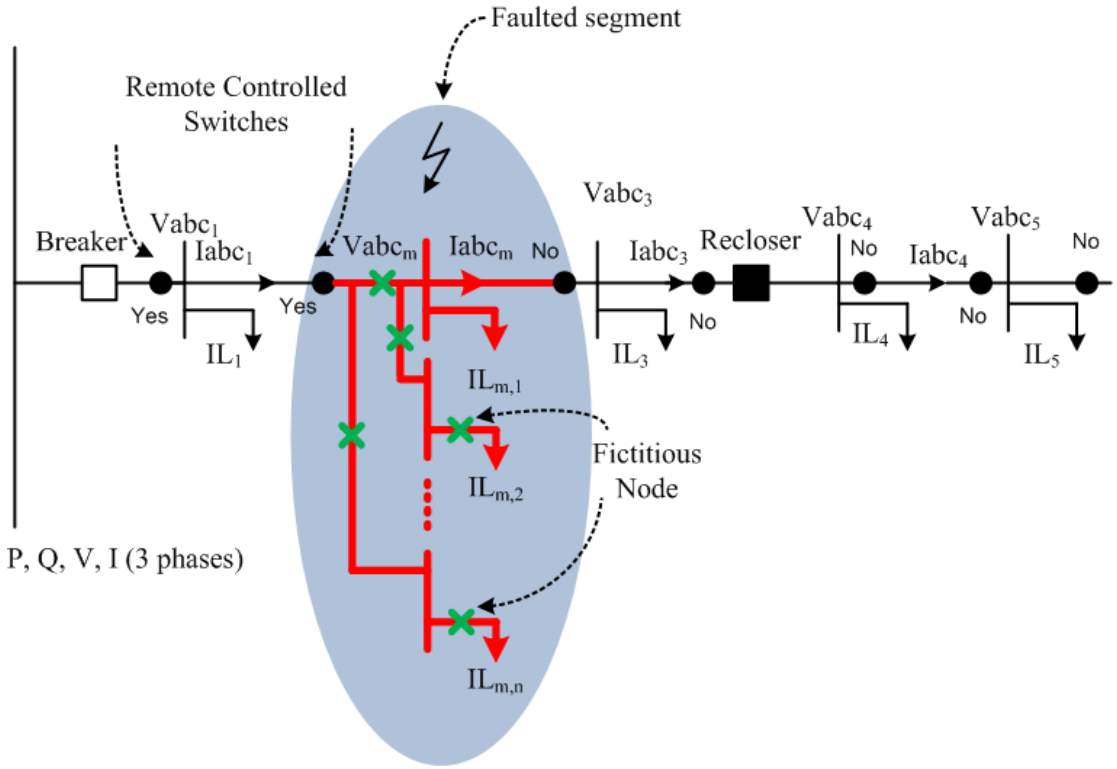

Figure 3.1: One-line diagram of distribution feeder with fictitious nodes

3 major steps needs to be executed. The first step is Initialization of SCADA measurement and topological statuses. In step 1, the information is populated from the Geographical Information System (GIS). The two important components which are obtained from the GIS are accurate data of the distribution feeder topology and real-time measurements of the topology data. The mathematical formulation for every system component such as distributed generators, feeder lines, transformers, voltage regulators, shunt capacitor, series reactor and loads. In step 2, load voltage measurements are required in order to design the load model from load voltage. The load currents are considered in the analysis because load currents are not less than the short circuit currents. In addition to this binary measurements (either ON or OFF)

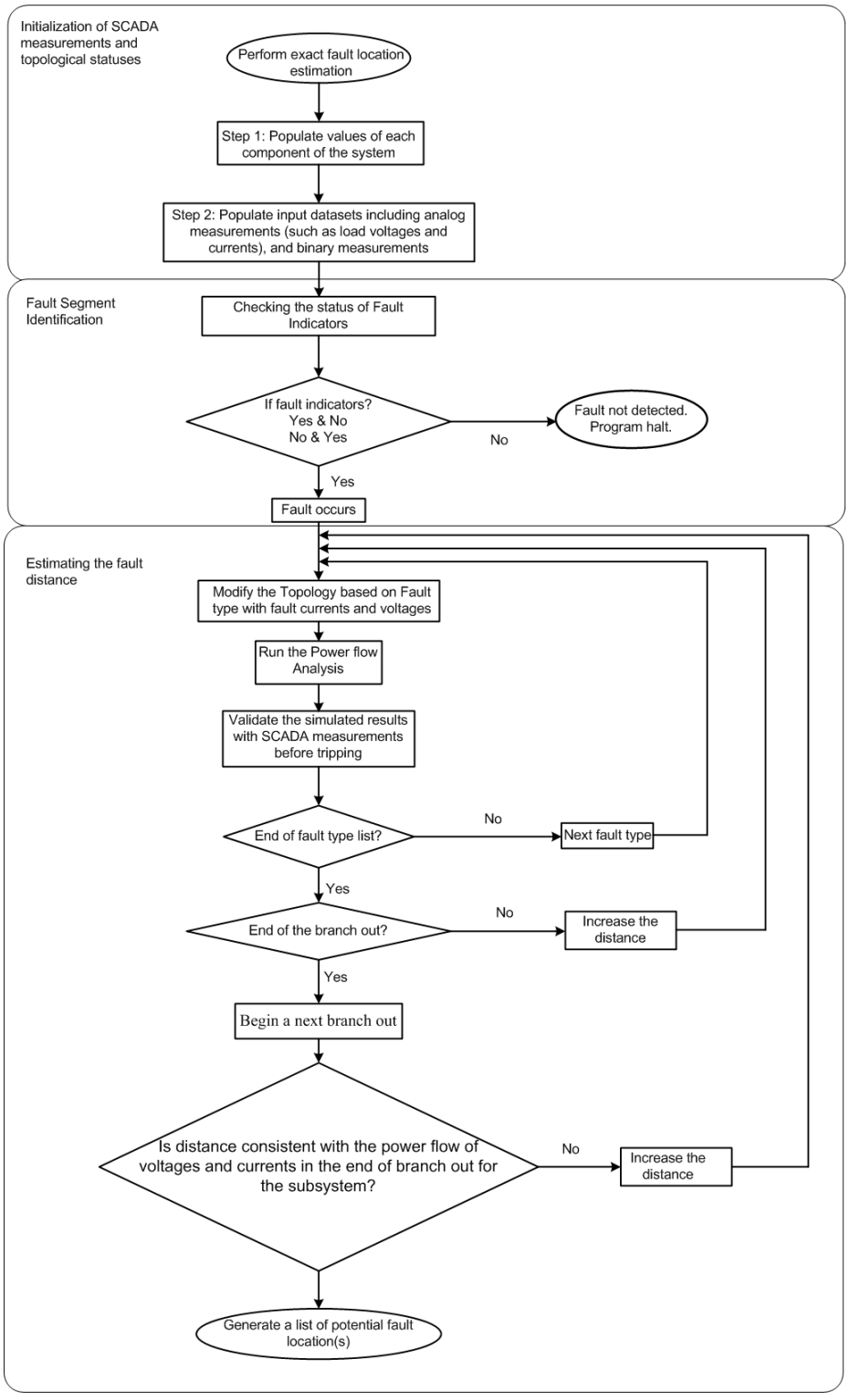

Figure 3.2: Flowchart for enhanced estimation of fault location point based on n number of branch out

of the Fault Indicators(FIs) are recorded to detect the exact location of the fault. In the computerized automated SCADA network, the FIs will help the crew members to navigate the exact location of the fault. The data of the FIs are centralized in the Distributed Automation System (DMS) system where the SCADA systems updates the information regrading the feeder topology and analog as well as binary measurements.

The fault location identification is the second major step for exact fault location estimation. The fault indicators will detect the fault in the distribution feeders. If the fault indicators indicates either (YES and NO) or (NO and YES) then it indicates that the fault has occurred in the segment which is connected between these two FIs. If the FIs indicates either (YES and YES) or (NO and NO) indicates that the fault is not detected and the program halts.

Once the fault occurs, the next and the final major step is estimating the fault distance. Depending up the type of faults and fault voltages and currents, the distribution feeder topology will be modified. The fault type can be classified into symmetrical faults (3 phase fault) and unsymmetrical faults which includes single line to ground fault, double line to ground fault, line to line fault etc. An algorithm will be executed depending upon the type of fault and the power analysis at each node of the distribution feeder will determined the voltages and currents and try to maintained within the specified limits. In order to execute the power flow analysis the system most

accurately, each component connected in the distribution feeder should be analyzed in more detail. This includes three phase transformers with various types of connection, composite loads, single, two and three phase unbalanced systems and effects due to voltage regulators and shunt capacitors. The simulated results obtained from power flow analysis are validated with the SCADA measurements before the tripping of the distribution feeder takes place. The incremental process continues till the next fault type is detected. The first iteration will detect if there are any other faults. If the fault is detected, again the process of topology modification, power flow analysis and comparison with the SCADA results will be carried out. The second iteration loop will verify whether the fault has occurred in the branch out and is the values of fault voltages and currents are consistent with the values of the voltages and currents obtained from the power flow analysis. If they are not consistent then increment the distance till the values become consistent. The third and the final loop will check whether the whole feeder is scanned for possible fault location. If the complete feeder is not scanned then the loop will increment the distance to carry out the process of estimation of fault distance. At the end of the feeder, the program will generate a list of potential fault locations.

3.4 Flowchart to Determine the Estimated Point(s) of Location

Fig. 3.3 depicts the flowchart to determine the exact location of fault in unidirectional power flow. The value current reference(I_ref) is calculated from the power flow analysis. The start_perc and end_perc are assumed to be 0 and 1 respectively and the value of CError is considered to be 999. The fault percentage is calculated by taking the average of the start_perc and end_perc. The currents at each node is calculated using the power flow analysis i.e. by using backward-forward sweep method. If the value of CError is greater than 0.1, then the difference of maximum absolute value of reference current and fault current is calculated. If the difference is less than zero, then fault. perc will equal to the ending_perc else fault.perc will be equal to start_perc. Finally, the exact fault distance is calculated.

3.5 Simulation Results

In order to determine the exact location of fault three cases are simulated using MATLAB programming depending on the topology reconfiguration. Various topologies such as radial feeder, various sub-feeder connected at different location of the

Figure 3.3: Flowchart for the determination of exact fault location

main feeder and various sub-feeders connected at a single point of the main feeder are considered during simulation studies.

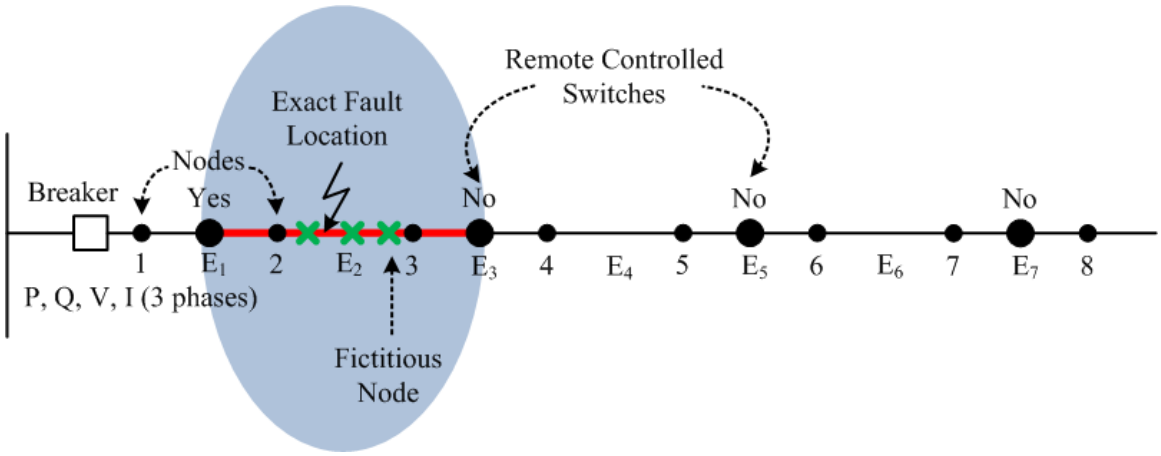

Figure 3.4: A case for determination of exact fault location

3.5.1 Case 1: Perfect Radial Network Setup

This topology consists of 8 nodes and 7 switches where the switches and the respective lines are connected topologically. Breakers and recloser are equipped with the relay. Under normal operating condition, the breaker is used to energized the feeder. The source is considered at node 1 and three phase loads are connected to all remaining 7 nodes. Using the matrix-based Backward-Forward Sweep method the voltages and the load currents at each nodes are calculated which are depicted in the Table 3.1.

Table 3.1
Node Voltages and Currents in Healthy Condition for Case 1

Node No.	Voltage			Load Current		
	Phase A	Phase B	Phase C	Phase A	Phase B	Phase C
1	7199.6∠0°	7199.6∠-120°	7199.6∠120°	983.0859∠-14.9051°	1040.9368∠-139.4749°	1082.5485∠95.7657°
2	7003.3338∠-0.899°	6982.2593∠-120.8724°	6971.3481∠119.2735°	983.0859∠-14.9051°	1040.9368∠-139.4749°	1082.5485∠95.7657°
3	6890.2296∠-1.3295°	6874.9924∠-121.3225°	6858.4751∠118.8277°	908.7012∠-21.261°	869.3071∠-138.9344°	906.0049∠99.2404°
4	6775.0515∠-1.8086°	6773.6496∠-121.9029°	6749.7778∠118.2421°	705.5937∠-20.8563°	673.9254∠-131.6606°	693.3597∠106.1805°
5	6661.9207∠-2.2922°	6677.6218∠-122.6257°	6621.358∠117.7731°	572.884∠-20.3255°	552.4364∠-123.7782°	600.6276∠94.2607°
6	6602.3593∠-2.6424°	6615.0259∠-122.9435°	6559.6823∠117.4741°	438.1184∠-12.7596°	436.1264∠-137.427°	430.7444∠101.3758°
7	6514.1105∠-2.879°	6562.383∠-123.3931°	6501.169∠116.9841°	348.308∠-33.454°	284.7439∠-121.1204°	275.026∠117.4099°
8	6507.1314∠-2.9139°	6561.3173∠-123.4634°	6499.1812∠116.9069°	184.4131∠-24.2511°	198.1309∠-85.9528°	184.6386∠154.4175°

Analysis of Three-Phase-to-Ground (LLLG) Fault

The system explained in case 1 is simulated for three phase to ground fault in which a fictitious node (node 9) is created between nodes 2 and 3 which is assumed to be at a distance of 20% from node 2 and 80% from node 3 of the total distance between these nodes. The fault resistance of 20 Ω is presumed. The initial voltage at node 9 is enforced as the average of the initial source voltage for the first iteration and due to this the final voltages on each phase of node 9 are equal in magnitude and angle which are shown in Table 3.2. The backward-forward sweep method continues until the mismatch occurs between the new and the previous iterations in the load voltages is within the specified tolerance. The final iteration results of voltages and load currents at each nodes are depicted in Table 3.2.

Table 3.2
Node Voltages and Currents for Three Phase to Ground Fault for Case 1

Node No.	Voltage			Load Current		
	Phase A	Phase B	Phase C	Phase A	Phase B	Phase C
1	7199.6∠0°	7199.6∠-120°	7199.6∠120°	2212.0241∠-77.7484°	2254.4046∠-82.8477°	2085.9201∠-78.7815°
2	6923.007∠1.4109°	7151.5421∠-122.6882°	7466.5546∠121.0368°	2212.0241∠-77.7484°	2254.4046∠-82.8477°	2085.9201∠-78.7815°
9	**4038.6524∠-65.1067°**	**4038.6524∠-65.1067°**	**4038.6524∠-65.1067°**	**2273.3453∠-80.6776°**	**2178.477∠-78.9782°**	**2249.5168∠-80.3575°**
3	3930.666∠-65.7774°	3941.7921∠-65.7971°	3933.0099∠-65.7792°	1664.0436∠-86.6201°	1562.9886∠-84.6279°	1639.0379∠-86.2695°
4	3788.0606∠-66.6472°	3827.5567∠-66.9937°	3808.6482∠-66.9449°	1307.8867∠-86.4854°	1217.9008∠-77.9637°	1264.8901∠-79.9106°
5	3646.2494∠-67.6415°	3732.239∠-68.6527°	3650.6711∠-67.6819°	1070.3975∠-86.1527°	999.2781∠-70.5291°	1103.8038∠-91.5546°
6	3576.5651∠-68.4394°	3660.1976∠-69.2796°	3577.4835∠-68.2769°	822.841∠-78.9421°	793.8333∠-84.1557°	794.7353∠-84.7044°
7	3451.9069∠-68.706°	3606.2813∠-70.4139°	3522.9638∠-69.3574°	658.0814∠-99.2695°	518.5148∠-68.2074°	507.7771∠-68.9892°
8	3440.3139∠-68.7403°	3606.1645∠-70.5953°	3522.9763∠-69.5287°	348.8054∠-90.0774°	360.4938∠-33.0847°	340.6211∠-32.0181°

Analysis of Three-Phase(LLL) Fault

In this case, the system in case 1 is simulated for three phase fault. As explained previously, a fictitious node 9 is created between nodes 2 and 3 respectively. The fault resistance is assumed to be 10 Ω. The final voltages and currents at each node obtained in the final iteration are shown in Table 3.3.

Table 3.3
Node Voltages and Currents for Three Phase Fault for Case 1

Node No.	Voltage			Load Current		
	Phase A	Phase B	Phase C	Phase A	Phase B	Phase C
1	7199.6∠0°	7199.6∠-120°	7199.6∠120°	3129.9477∠-79.1001°	3154.2419∠-82.4079°	3001.9057∠-79.8136°
2	6799.2223∠2.129°	7154.6257∠-123.8533°	7601.7648∠121.5328°	3129.9477∠-79.1001°	3154.2419∠-82.4079°	3001.9057∠-79.8136°
9	**3717.3682∠-68.3212°**	**3717.3682∠-68.3212°**	**3717.3682∠-68.3212°**	**3195.7026∠-81.1814°**	**3081.1428∠-79.6332°**	**3163.8247∠-80.8366°**
3	3593.3051∠-69.1956°	3607.4186∠-69.2023°	3596.6902∠-69.1913°	1862.1973∠-90.7761°	1735.3921∠-88.7022°	1827.585∠-90.3544°
4	3428.2431∠-70.3649°	3477.2765∠-70.7344°	3453.782∠-70.7057°	1472.5883∠-90.8405°	1355.8629∠-82.354°	1415.9566∠-84.3434°
5	3263.5237∠-71.7319°	3369.2864∠-72.8655°	3271.5383∠-71.7372°	1210.0993∠-90.6535°	1113.1466∠-75.1555°	1241.1997∠-95.8706°
6	3182.7306∠-72.824°	3286.9699∠-73.7003°	3187.25∠-72.5567°	932.3377∠-83.6701°	887.2832∠-88.7786°	895.5852∠-89.1905°
7	3036.2125∠-73.2818°	3226.5359∠-75.1893°	3125.6906∠-74.0117°	748.6424∠-103.8515°	579.7232∠-73.0154°	572.4958∠-73.6757°
8	3022.6399∠-73.3382°	3226.7634∠-75.424°	3126.1039∠-74.2376°	397.004∠-94.6754°	402.8805∠-37.9134°	383.8644∠-36.727°

Analysis of Double-Line-to-Ground(LLG) Fault

For double line to ground fault, case 1 is simulated with the assumption of fault resistance to be 20 Ω. The initial voltage at node 9 for phases a and b is enforced as the average of the initial source voltage for the first iteration and due to this the final voltages on phases a and b of node 9 are equal in magnitude and angle which are shown in Table 3.4.

Table 3.4
Node Voltages and Currents for Double Line to Ground Fault for Case 1

Node No.	Voltage			Load Current		
	Phase A	Phase B	Phase C	Phase A	Phase B	Phase C
1	7199.6∠0°	7199.6∠-120°	7199.6∠120°	1557.0985∠-42.0325°	1471.819∠-51.3713°	1088.0561∠94.9351°
2	6898.8347∠-0.03°	7298.6981∠-122.1123°	6952.9456∠118.8542°	1557.0985∠-42.0325°	1471.819∠-51.3713°	1088.0561∠94.9351°
9	**5799.1621∠-32.2103°**	**5799.1621∠-32.2103°**	**6928.2241∠118.7137°**	**1538.7104∠-46.8146°**	**1486.8872∠-45.027°**	**910.5738∠98.3207°**
3	5701.2471∠-32.5975°	5708.6149∠-32.6124°	6832.5754∠118.2271°	1111.9164∠-52.6318°	1055.7285∠-50.416°	910.5738∠98.3207°
4	5574.3058∠-33.1275°	5600.9468∠-33.3126°	6719.7596∠117.4734°	866.4376∠-52.2625°	819.9156∠-43.2732°	696.5065∠105.1545°
5	5444.3095∠-33.652°	5502.5532∠-34.1747°	6590.2762∠116.8344°	705.129∠-51.7584°	672.5497∠-35.4899°	604.0059∠93.2025°
6	5380.1921∠-34.0733°	5435.772∠-34.5261°	6525.6205∠116.4233°	540.0704∠-44.2715°	531.7909∠-49.1216°	433.162∠100.2629°
7	5278.5503∠-34.2935°	5382.6716∠-35.1683°	6466.5322∠115.8366°	429.971∠-64.8657°	347.2345∠-32.9162°	276.4948∠116.2559°
8	5269.7571∠-34.3287°	5381.8728∠-35.2742°	6465.3272∠115.7525°	227.7145∠-55.6658°	241.5516∠2.2364°	185.6055∠153.2632°

Analysis of Double-Line(LL) Fault

For double line fault, case 1 is simulated with the assumption of fault resistance to be 10 Ω. The initial voltage at node 9 for phases a and b is enforced as the average of the initial source voltage for the first iteration and due to this the final voltages on phases a and b of node 9 are equal in magnitude and angle. The final voltages and currents at each nodes are depicted in Table 3.5.

Table 3.5
Node Voltages and Currents for Double Line Fault for Case 1

Node No.	Voltage			Load Current		
	Phase A	Phase B	Phase C	Phase A	Phase B	Phase C
1	7199.6∠0°	7199.6∠-120°	7199.6∠120°	2036.8582∠-40.8321°	1939.2596∠-47.7831°	1089.8863∠94.7378°
2	6814.9379∠-0.1312°	7353.9002∠-122.6124°	6944.4179∠118.6799°	2036.8582∠-40.8321°	1939.2596∠-47.7831°	1089.8863∠94.7378°
9	**5691.6413∠-33.1389°**	**5691.6413∠-33.1389°**	**6918.7324∠118.5174°**	**2014.0312∠-44.5124°**	**1963.5016∠-43.0437°**	**912.1595∠98.1171°**
3	5592.3407∠-33.5401°	5599.8358∠-33.5556°	6822.5126∠118.0291°	1135.4047∠-53.6145°	1077.7161∠-51.4024°	912.1595∠98.1171°
4	5463.6147∠-34.0893°	5490.7054∠-34.2811°	6708.9765∠117.2723°	885.1403∠-53.2573°	837.2101∠-44.2842°	697.7642∠104.947°
5	5331.7642∠-34.6341°	5390.9906∠-35.1758°	6578.7651∠116.6299°	720.5592∠-52.7615°	686.7939∠-36.5191°	605.1282∠92.9968°
6	5266.7484∠-35.0717°	5323.3151∠-35.5409°	6513.7008∠116.2168°	551.9775∠-45.2882°	543.1926∠-50.1492°	433.9834∠100.0557°
7	5163.6764∠-35.3005°	5269.5747∠-36.2073°	6454.142∠115.6276°	439.551∠-65.873°	354.6968∠-33.9573°	277.0272∠116.0468°
8	5154.7649∠-35.3369°	5268.785∠-36.3171°	6452.9057∠115.5431°	232.7943∠-56.6741°	246.7362∠1.1935°	185.9627∠153.0537°

Analysis of Single-Line-to-Ground(SLG) Fault

In this case, the system in case 1 is simulated for single line to ground phase fault. As explained previously, a fictitious node 9 is created between nodes 2 and 3 respectively. The fault resistance is assumed to be 20 Ω. For the first iteration, voltages at node 9 is not enforced as carried out for the previous cases. The final voltages and currents at each node obtained in the final iteration are depicted in Table 3.6.

Table 3.6
Node Voltages and Currents for Single Line to Ground Fault for Case 1

Node No.	Voltage			Load Current		
	Phase A	Phase B	Phase C	Phase A	Phase B	Phase C
1	7199.6∠0°	7199.6∠-120°	7199.6∠120°	1359.3705∠-11.6171°	1042.5868∠-139.4505°	1082.237∠95.6837°
2	6946.1296∠-1.338°	6972.9605∠-120.851°	6973.3571∠119.2006°	1359.3705∠-11.6171°	1042.5868∠-139.4505°	1082.237∠95.6837°
9	**6916.7573∠-1.4784°**	**6950.3613∠-120.9373°**	**6951.0053∠119.1036°**	**1275.9335∠-15.9306°**	**870.7287∠-138.9097°**	**905.734∠99.1568°**
3	6825.6536∠-1.8302°	6864.4337∠-121.2983°	6860.6611∠118.7453°	917.8272∠-21.7792°	870.7287∠-138.9097°	905.734∠99.1568°
4	6709.6515∠-2.3179°	6762.9053∠-121.8787°	6751.861∠118.1591°	712.7962∠-21.3797°	675.0468∠-131.6366°	693.1542∠106.0963°
5	6595.6744∠-2.8104°	6666.6979∠-122.6019°	6623.3479∠117.6893°	578.7913∠-20.8526°	553.364∠-123.7549°	600.4533∠94.1765°
6	6535.6979∠-3.1673°	6603.9755∠-122.9197°	6561.6245∠117.3898°	442.6592∠-13.2918°	436.864∠-137.4032°	430.6207∠101.2914°
7	6446.8063∠-3.4082°	6551.2524∠-123.3696°	6503.0153∠116.8995°	351.9481∠-33.9834°	285.2281∠-121.0969°	274.9481∠117.3253°
8	6439.7777∠-3.4437°	6550.1819∠-123.44°	6501.0192∠116.8223°	186.3418∠-24.7809°	198.4678∠-85.9294°	184.5864∠154.3329°

Analysis of Exact Fault Location

For the analysis purpose,first, a bisection search algorithm has been employed. Second, an incremental adjustment to match the simulated current of fault with the measurements is conducted. Finally, the sensitivity analysis of a search can be improved with the proposed algorithm that leads to matching of telemetered and calculated values as depicted in Table 3.7.

Table 3.7
Determination of Exact Location of Fault for Case 1

Fault No.	Fault Type	Reference Current Value	Actual Value of Current	Actual Distance of Fault
1	LLLG	2212.0241∠-77.7484°	2212.7215∠-77.7581°	0.2031
		2254.4046∠-82.8477°	2255.1171∠-82.8548°	
		2085.9201∠-78.7815°	2086.62∠-78.7911°	
2	LLL	3129.9477∠-79.1001°	3129.4373∠-79.0945°	0.1992
		3154.2419∠-82.4079°	3153.7344∠-82.4033°	
		3001.9057∠-79.8136°	3001.3971∠-79.8081°	
3	LLG	1557.0985∠-42.0325°	1556.5689∠-42.0204°	0.1875
		1471.819∠-51.3713°	1471.2342∠-51.363°	
		1088.0561∠94.9351°	1088.0408∠94.9363°	
4	LL	2036.8582∠-40.8321°	2037.1314∠-40.8371°	0.2031
		1939.2596∠-47.7831°	1939.5538∠-47.7871°	
		1089.8863∠94.7378°	1089.8939∠94.7372°	
5	LG	1359.3705∠-11.6171°	1360.0281∠-11.6349°	0.2500
		1042.5868∠-139.4505°	1042.626∠-139.4499°	
		1082.237∠95.6837°	1082.2328∠95.6818°	

3.5.2 Case 2: Equal Distance Branchout Test Feeder

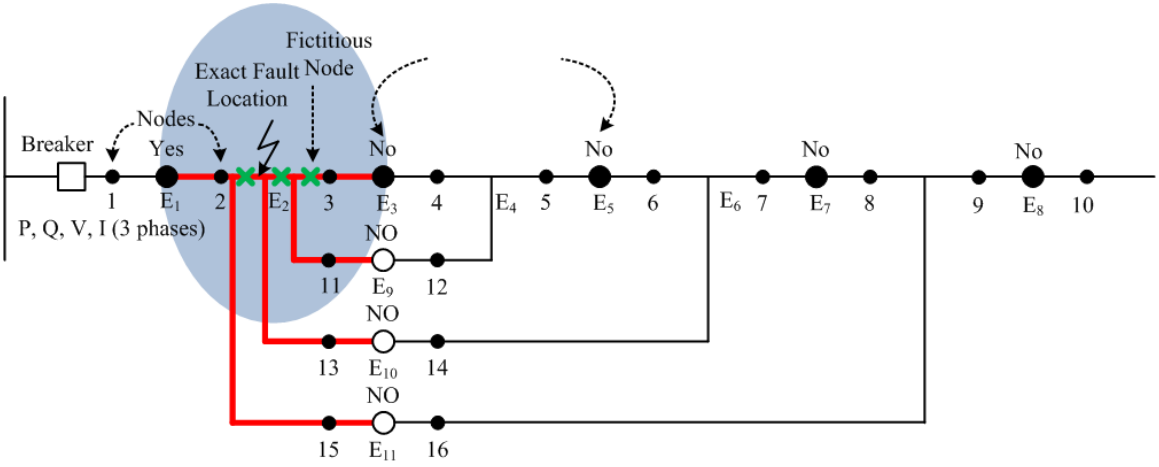

Figure 3.5: A case for determination of exact fault location

This topology consists of 18 nodes and 17 switches where the switches and the respective lines are connected topologically. Breakers and recloser are equipped with

the relay. Under normal operating condition, the breaker is used to energized the feeder. The source is considered at node 1 and three phase loads are connected to all remaining 17 nodes. Using the matrix-based Backward-Forward Sweep method the voltages and the load currents at each nodes are calculated which are depicted in the Table 3.8.

Table 3.8
Node Voltages and Currents in Healthy Condition for Case 2

Node No.	Voltage			Load Current		
	Phase A	Phase B	Phase C	Phase A	Phase B	Phase C
1	7199.6∠0°	7199.6∠-120°	7199.6∠120°	911.8118∠1.5616°	1358.2997∠-136.432°	1362.0796∠112.026°
2	7040.7921∠-1.2724°	6939.0028∠-121.3317°	6956.8943∠118.5857°	911.8118∠1.5616°	1358.2997∠-136.432°	1362.0796∠112.026°
3	6950.9448∠-1.9317°	6806.9155∠-122.0773°	6836.9587∠117.7038°	809.962∠-3.5899°	1186.5365∠-135.5247°	1211.8273∠116.9821°
4	6903.7519∠-2.0414°	6776.3444∠-122.3257°	6798.2345∠117.4313°	271.9325∠-33.5648°	241.423∠-121.8001°	263.5704∠113.6716°
5	6874.6504∠-2.0505°	6767.953∠-122.6138°	6756.6674∠117.3675°	145.4619∠-42.6842°	162.5307∠-85.1032°	177.6023∠76.7338°
6	6923.3826∠-2.4372°	6729.7199∠-122.6294°	6778.3362∠117.0246°	435.3443∠24.3067°	757.2321∠-132.2389°	786.7703∠129.1156°
7	6867.1764∠-2.5812°	6695.1901∠-122.9191°	6740.5124∠116.7194°	331.118∠-33.2027°	279.7207∠-120.7848°	265.9512∠117.0196°
8	6833.805∠-2.7401°	6689.8568∠-123.2583°	6730.8002∠116.359°	175.5976∠-24.0773°	194.324∠-85.7477°	178.2849∠153.8696°
9	6943.4882∠-2.6743°	6704.1044∠-122.9307°	6770.1666∠116.5742°	269.4188∠92.199°	332.2714∠-125.9574°	463.2881∠154.226°
10	6947.1364∠-2.7339°	6620.0483∠-122.6914°	6780.2036∠116.7102°	42.6634∠137.576°	363.7336∠174.4085°	51.519∠-88.1083°
11	6944.2566∠-3.0072°	6579.8835∠-122.5782°	6795.2357∠117.02°	172.8047∠34.5034°	197.5719∠174.4601°	206.0267∠-38.5741°
12	6935.3191∠-2.7828°	6720.6075∠-123.157°	6733.4062∠116.1069°	122.0206∠28.4515°	197.8851∠-39.5396°	516.6267∠125.3524°
13	6892.7446∠-2.9927°	6744.2555∠-123.2062°	6713.3183∠115.4213°	279.4622∠-11.5562°	143.0736∠9.0037°	491.9457∠143.7853°
14	6865.5349∠-3.4497°	6742.0321∠-123.3367°	6694.105∠114.8557°	290.4894∠20.8909°	41.2455∠-80.0934°	331.2015∠139.2747°
15	6862.7586∠-4.2789°	6710.1915∠-123.5852°	6705.3176∠114.0044°	387.9064∠45.8579°	163.9864∠-140.925°	428.412∠162.3397°
16	6850.0705∠-4.6724°	6671.5053∠-123.5431°	6699.9543∠113.6459°	206.6738∠34.6871°	192.3535∠175.7608°	218.1805∠147.9734°
17	6839.1158∠-4.7106°	6661.6779∠-123.6084°	6686.6857∠113.5821°	81.0628∠-26.8165°	84.2453∠-130.8466°	104.5949∠97.5551°
18	6822.4325∠-4.6102°	6672.3292∠-123.7831°	6690.5279∠113.3317°	153.9041∠-90.7542°	157.3663∠-61.4436°	186.8313∠175.6712°

Analysis of Three-Phase-to-Ground(LLLG) Fault

The system explained in case 2 is simulated for three phase to ground fault in which a fictitious node (node 19) is created between nodes 2 and 3 which is assumed to be at a distance of 20% from node 2 and 80% from node 3 of the total distance between these nodes. The fault resistance of 20 Ω is presumed. The initial voltage at node

19 is enforced as the average of the initial source voltage for the first iteration and due to this the final voltages on each phase of node 19 are equal in magnitude and angle which are shown in Table 3.9. The backward-forward sweep method continues until the mismatch occurs between the new and the previous iterations in the load voltages is within the specified tolerance. The final iteration results of voltages and load currents at each nodes are depicted in Table 3.9.

Table 3.9
Node Voltages and Currents for Three Phase to Ground Fault for Case 2

Node No.	Voltage			Load Current		
	Phase A	Phase B	Phase C	Phase A	Phase B	Phase C
1	7199.6∠0°	7199.6∠-120°	7199.6∠120°	2098.2909∠-67.0458°	2914.0567∠-82.5895°	2766.6691∠-69.8671°
2	6921.077∠0.7003°	7130.0236∠-123.7658°	7548.2838∠122.0588°	2098.2909∠-67.0458°	2914.0567∠-82.5895°	2766.6691∠-69.8671°
19	**3963.6942∠-67.32°**	**3963.6942∠-67.32°**	**3963.6942∠-67.32°**	**2136.1966∠-70.4126°**	**2840.3054∠-79.5763°**	**2918.8966∠-71.4912°**
3	3898.2278∠-68.2806°	3812.4111∠-68.4987°	3835.4104∠-69.1006°	1483.6332∠-71.7752°	2205.6477∠-83.1848°	2267.1924∠-72.6933°
4	3833.7474∠-68.3903°	3779.4888∠-69.1302°	3792.9595∠-69.7398°	491.6668∠-99.9225°	433.8828∠-68.9865°	475.0591∠-73.662°
5	3789.2015∠-68.3476°	3786.4517∠-69.9958°	3735.3869∠-69.7114°	263.9078∠-108.9813°	290.5095∠-32.4852°	321.2519∠-110.3451°
6	3894.0214∠-69.1701°	3686.712∠-69.5731°	3751.4956∠-70.9413°	786.4897∠-46.0015°	1432.7378∠-80.5552°	1482.0819∠-62.6162°
7	3813.7075∠-69.3415°	3648.2414∠-70.3779°	3714.7436∠-71.6336°	599.3846∠-99.9133°	515.325∠-68.6044°	483.7239∠-71.6103°
8	3757.1846∠-69.4981°	3647.6322∠-71.3266°	3714.8802∠-72.4472°	319.3881∠-90.8353°	356.3956∠-33.816°	323.0252∠-34.9366°
9	3945.2061∠-69.4373°	3625.2211∠-70.1094°	3732.0437∠-72.3323°	444.123∠22.9164°	647.993∠-75.7466°	855.1546∠-40.8664°
10	3979.6668∠-69.506°	3458.5453∠-69.3495°	3769.6933∠-72.2894°	71.2036∠71.4273°	701.3337∠-132.1393°	87.8693∠83.7339°
11	3977.9489∠-70.4187°	3391.7455∠-69.0351°	3799.6611∠-71.2811°	301.663∠-32.9081°	383.2835∠-131.9967°	368.4539∠133.1248°
12	3942.1755∠-69.5851°	3662.3084∠-70.4326°	3656.7878∠-73.6806°	220.571∠-46.6659°	358.1988∠11.3248°	988.804∠-67.7266°
13	3879.283∠-70.0185°	3715.3839∠-70.1328°	3615.2574∠-75.7007°	515.3763∠-80.8192°	250.4747∠60.8458°	924.2377∠-50.0478°
14	3847.6953∠-71.1941°	3725.2219∠-69.9994°	3573.531∠-77.277°	521.5975∠-49.0874°	80.6523∠-33.697°	629.5765∠-55.7471°
15	3868.8715∠-73.124°	3664.9349∠-69.8836°	3588.1647∠-79.7769°	686.4553∠-23.5264°	307.9372∠-87.592°	798.4359∠-32.1237°
16	3873.1927∠-74.1049°	3599.5992∠-69.3106°	3583.2474∠-80.9372°	366.2907∠-35.1996°	359.1549∠-129.9265°	408.0568∠-47.1777°
17	3860.422∠-74.1751°	3588.5885∠-69.4835°	3564.864∠-81.0972°	146.2828∠-96.5305°	158.1331∠-77.2751°	198.758∠-97.7526°
18	3826.3948∠-73.6322°	3604.3268∠-70.0837°	3583.2162∠-81.832°	274.4097∠-159.7762°	291.3165∠-7.7442°	348.8486∠-19.4925°

Analysis of Three-Phase(LLL) Fault

In this case, the system in case 2 is simulated for three phase fault. As explained previously, a fictitious node 19 is created between nodes 2 and 3 respectively. The fault resistance is assumed to be 10 Ω. The final voltages and currents at each node

obtained in the final iteration are shown in Table 3.10.

Table 3.10
Node Voltages and Currents for Three Phase Fault for Case 2

Node No.	Voltage			Load Current		
	Phase A	Phase B	Phase C	Phase A	Phase B	Phase C
1	7199.6∠0°	7199.6∠-120°	7199.6∠120°	2971.6466∠-70.7037°	3858.9515∠-83.0568°	3728.9854∠-73.4484°
2	6811.9666∠1.2484°	7125.8911∠-124.8619°	7679.199∠122.4831°	2971.6466∠-70.7037°	3858.9515∠-83.0568°	3728.9854∠-73.4484°
19	**3679.9684∠-70.3509°**	**3679.9684∠-70.3509°**	**3679.9684∠-70.3509°**	**3018.24∠-73.0692°**	**3785.8544∠-80.7825°**	**3883.4272∠-74.4923°**
3	3610.6259∠-71.4647°	3518.3533∠-71.7418°	3542.8098∠-72.4206°	1612.5018∠-75.4436°	2413.9428∠-86.8478°	2480.4847∠-76.8428°
4	3541.9829∠-71.6053°	3483.728∠-72.4801°	3498.0535∠-73.1695°	532.6805∠-103.1483°	471.0223∠-72.4209°	515.7592∠-77.1543°
5	3494.43∠-71.5663°	3492.0165∠-73.4802°	3436.4943∠-73.1517°	286.1697∠-112.2°	315.0042∠-35.9696°	349.1931∠-113.7853°
6	3606.537∠-72.4862°	3384.0193∠-73.0251°	3453.3025∠-74.5681°	852.1441∠-50.206°	1574.4575∠-84.4316°	1622.8989∠-67.2801°
7	3521.0627∠-72.7027°	3343.516∠-73.9761°	3414.7174∠-75.3823°	650.024∠-103.2836°	562.8214∠-72.3001°	526.6269∠-75.4359°
8	3460.9096∠-72.8976°	3343.9055∠-75.0852°	3415.8092∠-76.3274°	346.7297∠-94.2348°	388.767∠-37.5746°	351.3077∠-38.8168°
9	3660.9532∠-72.7793°	3318.189∠-73.6731°	3432.7759∠-76.1858°	470.3239∠18.9485°	716.8452∠-80.042°	930.2301∠-46.3287°
10	3697.8408∠-72.8508°	3137.7068∠-72.8305°	3473.0018∠-76.1233°	75.9239∠68.2726°	774.6727∠-135.5996°	94.2523∠80.1967°
11	3697.022∠-73.8955°	3065.3017∠-72.4787°	3503.7637∠-74.9469°	324.5856∠-36.3849°	424.1018∠-135.4404°	399.5703∠129.459°
12	3657.5327∠-72.9482°	3358.2753∠-74.0423°	3352.904∠-77.78°	239.6107∠-52.1008°	388.6165∠7.298°	1086.2981∠-72.749°
13	3590.6334∠-73.4592°	3414.7518∠-73.6799°	3310.3551∠-80.1548°	561.8036∠-84.815°	269.6867∠57.1725°	1010.2386∠-55.2261°
14	3557.8554∠-74.8195°	3425.160∠-73.5258°	3267.2707∠-82.0182°	564.9388∠-53.2628°	88.6137∠-39.0446°	689.7365∠-61.2501°
15	3582.6203∠-77.0316°	3360.7093∠-73.4114°	3286.9105∠-84.9367°	740.7985∠-27.5576°	337.6923∠-91.2833°	870.6422∠-37.4464°
16	3588.6007∠-78.1565°	3290.1396∠-72.7628°	3283.8295∠-86.2936°	395.3884∠-39.3489°	393.7043∠-133.3739°	445.1648∠-52.6779°
17	3575.0958∠-78.2413°	3278.4782∠-72.9706°	3264.373∠-86.4906°	158.4987∠-100.6835°	173.4999∠-80.9224°	217.6822∠-103.3161°
18	3538.1116∠-77.626°	3296.0767∠-73.6701°	3285.525∠-87.3377°	296.7685∠-163.77°	318.5605∠-11.3306°	380.4566∠-24.9982°

Analysis of Double-Line-to-Ground(LLG) Fault

In this case, the system in case 2 is simulated for three phase fault. As explained previously, a fictitious node 19 is created between nodes 2 and 3 respectively. The fault resistance is assumed to be 20 Ω. The final voltages and currents at each node obtained in the final iteration are shown in Table 3.11.

Table 3.11
Node Voltages and Currents for Double Line to Ground Fault for Case 2

Node No.	Voltage			Load Current		
	Phase A	Phase B	Phase C	Phase A	Phase B	Phase C
1	7199.6∠0°	7199.6∠-120°	7199.6∠120°	1477.1091∠-30.0334°	1844.8407∠-48.8391°	1367.072∠111.1003°
2	6923.7542∠-0.5559°	7350.386∠-122.6898°	6943.532∠118.0459°	1477.1091∠-30.0334°	1844.8407∠-48.8391°	1367.072∠111.1003°
19	**5819.4618∠-32.9425°**	**5819.4618∠-32.9425°**	**6918.0491∠117.8043°**	**1431.3032∠-34.8283°**	**1866.6946∠-43.8424°**	**1215.7322∠116.0005°**
3	5749.1023∠-33.535°	5694.5278∠-33.6146°	6820.0702∠116.9056°	986.4794∠-35.6885°	1432.0604∠-47.2186°	1215.7322∠116.0005°
4	5695.6245∠-33.6299°	5662.6056∠-33.9473°	6781.2482∠116.5826°	329.9996∠-65.129°	288.9768∠-33.4664°	264.124∠112.8261°
5	5656.4103∠-33.5905°	5657.6699∠-34.322°	6743.1023∠116.501°	176.7338∠-74.2125°	194.3941∠3.1992°	177.9573∠75.8687°
6	5728.5422∠-34.1148°	5595.1978∠-34.2409°	6762.7301∠116.0609°	527.9611∠-8.3885°	918.1606∠-44.0377°	788.9388∠128.0403°
7	5664.6071∠-34.2429°	5560.3314∠-34.6448°	6724.8273∠115.6974°	401.8085∠-64.8375°	337.1219∠-32.5914°	266.539∠115.9701°
8	5622.9454∠-34.3967°	5556.0783∠-35.1438°	6719.0374∠115.3081°	213.3421∠-55.7217°	233.9381∠2.3776°	178.5945∠152.8202°
9	5758.582∠-34.3809°	5550.6674∠-34.6001°	6758.1887∠115.5311°	318.2958∠59.8544°	405.8867∠-37.9588°	464.2833∠153.1091°
10	5784.8715∠-34.4106°	5448.4357∠-34.2612°	6758.7012∠115.5529°	50.9914∠106.2136°	442.0274∠-97.0945°	51.9509∠-89.2789°
11	5788.3362∠-34.7625°	5411.8432∠-34.0443°	6768.3056∠115.8037°	207.2494∠2.7604°	240.171∠-96.9955°	206.8437∠-39.7889°
12	5744.6257∠-34.5537°	5562.2496∠-34.8462°	6724.9233∠115.0685°	147.7531∠-5.9196°	238.4791∠48.2679°	518.2079∠124.2297°
13	5691.9974∠-34.9194°	5587.0705∠-34.8863°	6703.0676∠114.4108°	341.9022∠-44.1434°	170.8518∠96.9973°	493.2032∠142.6285°
14	5660.9532∠-35.5985°	5583.4546∠-34.9575°	6681.9463∠113.8153°	352.556∠-11.8854°	50.7895∠6.1561°	332.3144∠138.054°
15	5668.9742∠-36.7491°	5536.8357∠-35.1474°	6691.7579∠112.851°	468.962∠13.2678°	200.1041∠-52.5602°	429.2462∠161.1445°
16	5665.9583∠-37.3117°	5488.3444∠-34.9924°	6680.6464∠112.4163°	249.8568∠1.9634°	234.2972∠-95.6079°	218.6732∠146.7372°
17	5653.8473∠-37.3513°	5477.5856∠-35.0705°	6667.3141∠112.3361°	98.382∠-59.5252°	102.927∠-42.4213°	104.8342∠96.2594°
18	5631.4816∠-37.1713°	5487.3543∠-35.4054°	6674.8761∠112.0987°	186.392∠-123.3017°	191.3161∠26.9449°	187.2668∠174.4398°

Analysis of Double-Line(LL) Fault

For double line fault, case 2 is simulated with the assumption of fault resistance to be 10 Ω. The initial voltage at node 19 for phases a and b is enforced as the average of the initial source voltage for the first iteration and due to this the final voltages on phases a and b of node 19 are equal in magnitude and angle. The final voltages and currents at each nodes are depicted in Table 3.12.

Table 3.12
Node Voltages and Currents for Double Line Fault for Case 2

Node No.	Voltage			Load Current		
	Phase A	Phase B	Phase C	Phase A	Phase B	Phase C
1	7199.6∠0°	7199.6∠-120°	7199.6∠120°	1957.9534∠-31.7003°	2324.1733∠-46.6496°	1369.3736∠110.8969°
2	6839.8835∠-0.6669°	7404.6313∠-123.1978°	6934.731∠117.8704°	1957.9534∠-31.7003°	2324.1733∠-46.6496°	1369.3736∠110.8969°
19	**5715.5853∠-33.8495°**	**5715.5853∠-33.8495°**	**6909.9416∠117.6231°**	**1913.746∠-35.3693°**	**2351.8959∠-42.7359°**	**1217.781∠115.7915°**
3	5643.3099∠-34.4718°	5587.0375∠-34.5552°	6809.8398∠116.7072°	1006.7445∠-36.7146°	1461.8331∠-48.2224°	1217.781∠115.7915°
4	5589.1518∠-34.5703°	5554.7351∠-34.8997°	6770.7809∠116.3829°	336.5954∠-66.1006°	294.7643∠-34.4535°	264.5454∠112.6211°
5	5549.4059∠-34.5304°	5549.7603∠-35.2879°	6732.4933∠116.3005°	180.2862∠-75.1826°	198.2702∠2.2051°	178.2448∠75.6639°
6	5622.6467∠-35.0708°	5486.4378∠-35.2028°	6752.139∠115.8589°	538.6225∠-9.4872°	937.6389∠-45.0615°	790.287∠127.8265°
7	5557.897∠-35.2037°	5451.149∠-35.6212°	6713.9603∠115.494°	409.9064∠-65.8311°	344.0899∠-33.6059°	266.9882∠115.7619°
8	5515.7312∠-35.3626°	5446.9212∠-36.1372°	6708.0333∠115.1029°	217.6652∠-56.7191°	238.7455∠1.3553°	178.895∠152.6105°
9	5653.2195∠-35.3449°	5441.37∠-35.574°	6747.5453∠115.3271°	323.8377∠58.7758°	414.7602∠-39.018°	465.0468∠152.8894°
10	5679.8627∠-35.3753°	5337.6252∠-35.2223°	6747.8674∠115.3501°	51.9321∠105.2309°	451.5024∠-98.0792°	52.0374∠-89.4822°
11	5683.3158∠-35.7386°	5300.4081∠-34.9973°	6757.3505∠115.6013°	211.242∠1.7525°	245.3488∠-97.9764°	207.1874∠-39.9957°
12	5639.1862∠-35.5235°	5453.2496∠-35.8291°	6714.2734∠114.8627°	150.7829∠-7.1918°	243.2394∠47.2151°	519.1058∠124.0134°
13	5585.9883∠-35.9011°	5478.5931∠-35.8705°	6692.3672∠114.2031°	349.1243∠-45.2216°	174.1377∠95.9794°	494.0405∠142.4102°
14	5554.672∠-36.6024°	5475.066∠-35.9442°	6671.1476∠113.6051°	359.7086∠-12.9909°	51.8391∠4.941°	332.892∠137.8332°
15	5563.1009∠-37.7898°	5427.996∠-36.1401°	6680.8467∠112.6366°	478.242∠12.178°	204.3301∠-53.5975°	429.9689∠160.924°
16	5560.2153∠-38.3707°	5378.9081∠-35.9796°	6669.6056∠112.2005°	254.8138∠0.8604°	239.235∠-96.621°	219.0457∠146.5159°
17	5547.9711∠-38.4118°	5368.0118∠-36.0606°	6656.2129∠112.1199°	100.3687∠-60.6285°	105.1133∠-43.4551°	105.0154∠96.0383°
18	5525.3405∠-38.2259°	5377.9741∠-36.4069°	6663.7618∠111.882°	190.1249∠-124.3914°	195.3059∠25.9144°	187.587∠174.2183°

Analysis of Single-Line-to-Ground(SLG) Fault

In this case, the system in case 2 is simulated for single line to ground phase fault. As explained previously, a fictitious node 19 is created between nodes 2 and 3 respectively. The fault resistance is assumed to be 20 Ω. For the first iteration, voltages at node 19 is not enforced as carried out for the previous cases. The final voltages and currents at each node obtained in the final iteration are depicted in Table 3.13.

Table 3.13
Node Voltages and Currents for Single Line to Ground Fault for Case 2

Node No.	Voltage			Load Current		
	Phase A	Phase B	Phase C	Phase A	Phase B	Phase C
1	7199.6∠0°	7199.6∠-120°	7199.6∠120°	1292.4403∠0.1929°	1360.4945∠-136.4116°	1361.6548∠111.9451°
2	6983.9898∠-1.7118°	6929.6138∠-121.3114°	6958.8868∠118.5134°	1292.4403∠0.1929°	1360.4945∠-136.4116°	1361.6548∠111.9451°
19	**6959.323∠-1.8978°**	**6901.9788∠-121.4559°**	**6935.0383∠118.3306°**	**1190.0343∠-3.4218°**	**1188.4985∠-135.5046°**	**1211.4281∠116.9003°**
3	6887.1245∠-2.436°	6796.1764∠-122.0554°	6839.1774∠117.6223°	817.776∠-4.1158°	1188.4985∠-135.5046°	1211.4281∠116.9003°
4	6839.6063∠-2.5476°	6765.5599∠-122.304°	6800.4084∠117.3496°	274.4937∠-34.0715°	241.8089∠-121.7785°	263.4861∠113.5898°
5	6810.26∠-2.5569°	6757.1649∠-122.5925°	6758.8178∠117.2856°	146.8373∠-43.1906°	162.7902∠-85.0819°	177.5458∠76.652°
6	6859.5118∠-2.9502°	6718.7816∠-122.6086°	6780.5561∠116.9429°	439.4947∠23.7535°	758.5089∠-132.2201°	786.5076∠129.0339°
7	6802.9174∠-3.0967°	6684.2014∠-122.8985°	6742.6751∠116.6375°	334.2608∠-33.7191°	280.1825∠-120.7644°	265.8668∠116.9377°
8	6769.3227∠-3.2581°	6678.8477∠-123.2383°	6732.9263∠116.2771°	177.2703∠-24.5953°	194.6444∠-85.7277°	178.2286∠153.7877°
9	6879.8813∠-3.1911°	6693.0675∠-122.911°	6772.4226∠116.4927°	271.7291∠91.6504°	332.8466∠-125.9417°	463.1303∠154.1449°
10	6883.6756∠-3.2518°	6608.8854∠-122.671°	6782.4448∠116.6287°	43.0429∠137.0609°	364.3526∠174.4291°	51.5038∠-88.1907°
11	6880.7823∠-3.5297°	6568.6371∠-122.5573°	6797.4679∠116.9381°	174.3988∠33.9809°	197.9102∠174.4811°	205.959∠-38.656°
12	6871.6716∠-3.3018°	6709.5598∠-123.1378°	6735.6852∠116.0255°	123.2003∠27.8351°	198.2025∠-39.5236°	516.451∠125.2708°
13	6828.8051∠-3.5157°	6733.2062∠-123.1866°	6715.5809∠115.3401°	282.2232∠-12.1013°	143.2951∠9.0225°	491.7779∠143.7037°
14	6801.4457∠-3.981°	6730.9042∠-123.3169°	6696.3752∠114.7743°	293.2727∠20.3349°	41.3151∠-80.0923°	331.0881∠139.193°
15	6798.8418∠-4.8245°	6698.871∠-123.5659°	6707.6231∠113.9228°	391.5497∠45.3069°	164.27∠-140.9071°	428.2649∠162.2581°
16	6786.1788∠-5.2252°	6660.0652∠-123.5233°	6702.2667∠113.5641°	208.6204∠34.1315°	192.686∠175.7806°	218.1055∠147.892°
17	6775.1557∠-5.2641°	6650.2217∠-123.5887°	6688.9911∠113.5003°	81.8355∠-27.3723°	84.3913∠-130.828°	104.5582∠97.4739°
18	6758.3626∠-5.1618°	6660.9092∠-123.7639°	6692.8035∠113.2502°	155.3631∠-91.3058°	157.6361∠-61.4244°	186.7678∠175.5897°

Analysis of Exact Fault Location

For the analysis purpose,first, a bisection search algorithm has been employed. Second, an incremental adjustment to match the simulated current of fault with the measurements is conducted. Finally, the sensitivity analysis of a search can be improved with the proposed algorithm that leads to matching of telemetered and calculated values as depicted in Table 3.14.

Table 3.14
Determination of Exact Location of Fault for Case 2

Fault No.	Fault Type	Reference Current Value	Actual Value of Current	Actual Distance of Fault
1	LLLG	2098.2909∠-67.0458°	2099.1424∠-67.0625°	0.2031
		2914.0567∠-82.5895°	2915.1028∠-82.6017°	
		2766.6691∠-69.8671°	2767.7534∠-69.882°	
2	LLL	2971.6466∠-70.7037°	2971.1454∠-70.6969°	0.1992
		3858.9515∠-83.0568°	3858.327∠-83.0511°	
		3728.9854∠-73.4484°	3728.3514∠-73.4416°	
3	LLG	1477.1091∠-30.0334°	1477.1091∠-30.0334°	0.1875
		1844.8407∠-48.8391°	1844.8407∠-48.8391°	
		1367.072∠111.1003°	1367.072∠111.1003°	
4	LL	1957.9534∠-31.7003°	1956.9154∠-31.6755°	0.1875
		2324.1733∠-46.6496°	2323.0287∠-46.6309°	
		1369.3736∠110.8969°	1369.3333∠110.8994°	
5	LG	1292.4403∠0.1929°	1292.9756∠0.1693°	0.2500
		1360.4945∠-136.4116°	1360.5481∠-136.411°	
		1361.6548∠111.9451°	1361.6497∠111.943°	

3.5.3 Case 3: Distance Branching from a Common Node

This topology consists of 12 nodes and 11 switches where the switches and the respective lines are connected topologically. Breakers and recloser are equipped with the relay. Under normal operating condition, the breaker is used to energized the feeder. The source is considered at node 1 and three phase loads are connected to all remaining 11 nodes. Using the matrix-based Backward-Forward Sweep method the voltages and the load currents at each nodes are calculated which are depicted in the Table 3.15.

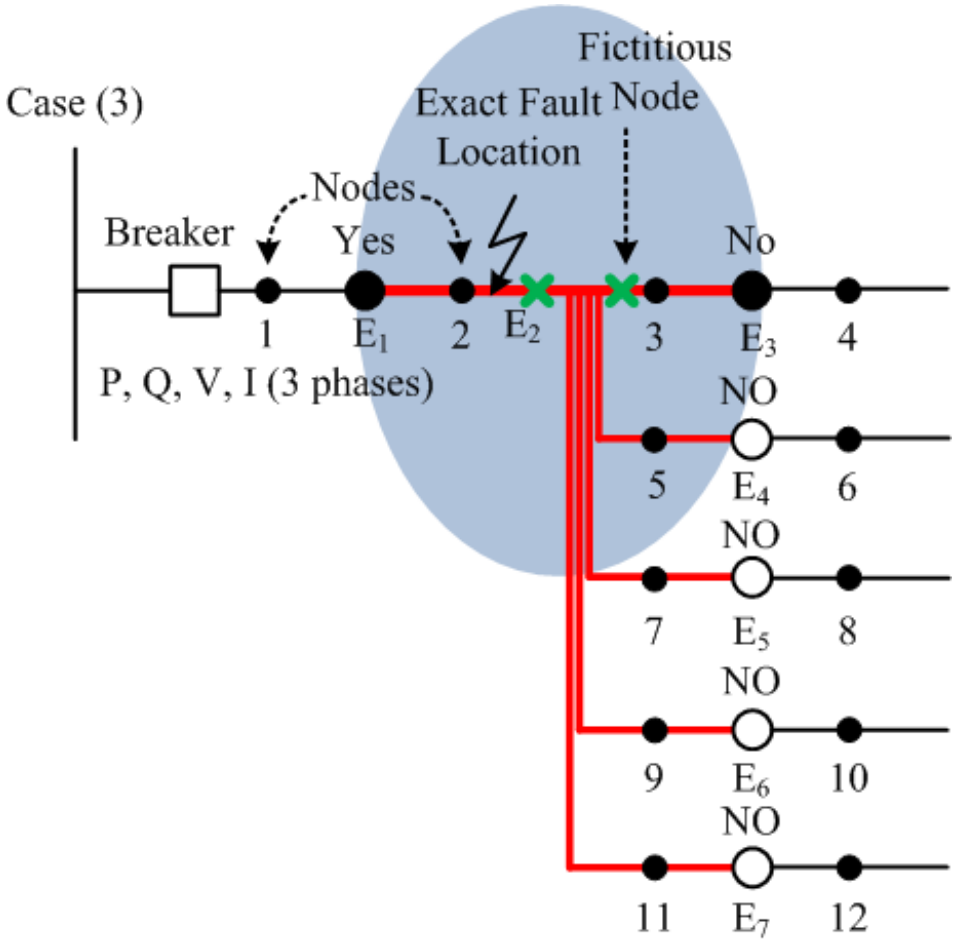

Figure 3.6: A case for determination of exact fault location

Table 3.15
Node Voltages and Currents in Healthy Condition for Case 3

Node No.	Voltage			Load Current		
	Phase A	Phase B	Phase C	Phase A	Phase B	Phase C
1	7199.6∠0°	7199.6∠-120°	7199.6∠120°	633.5431∠7.2918°	1475.877∠-139.0941°	973.7994∠98.0213°
2	7098.9977∠-1.0105°	6910.1189∠-121.2795°	6991.1989∠119.4067°	633.5431∠7.2918°	1475.877∠-139.0941°	973.7994∠98.0213°
3	7043.4895∠-1.5014°	6760.5975∠-121.9965°	6890.031∠119.0459°	526.5315∠0.5441°	1302.5904∠-138.6248°	800.5964∠102.4127°
4	7019.9035∠-1.602°	6736.7568∠-122.0156°	6884.6241∠118.8282°	128.2069∠-22.9391°	148.4394∠-162.6493°	159.7763∠156.3388°
5	7005.9582∠-1.7751°	6710.0728∠-122.3587°	6812.8851∠118.9724°	233.3093∠-1.2052°	266.8275∠-126.0746°	352.9395∠78.3344°
6	6999.6552∠-1.9666°	6679.7113∠-122.4099°	6787.2282∠118.9637°	157.1506∠35.544°	179.6485∠-163.0436°	176.8027∠78.33°
7	6960.0345∠-1.7134°	6708.9879∠-122.4289°	6833.5825∠118.6017°	326.5708∠-32.327°	279.0471∠-120.2732°	262.2092∠118.9251°
8	6931.0434∠-1.8508°	6704.3567∠-122.7262°	6824.9822∠118.2925°	173.1341∠-23.188°	193.9038∠-85.2156°	175.8246∠155.8032°
9	7077.3232∠-1.4373°	6744.2634∠-122.1633°	6911.0319∠118.8284°	277.6476∠157.8242°	218.8211∠-131.9657°	287.5906∠-159.8116°
10	7082.0406∠-1.2459°	6726.0233∠-122.1078°	6904.6475∠118.652°	183.5629∠-156.84°	163.5439∠174.9305°	173.796∠156.1626°
11	7080.1174∠-1.7032°	6713.8329∠-122.1768°	6874.1873∠119.4839°	208.5943∠97.3945°	222.6217∠-143.9124°	253.3973∠3.2521°
12	7126.4444∠-1.6037°	6709.8612∠-122.5267°	6836.6892∠119.6108°	196.4514∠146.7552°	149.0344∠-85.0161°	160.8966∠56.6492°

Analysis of Three-Phase-to-Ground(LLLG) Fault

The system explained in case 3 is simulated for three phase to ground fault in which a fictitious node (node 13) is created between nodes 2 and 3 which is assumed to be at a distance of 20% from node 2 and 80% from node 3 of the total distance between these nodes. The fault resistance of 20 Ω is presumed. The initial voltage at node 13 is enforced as the average of the initial source voltage for the first iteration and due to this the final voltages on each phase of node 13 are equal in magnitude and angle which are shown in Table 3.16. The backward-forward sweep method continues until the mismatch occurs between the new and the previous iterations in the load voltages is within the specified tolerance. The final iteration results of voltages and load currents at each nodes are depicted in Table 3.16.

Table 3.16
Node Voltages and Currents for Three Phase to Ground Fault for Case 3

Node No.	Voltage			Load Current		
	Phase A	Phase B	Phase C	Phase A	Phase B	Phase C
1	7199.6∠0°	7199.6∠-120°	7199.6∠120°	1551.6215∠-61.38°	2967.4507∠-83.1316°	1870.6801∠-76.368°
2	6998.8813∠0.1497°	7125.0976∠-124.0002°	7429.6863∠120.9578°	1551.6215∠-61.38°	2967.4507∠-83.1316°	1870.6801∠-76.368°
13	**4072.4633∠-65.9296°**	**4072.4633∠-65.9296°**	**4072.4633∠-65.9296°**	**1576.9491∠-65.9992°**	**2892.7568∠-80.1793°**	**2032.5539∠-78.32°**
3	4047.5731∠-66.5481°	3903.9727∠-67.1242°	3984.5937∠-66.523°	940.48∠-66.0462°	2281.2556∠-84.1172°	1417.5024∠-83.8486°
4	4020.7095∠-66.6709°	3868.1038∠-67.0659°	3987.4996∠-67.1137°	223.8411∠-88.0081°	258.5246∠-107.6995°	275.8621∠-29.6031°
5	4013.7994∠-67.2407°	3856.5265∠-67.8805°	3878.1615∠-66.4495°	407.7279∠-66.9098°	465.8768∠-71.6792°	621.9104∠-107.07°
6	4019.2649∠-67.7789°	3818.3522∠-67.8527°	3840.1787∠-66.4232°	273.6819∠-30.2683°	314.2717∠-108.4863°	312.4855∠-107.0569°
7	3933.6744∠-66.7581°	3850.3908∠-68.1467°	3933.7598∠-67.4153°	580.1747∠-97.3235°	487.5404∠-66.2407°	456.2013∠-67.2875°
8	3886.7761∠-66.8757°	3849.2256∠-68.8676°	3933.5963∠-68.0372°	308.7392∠-88.2129°	337.7303∠-31.357°	305.0644∠-30.5266°
9	4106.6073∠-66.0318°	3850.1514∠-67.5096°	4021.4779∠-67.2872°	475.56∠93.3234°	385.3033∠-77.5293°	492.1653∠13.8366°
10	4128.9401∠-65.3606°	3808.271∠-67.3118°	4018.6365∠-68.0199°	314.8508∠139.0453°	288.845∠-130.2735°	298.6087∠-30.5093°
11	4113.8922∠-67.1966°	3833.1686∠-67.6143°	3958.6146∠-65.2654°	355.2627∠31.4997°	392.3591∠-89.4851°	441.0573∠178.9288°
12	4194.4487∠-66.8879°	3823.9094∠-68.5256°	3891.8657∠-64.9076°	333.7745∠81.471°	261.5125∠-31.015°	282.6408∠-127.8692°

Analysis of Three-Phase(LLL) Fault

In this case, the system in case 3 is simulated for three phase fault. As explained previously, a fictitious node 13 is created between nodes 2 and 3 respectively. The fault resistance is assumed to be 10 Ω. The final voltages and currents at each node obtained in the final iteration are shown in Table 3.17.

Table 3.17
Node Voltages and Currents for Three Phase Fault for Case 3

Node No.	Voltage			Load Current		
	Phase A	Phase B	Phase C	Phase A	Phase B	Phase C
1	7199.6∠0°	7199.6∠-120°	7199.6∠120°	2318.0498∠-65.383°	3810.825∠-82.448°	2666.6707∠-76.5005°
2	6904.1938∠0.5594°	7121.3612∠-124.8969°	7524.941∠121.3326°	2318.0498∠-65.383°	3810.825∠-82.448°	2666.6707∠-76.5005°
13	**3840.3539∠-68.3004°**	**3840.3539∠-68.3004°**	**3840.3539∠-68.3004°**	**2351.7963∠-68.4731°**	**3739.4486∠-80.131°**	**2826.7229∠-77.8576°**
3	3814.5684∠-68.9758°	3666.0509∠-69.6047°	3749.4181∠-68.947°	1001.9352∠-68.7059°	2434.0319∠-86.6597°	1512.2837∠-86.3804°
4	3786.8266∠-69.1105°	3628.9773∠-69.5398°	3752.4059∠-69.5953°	237.666∠-90.4476°	275.5597∠-110.1734°	293.1453∠-32.0847°
5	3779.7321∠-69.735°	3616.9868∠-70.4358°	3639.3651∠-68.8631°	433.1004∠-69.4352°	497.0143∠-74.2563°	663.0536∠-109.4816°
6	3785.4222∠-70.3249°	3577.545∠-70.4047°	3600.0814∠-68.8328°	290.5885∠-32.8143°	335.4255∠-111.0384°	333.3258∠-109.4665°
7	3696.8474∠-69.2044°	3610.648∠-70.7282°	3696.8783∠-69.926°	617.7429∠-99.7699°	520.1799∠-68.8627°	485.6396∠-69.8311°
8	3648.3747∠-69.3331°	3609.4678∠-71.5214°	3696.7363∠-70.6092°	328.9136∠-90.6703°	360.1639∠-34.0108°	324.6107∠-33.0986°
9	3875.5361∠-68.4101°	3610.4144∠-70.0284°	3787.5037∠-69.785°	503.5321∠90.9602°	411.1864∠-80.0768°	522.3076∠11.3069°
10	3898.6228∠-67.676°	3567.1588∠-69.8096°	3784.6387∠-70.5883°	333.4511∠136.73°	308.3687∠-132.7712°	317.0712∠-33.0777°
11	3883.0445∠-69.6844°	3592.8651∠-70.1431°	3722.6793∠-67.564°	375.8334∠28.9567°	419.023∠-92.0384°	469.1486∠176.6951°
12	3966.1549∠-69.3451°	3583.3174∠-71.1474°	3653.7372∠-67.1666°	352.9867∠79.0138°	279.071∠-33.6368°	301.0616∠-130.1283°

Analysis of Double-Line-to-Ground(LLG) Fault

In this case, the system in case 3 is simulated for three phase fault. As explained previously, a fictitious node 13 is created between nodes 2 and 3 respectively. The fault resistance is assumed to be 20 Ω. The final voltages and currents at each node obtained in the final iteration are shown in Table 3.18.

Table 3.18
Node Voltages and Currents for Double Line to Ground Fault for Case 3

Node No.	Voltage			Load Current		
	Phase A	Phase B	Phase C	Phase A	Phase B	Phase C
1	7199.6∠0°	7199.6∠-120°	7199.6∠120°	1131.2392∠-25.5626°	1943.4414∠-50.6676°	975.386∠97.1574°
2	7010.0377∠-0.5499°	7347.8794∠-122.8739°	6982.2578∠118.834°	1131.2392∠-25.5626°	1943.4414∠-50.6676°	975.386∠97.1574°
13	**5887.652∠-32.4189°**	**5887.652∠-32.4189°**	**6961.0453∠118.6916°**	**1078.0373∠-31.6277°**	**1960.3234∠-45.898°**	**801.5834∠101.4848°**
3	5851.1215∠-32.7783°	5750.2177∠-33.0599°	6879.4413∠118.1973°	637.8649∠-31.0817°	1535.6389∠-49.7295°	801.5834∠101.4848°
4	5829.4654∠-32.9004°	5722.6003∠-33.0946°	6871.2233∠117.9437°	154.3881∠-54.2376°	174.7457∠-73.7283°	160.0879∠155.4543°
5	5808.5265∠-33.0958°	5698.6556∠-33.397°	6802.4279∠118.0351°	281.4743∠-32.5712°	314.5807∠-37.1046°	353.546∠77.371°
6	5805.7056∠-33.3535°	5665.1314∠-33.374°	6774.3609∠117.9745°	189.4688∠4.1571°	211.8221∠-74.0077°	177.1385∠77.3408°
7	5756.2173∠-32.9663°	5698.8766∠-33.6402°	6822.7829∠117.6679°	395.307∠-63.567°	328.7798∠-31.5564°	262.6004∠117.9663°
8	5720.0038∠-33.0988°	5695.2854∠-34.0615°	6817.6014∠117.3335°	209.7901∠-54.436°	228.259∠3.4491°	176.015∠154.8441°
9	5897.5855∠-32.6147°	5716.3162∠-33.3372°	6904.6513∠117.9326°	332.7097∠126.6424°	258.4319∠-43.2512°	287.8415∠-160.7207°
10	5911.0197∠-32.3394°	5684.3803∠-33.3096°	6896.8532∠117.737°	219.9282∠172.0665°	193.5127∠-96.2712°	173.9924∠155.2476°
11	5897.7006∠-32.9783°	5699.065∠-33.1689°	6865.2684∠118.5455°	249.801∠66.1008°	262.5373∠-54.8507°	253.6787∠2.2639°
12	5947.9136∠-32.7782°	5684.2415∠-33.5542°	6836.5437∠118.6394°	235.3767∠115.5807°	175.925∠3.9564°	160.9∠55.6777°

Analysis of Double-Line(LL) Fault

For double line fault, case 3 is simulated with the assumption of fault resistance to be 10 Ω. The initial voltage at node 13 for phases a and b is enforced as the average of the initial source voltage for the first iteration and due to this the final voltages on phases a and b of node 13 are equal in magnitude and angle. The final voltages and currents at each nodes are depicted in Table 3.19.

Analysis of Single-Line-to-Ground(SLG) Fault

In this case, the system in case 3 is simulated for single line to ground phase fault. As explained previously, a fictitious node 13 is created between nodes 2 and 3 respectively. The fault resistance is assumed to be 20 Ω. For the first iteration, voltages at node 13

Table 3.19
Node Voltages and Currents for Double Line Fault for Case 3

Node No.	Voltage			Load Current		
	Phase A	Phase B	Phase C	Phase A	Phase B	Phase C
1	7199.6∠0°	7199.6∠-120°	7199.6∠120°	1596.3037∠-28.4261°	2411.9725∠-48.1758°	976.8273∠96.9639°
2	6927.8901∠-0.6757°	7402.1203∠-123.3777°	6973.8394∠118.6609°	1596.3037∠-28.4261°	2411.9725∠-48.1758°	976.8273∠96.9639°
13	5782.5313∠-33.3398°	5782.5313∠-33.3398°	6951.6767∠118.4968°	1546.4459∠-32.8017°	2435.7653∠-44.3844°	802.788∠101.2856°
3	5745.5825∠-33.7122°	5643.172∠-34.003°	6869.5465∠118.0001°	650.0468∠-32.0596°	1565.3267∠-50.6835°	802.788∠101.2856°
4	5723.6723∠-33.8382°	5615.2068∠-34.0387°	6861.2044∠117.746°	157.2417∠-55.1754°	178.0878∠-74.6724°	160.3217∠155.2566°
5	5702.4332∠-34.0418°	5590.9038∠-34.3531°	6792.2257∠117.8363°	286.7313∠-33.5219°	320.6785∠-38.0652°	354.0813∠77.1721°
6	5699.5998∠-34.3087°	5556.906∠-34.3299°	6764.0414∠117.7753°	192.996∠3.2019°	215.9475∠-74.9636°	177.4087∠77.1416°
7	5649.4122∠-33.9071°	5591.2017∠-34.6036°	6812.4665∠117.4687°	402.8257∠-64.5091°	335.146∠-32.5277°	263.0038,∠117.7666°
8	5612.7375∠-34.0439°	5587.635∠-35.0391°	6807.1618∠117.1327°	213.7994∠-55.3811°	232.6566∠2.4715°	176.2849∠154.6433°
9	5792.769∠-33.5423°	5608.8264∠-34.2889°	6894.8046∠117.7348°	338.6912∠125.7167°	263.409∠-44.2087°	288.254∠-160.9184°
10	5806.4531∠-33.2579°	5576.4863∠-34.2602°	6886.9892∠117.5396°	223.8888∠171.148°	197.2568∠-97.2218°	174.2416∠155.0502°
11	5792.7467∠-33.9192°	5591.1641∠-34.1164°	6855.3039∠118.3483°	254.2651∠65.1522°	267.6501∠-55.8001°	254.0485∠2.0664°
12	5843.6751∠-33.7132°	5576.1211∠-34.5159°	6826.6367∠118.4415°	239.5753∠114.6457°	179.3361∠2.9947°	161.1335∠55.4799°

is not enforced as carried out for the previous cases. The final voltages and currents at each node obtained in the final iteration are depicted in Table 3.20.

Table 3.20
Node Voltages and Currents for Single Line to Ground Fault for Case 3

Node No.	Voltage			Load Current		
	Phase A	Phase B	Phase C	Phase A	Phase B	Phase C
1	7199.6∠0°	7199.6∠-120°	7199.6∠120°	1005.5623∠3.7204°	1478.2015∠-139.0743°	973.4888∠97.9419°
2	7043.4019∠-1.4448°	6900.7938∠-121.2604°	6993.255∠119.3349°	1005.5623∠3.7204°	1478.2015∠-139.0743°	973.4888∠97.9419°
13	7025.7438∠-1.5964°	6869.6878∠-121.3991°	6973.2583∠119.2547°	900.2093∠-0.635°	1304.6809∠-138.605°	800.3269∠102.3317°
3	6981.1828∠-1.9963°	6749.9356∠-121.9762°	6892.3102∠118.9649°	531.3684∠0.0325°	1304.6809∠-138.605°	800.3269∠102.3317°
4	6957.4707∠-2.0987°	6726.0521∠-121.9951°	6886.8775∠118.7473°	129.3574∠-23.4358°	148.6756∠-162.6288°	159.7241∠156.2579°
5	6943.3849∠-2.2751°	6699.3043∠-122.3388°	6815.1516∠118.8909°	235.4191∠-1.7068°	267.2592∠-126.0551°	352.8217∠78.2527°
6	6937.0633∠-2.4701°	6668.8686∠-122.39°	6789.5031∠118.8819°	158.5685∠35.0405°	179.9406∠-163.0237°	176.7434∠78.2483°
7	6897.1463∠-2.2119°	6698.2493∠-122.4089°	6835.7743∠118.5205°	329.561∠-32.8263°	279.4961∠-120.2534°	262.1259∠118.8439°
8	6867.9584∠-2.3514°	6693.6003∠-122.7068°	6827.1417∠118.2112°	174.7244∠-23.6886°	194.2154∠-85.1961°	175.769∠155.7218°
9	7015.3698∠-1.9307°	6733.5708∠-122.1441°	6913.3322∠118.7478°	280.0896∠157.3317°	219.169∠-131.9467°	287.496∠-159.8919°
10	7020.1933∠-1.7362°	6715.3244∠-122.0886°	6906.9448∠118.572°	185.1801∠-157.3302°	163.8044∠174.9497°	173.7382∠156.0826°
11	7018.0913∠-2.2013°	6703.0674∠-122.1572°	6876.5112∠119.4024°	210.4195∠96.893°	222.9828∠-143.8932°	253.3104∠3.1703°
12	7064.7682∠-2.1001°	6699.0802∠-122.5086°	6839.0744∠119.5295°	198.1664∠146.2588°	149.2742∠-84.998°	160.8405∠56.5679°

Analysis of Exact Fault Location

For the analysis purpose,first, a bisection search algorithm has been employed. Second, an incremental adjustment to match the simulated current of fault with the measurements is conducted. Finally, the sensitivity analysis of a search can be improved with the proposed algorithm that leads to matching of telemetered and calculated values as depicted in Table 3.21.

Table 3.21
Determination of Exact Location of Fault for Case 3

Fault No.	Fault Type	Reference Current Value	Actual Value of Current	Actual Distance of Fault
1	LLLG	1551.6215∠-61.38°	1552.1211∠-61.3926°	0.2031
		2967.4507∠-83.1316°	2968.1092∠-83.1386°	
		1870.6801∠-76.368°	1871.2662∠-76.3795°	
2	LLL	2318.0498∠-65.383°	2319.1824∠-65.401°	0.2031
		3810.825∠-82.448°	3812.3637∠-82.46°	
		2666.6707∠-76.5005°	2667.9786∠-76.5175°	
3	LLG	1131.2392∠-25.5626°	1132.6707∠-25.6234°	0.2500
		1943.4414∠-50.6676°	1944.5558∠-50.697°	
		975.386∠97.1574°	975.4278∠97.153°	
4	LL	1596.3037∠-28.4261°	1595.5427∠-28.4031°	0.1875
		2411.9725∠-48.1758°	2411.1248∠-48.1612°	
		976.8273∠96.9639°	976.8048∠96.9661°	
5	LG	1005.5623∠3.7204°	1005.9051∠3.6976°	0.2500
		1478.2015∠-139.0743°	1478.2583∠-139.0738°	
		973.4888∠97.9419°	973.4848∠97.94°	

3.6 Conclusion

This chapter provides a groundwork on the reversal from a presumed location and different types of faults to determine the exact location of faults in unidirectional flow of power in distribution feeders. Exact location of fault was carried out on radial distribution system as well as on distribution system consisting of laterals and sub-laterals. This chapter explores a modern algorithm called the bisection method and incremental distance to detect the exact location of fault. The advantage of this method is that it reduces the time for fault detection and increases the overall reliability of the system.

Chapter 4

Fault Localization Under Bidirectional Flow Conditions

For the last ten years, due to the tremendous increase in the power supply form the distributed energy resources (DER), the traditional radial passive distribution system is transformed into active multi-source distribution system. As discussed earlier in chapter 3 about various modern fault diagnosis algorithm for unidirectional flow of power, this chapter explores the same modern fault diagnosis algorithm for bidirectional flow of power.

4.1 Modeling with Distributed Energy Resource

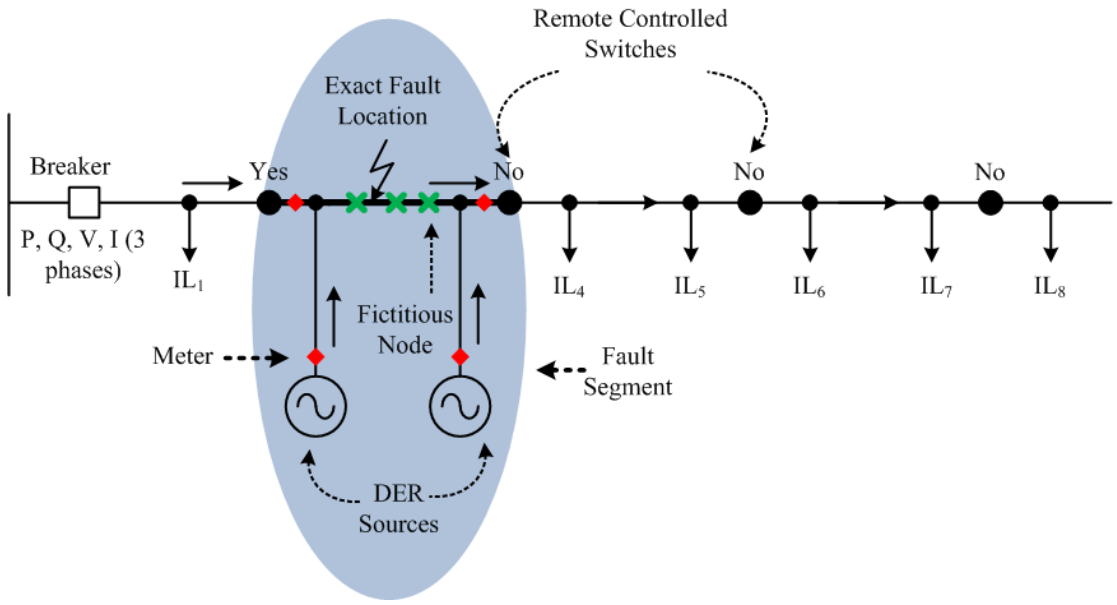

Figure 4.1: Single line diagram of distribution feeder with fictitious nodes and DER integration

The distribution feeder in the power system is radial network consisting of n number of line segments and integrated with renewable energy resources (RES) as shown in 4.1. Due to the radial network, the measured values of the voltages and the currents are available at the substation. Therefore, an estimation procedure is required to calculate the voltage as well as the currents at the beginning of the faulted line segment depending on the loading condition of the customer and the pre-fault and the post fault measurements of the voltages and the currents at the substation. It is observed that same voltages and currents will be measured at various fault locations as the distribution feeder in a large power system is radial in nature and number

of laterals are connected to the main feeder.The first step is to find the possible fault locations which can be determined by scanning the network and the applying algorithm for the fault distance on a section by section basis.

Assumptions include:

1. The radial distribution feeder system is considered.
2. The fault occurred within the segment circled in Fig. 4.1 that could branch out with multiple locations.
3. Fault can be either symmetrical or unsymmetrical.
4. Incremental change in the distance will be equal.
5. Fault location is initially inferred between Yes and No from the fault indicators.
6. The breaker tripped in distribution substation could provide a hint to capture potential fault segment.
7. Known statuses of fault indicators, i.e., between “yes” and “no” from the remote controlled switches information before occurrence of the fault.
8. The distributed energy resources (DER) are modeled as negative loads
9. Single-event fault with potential multiple fault types that does not disrupt the majority of the electrical overhead lines. It is rather a localized fault that is

generally deemed an "abnormal" condition, not the extreme scenarios like those incurred by hurricanes nor tornadoes.

4.2 Combinatorial Search of Faulted Candidate Locations

The flowchart shown in Fig. 4.2 and Fig. 4.1 gives the information to be computed to determine the exact fault location. In order to determine the exact fault location 3 major steps needs to be executed. The first step is Initialization of SCADA measurement and topological statuses. In step 1, the information is populated from the Geographical Information System (GIS). The two important components which are obtained from the GIS are accurate data of the distribution feeder topology and real-time measurements of the topology data. The mathematical formulation for every system component such as distributed generators, feeder lines, transformers, voltage regulators, shunt capacitor, series reactor and loads. In step 2, the distributed energy resources are modeled as negative loads for the analysis purpose. In step 3 load voltage measurements are required in order to design the load model from load voltage. The load currents are considered in the analysis because load currents are not less than the short circuit currents. In addition to this binary measurements (either ON or OFF) of the Fault Indicators(FIs) are recorded to detect the exact location

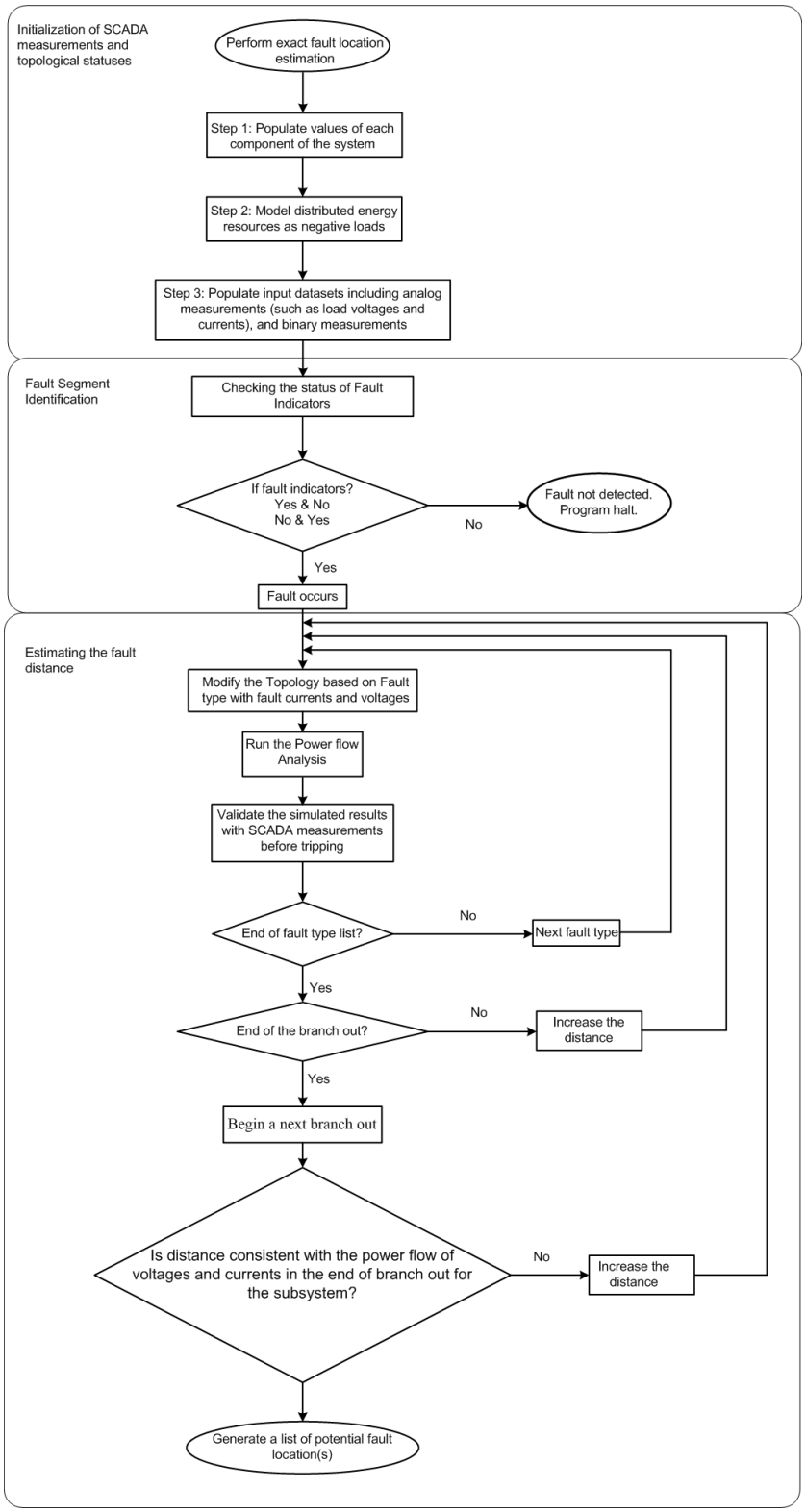

Figure 4.2: Flowchart for enhanced estimation of fault location point based on n number of branch out for bidirectional power flow

of the fault. In the computerized automated SCADA network, the FIs will help the crew members to navigate the exact location of the fault. The data of the FIs are centralized in the Distributed Automation System (DMS) system where the SCADA systems updates the information regrading the feeder topology and analog as well as binary measurements.

The fault location identification is the second major step for exact fault location estimation. The fault indicators will detect the fault in the distribution feeders. If the fault indicators indicates either (YES and NO) or (NO and YES) then it indicates that the fault has occurred in the segment which is connected between these two FIs. If the FIs indicates either (YES and YES) or (NO and NO) indicates that the fault is not detected and the program halts.

Once the fault occurs, the next and the final major step is estimating the fault distance. Depending up the type of faults and fault voltages and currents, the distribution feeder topology will be modified. The fault type can be classified into symmetrical faults (3 phase fault) and unsymmetrical faults which includes single line to ground fault, double line to ground fault, line to line fault etc. An algorithm will be executed depending upon the type of fault and the power analysis at each node of the distribution feeder will determined the voltages and currents and try to maintained within the specified limits. In order to execute the power flow analysis the system most accurately, each component connected in the distribution feeder should be analyzed

in more detail. This includes three phase transformers with various types of connection, composite loads, single, two and three phase unbalanced systems and effects due to voltage regulators and shunt capacitors. The simulated results obtained from power flow analysis are validated with the SCADA measurements before the tripping of the distribution feeder takes place. The incremental process continues till the next fault type is detected. The first iteration will detect if there are any other faults. If the fault is detected, again the process of topology modification, power flow analysis and comparison with the SCADA results will be carried out. The second iteration loop will verify whether the fault has occurred in the branch out and is the values of fault voltages and currents are consistent with the values of the voltages and currents obtained from the power flow analysis. If they are not consistent then increment the distance till the values become consistent. The third and the final loop will check whether the whole feeder is scanned for possible fault location. If the complete feeder is not scanned then the loop will increment the distance to carry out the process of estimation of fault distance. At the end of the feeder, the program will generate a list of potential fault locations.

4.3 Proposed Flowchart

The proposed flowchart for the determination of exact fault location is shown in Fig. 4.3. The first step is to define I_ref value obtained from the meters, Cerror

as 999, start_perc as 0 and end _perc as 1. For the 25% and 75% fault location variables A and B are determined which are maximum absolute values of currents. These values A and B are calculated using power flow analysis. After the condition for CError is determined, fault percentage is calculated by assuming the average of start_perc and the ending_perc. The values current at each node is calculated using power flow analysis. As the distance increases the value of current can increase or decrease. Depending on this condition, the endingperc and the start_perc are determined. Once the ending_perc and start_perc are determined the final exact fault location is calculated the averaging the start and end_perc respectively.

4.4 Simulation Results

In order to determine the exact location of fault three cases are simulated using MATLAB ®programming depending on the topology reconfiguration. This numerical experience includes variation of topological configuration, location of where the presumed fault would be in the simulation studies.

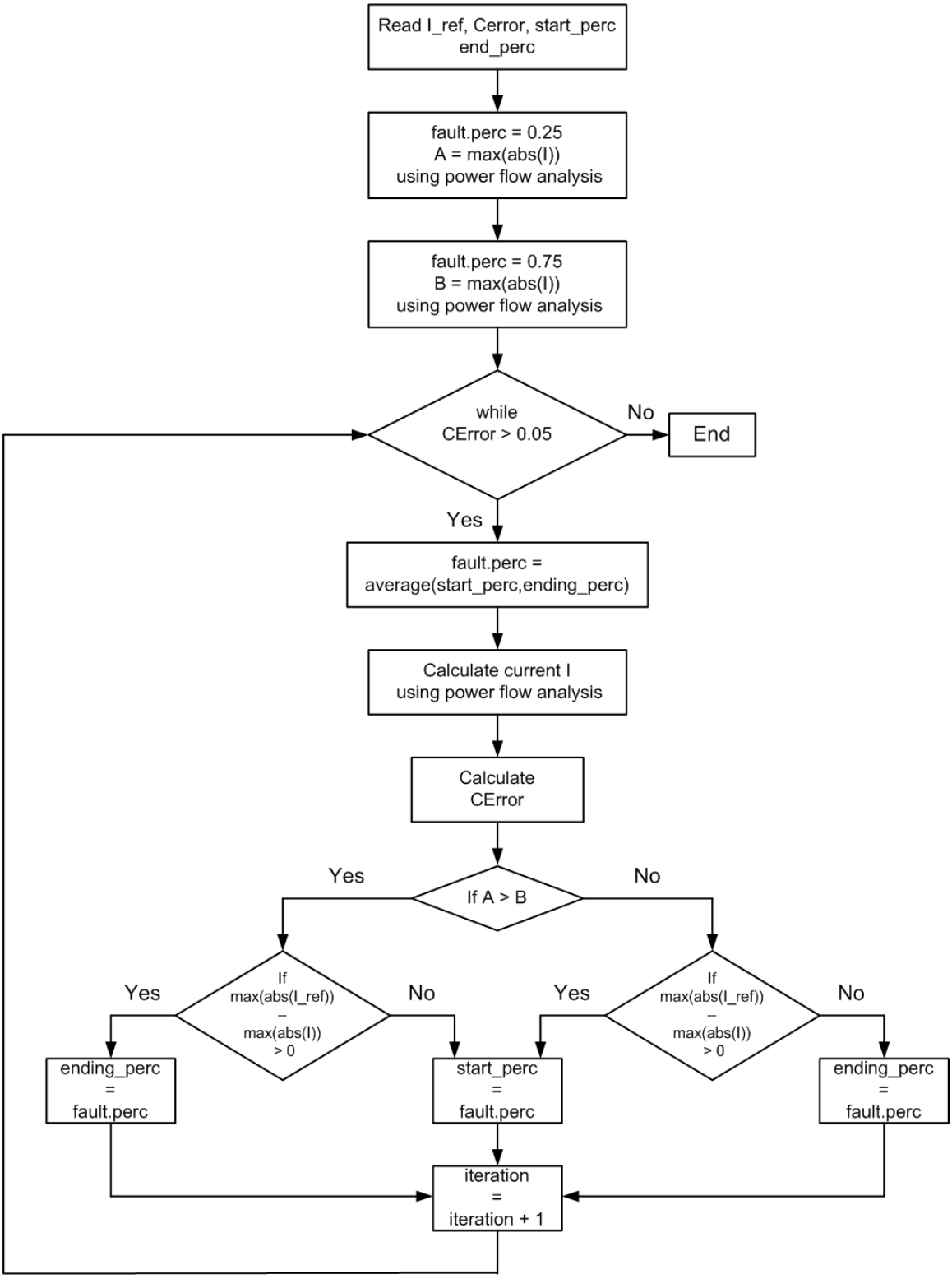

Figure 4.3: Flowchart for determination of exact fault location for bidirectional power flow

4.4.1 Case 1: Perfect Radial Network Setup

This topology consists of 8 nodes and 7 switches where the switches and the respective lines are connected topologically. Breakers and recloser are equipped with the relay. Under normal operating condition, the breaker is used to energized the feeder. The source is considered at node 1 and three phase loads are connected to all remaining 7 nodes. Distributed energy sources (DER) are connected to nodes 3,5 and 7 respectively. These sources are considered negative sources during analysis purpose as shown in Fig. 4.4.

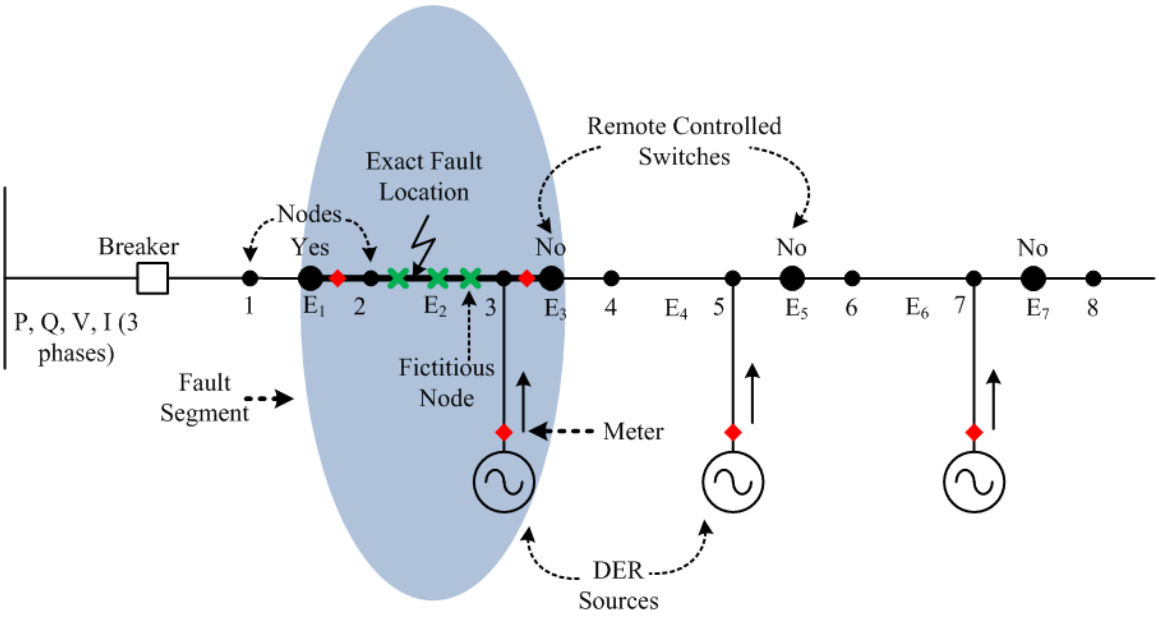

Figure 4.4: A case for determination of exact fault location with integration of DER's

Analysis of Three-Phase-to-Ground (LLLG) Fault

The system explained in case 1 is simulated for three phase to ground fault in which a fictitious node (node 9) is created between nodes 2 and 3 which is assumed to be at a distance of 40% from node 2 and 60% from node 3 of the total distance between these nodes. The fault resistance of 40 Ω is presumed. The initial voltage at node 9 is enforced as the average of the initial source voltage for the first iteration and due to this the final voltages on each phase of node 9 are equal in magnitude and angle which are shown in Table 4.1. The backward-forward sweep method continues until the mismatch occurs between the new and the previous iterations in the load voltages is within the specified tolerance. The final iteration results of voltages and load currents at each nodes are depicted in Table 4.1.

Table 4.1
Node Voltages and Currents in Three Phase to Ground Fault for Case 1

Node No.	Voltage			Load Current		
	Phase A	Phase B	Phase C	Phase A	Phase B	Phase C
1	7199.6∠0°	7199.6∠-120°	7199.6∠120°	544.6549∠1.4271°	290.3465∠-80.1562°	758.8027∠21.1433°
2	7138.6554∠-0.5752°	7164.331∠-120.4619°	7098.11∠120.8859°	544.6549∠1.4271°	290.3465∠-80.1562°	758.8027∠21.1433°
9	4800.0659∠-61.8424°	4800.0659∠-61.8424°	4800.0659∠-61.8424°	448.0509∠-7.9792°	257.2141∠-45.1927°	683.0998∠7.8416°
3	4815.6621∠-62.0099°	4798.8117∠-61.8006°	4834.995∠-62.1796°	361.8971∠29.0718°	77.3728∠45.8903°	641.4458∠31.091°
4	4819.9922∠-62.612°	4756.552∠-61.7349°	4869.9501∠-62.9538°	367.7464∠-17.8809°	250.0531∠-93.0833°	475.9886∠1.0306°
5	4855.105∠-63.2307°	4741.7221∠-61.6894°	4908.7564∠-63.3886°	338.2214∠12.4245°	54.4336∠-54.5348°	291.7277∠21.2221°
6	4854.7726∠-63.6659°	4735.8739∠-62.0562°	4904.0353∠-63.7042°	308.3988∠-24.3588°	280.3073∠-29.8109°	250.1165∠-31.7395°
7	4843.444∠-63.7474°	4780.0559∠-62.6713°	4949.9793∠-64.2165°	82.2364∠-19.4036°	317.7383∠19.8411°	292.9629∠21.107°
8	4834.4472∠-63.773°	4780.3464∠-62.7834°	4950.5749∠-64.3135°	248.2187∠-85.1102°	271.9468∠-25.2728°	242.3961∠-26.8029°

Analysis of Three-Phase(LLL) Fault

In this case, the system in case 1 is simulated for three phase fault. As explained previously, a fictitious node 9 is created between nodes 2 and 3 respectively. The fault resistance is assumed to be 10 Ω. The final voltages and currents at each node obtained in the final iteration are shown in Table 4.2.

Table 4.2
Node Voltages and Currents in Three Phase Fault for Case 1

Node No.	Voltage			Load Current		
	Phase A	Phase B	Phase C	Phase A	Phase B	Phase C
1	7199.6∠0°	7199.6∠-120°	7199.6∠120°	1214.0241∠-40.6114°	1151.904∠-69.4896°	1227.0885∠-26.1251°
2	7015.8032∠-0.317°	7199.2083∠-121.4356°	7189.7791∠121.59°	1214.0241∠-40.6114°	1151.904∠-69.4896°	1227.0885∠-26.1251°
9	**4556.7554∠-65.2127°**	**4556.7554∠-65.2127°**	**4556.7554∠-65.2127°**	**1193.5306∠-46.6418°**	**1115.4411∠-61.2613°**	**1291.813∠-33.8139°**
3	4573.1509∠-65.3774°	4555.2975∠-65.1697°	4593.2888∠-65.5415°	380.1654∠25.732°	80.7866∠42.711°	673.9329∠27.765°
4	4580.4591∠-66.0068°	4512.7883∠-65.1321°	4632.0367∠-66.3291°	386.4841∠-21.3298°	263.7909∠-96.5993°	499.7277∠-2.3621°
5	4618.6058∠-66.6304°	4497.7609∠-65.0954°	4672.9578∠-66.757°	355.2986∠9.0191°	57.216∠-58.504°	305.9936∠17.8659°
6	4620.4678∠-67.0873°	4493.7315∠-65.4858°	4669.8374∠-67.0914°	324.0179∠-27.7891°	295.1194∠-33.302°	262.4115∠-35.1786°
7	4609.5718∠-67.1811°	4540.8893∠-66.099°	4718.3009∠-67.5951°	86.3824∠-22.8571°	334.4286∠16.4145°	307.3155∠17.73°
8	4600.7211∠-67.2148°	4541.7389∠-66.2166°	4719.3895∠-67.6962°	260.8287∠-88.5519°	286.234∠-28.7059°	254.2702∠-30.1856°

Analysis of Double-Line-to-Ground (LLG) Fault

For double line to ground fault, case 1 is simulated with the assumption of fault resistance to be 40 Ω. The initial voltage at node 9 for phases a and b is enforced as the average of the initial source voltage for the first iteration and due to this the final voltages on phases a and b of node 9 are equal in magnitude and angle which are shown in Table 4.3.

Table 4.3
Node Voltages and Currents in Double Line to Ground Fault for Case 1

Node No.	Voltage			Load Current		
	Phase A	Phase B	Phase C	Phase A	Phase B	Phase C
1	7199.6∠0°	7199.6∠-120°	7199.6∠120°	467.7557∠26.6927°	162.6103∠-68.4083°	331.5785∠-170.3338°
2	7171.9569∠-0.8121°	7201.1014∠-120.2789°	7236.433∠119.4204°	467.7557∠26.6927°	162.6103∠-68.4083°	331.5785∠-170.3338°
9	**6247.6195∠-31.1539°**	**6247.6195∠-31.1539°**	**7254.5078∠119.2874°**	**344.8655∠23.0679°**	**196.3527∠-14.0679°**	**429.7404∠-147.343°**
3	6264.3666∠-31.3149°	6251.5501∠-31.1897°	7282.6012∠119.1176°	279.8449∠60.0365°	60.9774∠77.7468°	429.7404∠-147.343°
4	6268.9654∠-31.7936°	6220.7645∠-31.2709°	7302.2574∠118.666°	282.8642∠13.2386°	189.891∠-62.4632°	318.3771∠-177.009°
5	6300.3481∠-32.2478°	6214.2421∠-31.3287°	7335.8844∠118.3918°	260.8971∠43.5123°	40.94∠-22.3648°	196.0875∠-156.7328°
6	6297.0357∠-32.5589°	6206.9391∠-31.5971°	7334.5447∠118.1394°	237.578∠6.7539°	213.8722∠0.9334°	167.174∠150.4681°
7	6294.3205∠-32.7054°	6246.5323∠-32.0634°	7376.0701∠117.8195°	63.2182∠11.7392°	243.2429∠50.4632°	196.6911∠-156.848°
8	6286.8123∠-32.7344°	6246.1067∠-32.1445°	7375.3338∠117.7527°	190.8757∠-54.0716°	208.1297∠5.3661°	162.7045∠155.2633°

Analysis of Double-Line (LL) Fault

For double line fault, case 1 is simulated with the assumption of fault resistance to be 10 Ω. The initial voltage at node 9 for phases a and b is enforced as the average of the initial source voltage for the first iteration and due to this the final voltages on phases a and b of node 9 are equal in magnitude and angle. The final voltages and currents at each nodes are depicted in Table 4.4.

Table 4.4
Node Voltages and Currents in Double Line Fault for Case 1

Node No.	Voltage			Load Current		
	Phase A	Phase B	Phase C	Phase A	Phase B	Phase C
1	7199.6∠0°	7199.6∠-120°	7199.6∠120°	976.9154∠-8.0811°	779.6244∠-39.6756°	332.1475∠-170.631°
2	7063.0697∠-1.0624°	7281.9987∠-120.9059°	7228.7592∠119.1819°	976.9154∠-8.0811°	779.6244∠-39.6756°	332.1475∠-170.631°
9	**6103.6047∠-32.58°**	**6103.6047∠-32.58°**	**7245.0974∠118.9922°**	**890.5708∠-13.8398°**	**831.1913∠-28.5181°**	**430.2636∠-147.6344°**
3	6120.7841∠-32.7408°	6107.6314∠-32.6157°	7273.3012∠118.8233°	286.1828∠58.6167°	62.2556∠76.3833°	430.2636∠-147.6344°
4	6126.6888∠-33.2294°	6077.076∠-32.706°	7293.2523∠118.3719°	289.3219∠11.7841°	194.4441∠-63.9345°	318.7507∠-177.3023°
5	6159.3114∠-33.6866°	6070.7127∠-32.7667°	7327.0583∠118.0988°	266.8126∠42.071°	41.8775∠-23.9842°	196.3128∠-157.0237°
6	6156.8611∠-34.0055°	6064.1443∠-33.0431°	7325.884∠117.846°	242.9779∠5.3047°	218.8483∠-0.5333°	167.363∠150.1736°
7	6154.5539∠-34.156°	6105.0043∠-33.5108°	7367.6187∠117.5274°	64.6474∠10.2835°	248.8715∠49.0159°	196.9159∠-157.14°
8	6147.1287∠-34.1874°	6104.8022∠-33.5937°	7366.9262∠117.4605°	195.2131∠-55.5246°	212.9471∠3.9169°	162.8902∠154.9711°

Analysis of Single-Line-to-Ground (SLG) Fault

In this case, the system in case 1 is simulated for single line to ground phase fault. As explained previously, a fictitious node 9 is created between nodes 2 and 3 respectively. The fault resistance is assumed to be 40 Ω. For the first iteration, voltages at node 9 is not enforced as carried out for the previous cases. The final voltages and currents at each node obtained in the final iteration are depicted in Table 4.5.

Table 4.5
Node Voltages and Currents in Double Line Fault for Case 1

Node No.	Voltage			Load Current		
	Phase A	Phase B	Phase C	Phase A	Phase B	Phase C
1	7199.6∠0°	7199.6∠-120°	7199.6∠120°	420.6607∠48.6298°	138.0345∠-124.4007°	331.8585∠-170.1705°
2	7204.2321∠-0.7713°	7178.6468∠-120.2008°	7237.6637∠119.4799°	420.6607∠48.6298°	138.0345∠-124.4007°	331.8585∠-170.1705°
9	**7206.9631∠-0.9064°**	**7182.3363∠-120.2123°**	**7256.0133∠119.361°**	**299.5228∠53.5598°**	**53.8271∠-10.6187°**	**430.2116∠-147.2273°**
3	7220.419∠-1.0324°	7189.432∠-120.2329°	7283.1561∠119.196°	243.8113∠90.4446°	53.8271∠-10.6187°	430.2116∠-147.2273°
4	7217.044∠-1.4199°	7165.8691∠-120.3146°	7304.3828∠118.8022°	245.7211∠43.7798°	164.0966∠-151.4984°	318.6524∠-176.8419°
5	7241.452∠-1.779°	7164.5051∠-120.3946°	7336.9452∠118.5608°	226.9997∠74.0406°	34.9863∠-110.5869°	196.4349∠-156.5869°
6	7239.1361∠-2.0478°	7158.0918∠-120.638°	7332.3102∠118.3415°	206.568∠37.2767°	185.226∠-87.9217°	167.44∠150.7231°
7	7243.9739∠-2.1932°	7195.0774∠-120.963°	7365.1081∠118.0007°	54.9034∠42.3024°	211.231∠-38.4248°	197.0043∠-156.6684°
8	7237.7599∠-2.2238°	7194.2238∠-121.0221°	7363.5726∠117.938°	165.7972∠-23.561°	180.7005∠-83.5115°	162.9644∠155.4486°

Analysis of Exact Fault Location

For the analysis purpose,first, a bisection search algorithm has been employed. Second, an incremental adjustment to match the simulated current of fault with the measurements is conducted. Finally, the sensitivity analysis of a search can be improved with the proposed algorithm that leads to matching of telemetered and calculated values as depicted in Table 4.6.

Table 4.6
Determination of Exact Location of Fault for Case 1

Fault No.	Fault Type	Reference Current Value	Actual Value of Current	Actual Distance of Fault
1	LLLG	544.6549∠1.4271°	544.655∠1.4271°	0.3999
		290.3465∠-80.1562°	290.3463∠-80.1561°	
		758.8027∠21.1433°	758.8024∠21.1433°	
2	LLL	1214.0241∠-40.6114°	1214.0246∠-40.6115°	0.4000
		1151.904∠-69.4896°	1151.9048∠-69.4897°	
		1227.0885∠-26.1251°	1227.089∠-26.1251°	
3	LLG	467.7557∠26.6927°	467.7555∠26.6926°	0.4004
		162.6103∠-68.4083°	162.6108∠-68.4085°	
		331.5785∠-170.3338°	331.5786∠-170.3338°	
4	LL	976.9154∠-8.0811°	976.9156∠-8.0811°	0.4000
		779.6244∠-39.6756°	779.6247∠-39.6757°	
		332.1475∠-170.631°	332.1476∠-170.631°	
5	LG	420.6607∠48.6298°	420.661∠48.63°	0.3984
		138.0345∠-124.4007°	138.0345∠-124.4007°	
		331.8585∠-170.1705°	331.8585∠-170.1705°	

4.4.2 Case 2: Equal Distance Branchout Test Feeder

This topology consists of 18 nodes and 17 switches where the switches and the respective lines are connected topologically. Breakers and recloser are equipped with the relay. Under normal operating condition, the breaker is used to energized the feeder. The source is considered at node 1 and three phase loads are connected to all remaining 17 nodes. For analysis purpose, the distributed energy sources are considered at nodes 2 and 3 respectively.

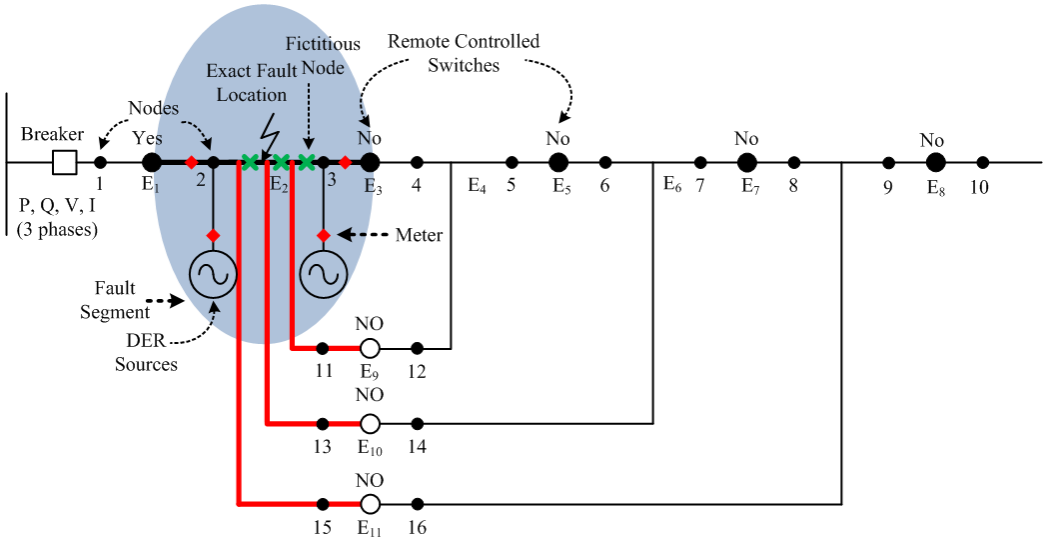

Figure 4.5: A case for determination of exact fault location with integration of DER's

Analysis of Three-Phase-to-Ground (LLLG) Fault

The system explained in case 2 is simulated for three phase to ground fault in which a fictitious node (node 19) is created between nodes 2 and 3 which is assumed to be at a distance of 40% from node 2 and 60% from node 3 of the total distance between these nodes. The fault resistance of 40 Ω is presumed. The initial voltage at node 19 is enforced as the average of the initial source voltage for the first iteration and due to this the final voltages on each phase of node 19 are equal in magnitude and angle which are shown in Table 4.7. The backward-forward sweep method continues until the mismatch occurs between the new and the previous iterations in the load voltages is within the specified tolerance. The final iteration results of voltages and load currents at each nodes are depicted in Table 4.7.

Table 4.7
Node Voltages and Currents in Three Phase to Ground Fault for Case 2

Node No.	Voltage			Load Current		
	Phase A	Phase B	Phase C	Phase A	Phase B	Phase C
1	7199.6∠0°	7199.6∠-120°	7199.6∠120°	1034.4848∠-63.0371°	1592.2776∠-60.5388°	1866.5983∠-56.7464°
2	7084.3351∠0.3679°	7264.7096∠-121.8901°	7403.542∠121.7935°	1034.4848∠-63.0371°	1592.2776∠-60.5388°	1866.5983∠-56.7464°
19	**4395.4071∠-65.2822°**	**4395.4071∠-65.2822°**	**4395.4071∠-65.2822°**	**1018.0988∠-55.9993°**	**1621.5972∠-66.3376°**	**1740.286∠-52.8681°**
3	4382.4282∠-65.6159°	4336.6814∠-65.9352°	4356.6102∠-66.2791°	728.6609∠-52.2567°	1326.8051∠-66.5721°	1453.7091∠-50.3691°
4	4325.704∠-65.6919°	4307.8386∠-66.4109°	4319.5181∠-66.7593°	435.1444∠-97.2127°	380.2407∠-66.1433°	416.3195∠-70.5928°
5	4286.6576∠-65.6517°	4313.2954∠-67.0709°	4269.8458∠-66.7266°	233.282∠-106.2854°	255.0254∠-29.5603°	281.0406∠-107.3603°
6	4378.7438∠-66.3112°	4229.3751∠-66.7145°	4287.2979∠-67.6332°	694.8317∠-41.8414°	1232.2974∠-77.1002°	1275.9144∠-57.6856°
7	4308.2351∠-66.4325°	4196.0467∠-67.3064°	4255.4161∠-68.146°	529.609∠-96.9977°	447.3287∠-65.3918°	421.698∠-68.01°
8	4258.7298∠-66.5457°	4194.8128∠-68.0118°	4254.9289∠-68.7556°	281.7742∠-87.8829°	309.9066∠-30.5012°	282.0259∠-31.245°
9	4424.1183∠-66.5285°	4177.2081∠-67.0963°	4272.8595∠-68.6505°	405.7372∠26.8395°	551.6459∠-71.6756°	743.0132∠-34.5611°
10	4453.8738∠-66.5864°	4037.599∠-66.4935°	4305.1103∠-68.6274°	64.5093∠74.1246°	598.9212∠-129.3201°	78.382∠87.0271°
11	4451.5437∠-67.3034°	3981.8252∠-66.2458°	4331.8584∠-67.871°	269.5694∠-29.7928°	326.4834∠-129.2074°	323.1869∠136.535°
12	4421.9893∠-66.6432°	4208.5456∠-67.3431°	4210.2086∠-69.6151°	193.8745∠-40.6459°	313.8896∠15.0485°	845.7175∠-62.2168°
13	4367.2879∠-66.9721°	4254.2631∠-67.1276°	4175.504∠-71.0679°	451.1452∠-77.0001°	222.0127∠64.0927°	796.8476∠-44.2296°
14	4339.4661∠-67.8776°	4262.562∠-67.0265°	4140.9987∠-72.1808°	460.9108∠-44.9607°	69.3169∠-28.0634°	540.1709∠-49.4115°
15	4356.5711∠-69.3801°	4210.2419∠-66.93°	4151.6363∠-73.9696°	610.0462∠-19.5919°	265.7877∠-84.4269°	690.8231∠-26.0313°
16	4359.2955∠-70.1423°	4154.4324∠-66.4889°	4146.6374∠-74.7993°	325.3064∠-31.0903°	310.3012∠-127.1209°	352.5181∠-40.7995°
17	4348.0908∠-70.1944°	4144.8244∠-66.6126°	4131.5088∠-74.9072°	129.1728∠-92.4453°	136.4074∠-74.1792°	170.55∠-91.3254°
18	4319.1001∠-69.7746°	4157.631∠-67.0629°	4145.8891∠-75.4381°	243.1062∠-155.9186°	252.5477∠-4.7234°	301.5035∠-13.0986°

Analysis of Three-Phase (LLL) Fault

In this case, the system in case 2 is simulated for three phase fault. As explained previously, a fictitious node 19 is created between nodes 2 and 3 respectively. The fault resistance is assumed to be 10 Ω. The final voltages and currents at each node obtained in the final iteration are shown in Table 4.8.

Analysis of Double-Line-to-Ground (LLG) Fault

In this case, the system in case 2 is simulated for three phase fault. As explained previously, a fictitious node 19 is created between nodes 2 and 3 respectively. The fault resistance is assumed to be 40 Ω. The final voltages and currents at each node

Table 4.8

Node Voltages and Currents in Three Phase Fault for Case 2

Node No.	Voltage			Load Current		
	Phase A	Phase B	Phase C	Phase A	Phase B	Phase C
1	7199.6∠0°	7199.6∠-120°	7199.6∠120°	2134.7033∠-68.6997°	2743.0912∠-67.7464°	3046.3189∠-64.4586°
2	6933.7418∠0.9904°	7271.7754∠-123.3659°	7573.8991∠122.5598°	2134.7033∠-68.6997°	2743.0912∠-67.7464°	3046.3189∠-64.4586°
19	**3990.5728∠-69.8055°**	**3990.5728∠-69.8055°**	**3990.5728∠-69.8055°**	**2099.9829∠-65.3146°**	**2784.9786∠-71.0557°**	**2904.9344∠-62.5841°**
3	3975.8765∠-70.2223°	3923.9255∠-70.6359°	3945.1598∠-71.0718°	811.3112∠-58.1123°	1486.4964∠-72.1482°	1624.4062∠-56.8145°
4	3912.561∠-70.3322°	3892.0945∠-71.2337°	3904.0406∠-71.6785°	481.6466∠-101.8646°	421.1983∠-71.0631°	461.3174∠-75.583°
5	3868.8111∠-70.2941°	3899.1011∠-72.0512°	3848.0577∠-71.6538°	258.4773∠-110.9277°	282.1163∠-34.5406°	311.8456∠-112.2875°
6	3971.8773∠-71.0832°	3802.334∠-71.6533°	3864.8484∠-72.8178°	769.8626∠-47.7105°	1384.5493∠-82.5161°	1432.6508∠-64.1672°
7	3893.0335∠-71.2533°	3765.2514∠-72.4119°	3829.3472∠-73.4732°	586.9852∠-101.8272°	499.0964∠-70.608°	469.0833∠-73.4267°
8	3837.6295∠-71.4084°	3764.892∠-73.3042°	3829.7071∠-74.241°	312.693∠-92.7455°	345.2954∠-35.7936°	313.3399∠-36.7304°
9	4022.224∠-71.3411°	3742.8755∠-72.1598°	3846.9262∠-74.1334°	437.1962∠21.209°	624.5654∠-77.582°	827.7184∠-42.1113°
10	4055.8557∠-71.4056°	3581.304∠-71.4552°	3883.5085∠-74.0924°	70.0372∠69.5022°	676.825∠-134.2578°	85.6577∠81.8729°
11	4054.2709∠-72.2848°	3516.5889∠-71.1641°	3912.5107∠-73.1373°	295.9842∠-34.7742°	369.6764∠-134.1257°	357.8265∠131.2687°
12	4019.3571∠-71.4855°	3778.9487∠-72.4607°	3774.6271∠-75.4081°	215.5699∠-48.0879°	347.6243∠9.45°	954.2551∠-69.1664°
13	3957.8127∠-71.9075°	3830.4841∠-72.1736°	3735.2382∠-77.3109°	503.8309∠-82.5995°	243.7633∠58.8737°	893.3395∠-51.4107°
14	3927.1385∠-73.0418°	3839.9755∠-72.0443°	3695.5173∠-78.793°	510.6298∠-50.8074°	77.8766∠-35.1573°	607.7694∠-57.007°
15	3948.2928∠-74.901°	3781.1286∠-71.9345°	3710.4231∠-81.1391°	672.6843∠-25.2713°	297.8751∠-89.6043°	772.2294∠-33.4243°
16	3952.6022∠-75.8459°	3717.4696∠-71.396°	3705.8769∠-82.2294°	358.8828∠-36.9164°	347.5397∠-132.0194°	394.495∠-48.4197°
17	3940.0486∠-75.9144°	3706.8353∠-71.5582°	3688.1122∠-82.3804°	143.1869∠-98.2595°	152.9446∠-79.3031°	191.8767∠-98.993°
18	3906.5661∠-75.3956°	3722.2184∠-72.1221°	3706.0889∠-83.0704°	268.7783∠-161.5396°	282.0898∠-9.7826°	337.2828∠-20.7309°

obtained in the final iteration are shown in Table 4.9.

Table 4.9

Node Voltages and Currents in Double Line to Ground Fault for Case 2

Node No.	Voltage			Load Current		
	Phase A	Phase B	Phase C	Phase A	Phase B	Phase C
1	7199.6∠0°	7199.6∠-120°	7199.6∠120°	679.5504∠-30.9606°	1225.4896∠-25.0207°	789.71∠147.3844°
2	7074.3469∠-0.2203°	7395.0651∠-121.2655°	7143.9352∠118.3974°	679.5504∠-30.9606°	1225.4896∠-25.0207°	789.71∠147.3844°
19	**6020.0498∠-32.1789°**	**6020.0498∠-32.1789°**	**7122.2788∠118.0041°**	**736.2353∠-21.7248°**	**1159.3121∠-32.1474°**	**869.9668∠136.0766°**
3	6000.1098∠-32.4811°	5967.0642∠-32.6526°	7091.3984∠117.4397°	525.9807∠-17.4658°	944.0316∠-32.1402°	869.9668∠136.0766°
4	5948.5673∠-32.5685°	5936.4036∠-32.9571°	7054.03∠117.1399°	315.9767∠-64.0781°	275.622∠-32.4712°	253.8674∠113.395°
5	5910.8077∠-32.5319°	5931.668∠-33.2999°	7017.2779∠117.0644°	169.1816∠-73.1656°	185.4453∠4.2107°	171.0065∠76.4307°
6	5980.3063∠-33.0168°	5871.7293∠-33.2261°	7036.3766∠116.6559°	505.1691∠-7.051°	873.2147∠-42.9527°	757.1415∠128.7884°
7	5918.6765∠-33.1346°	5838.2526∠-33.5951°	6999.896∠116.3189°	384.5622∠-63.7377°	321.0227∠-31.5294°	256.0079∠116.6041°
8	5878.5048∠-33.2763°	5834.1217∠-34.0512°	6994.338∠115.9583°	204.1335∠-54.6135°	222.827∠3.4594°	171.5673∠153.4689°
9	6009.2664∠-33.2633°	5828.9684∠-33.5548°	7032.1106∠116.1646°	306.4506∠61.1612°	385.4314∠-36.7876°	446.1068∠153.97°
10	6034.5558∠-33.2911°	5730.9114∠-33.2457°	7032.7053∠116.1842°	48.9825∠107.285°	420.1771∠-96.1°	49.9874∠-88.6813°
11	6037.864∠-33.6166°	5695.8534∠-33.0481°	7042.0812∠116.4167°	198.7458∠3.894°	228.2362∠-96.0097°	198.8049∠-39.1774°
12	5995.8544∠-33.4229°	5840.0451∠-33.7796°	7000.0425∠115.736°	141.2203∠-4.1838°	227.468∠49.4271°	497.1151∠125.0293°
13	5945.1287∠-33.7604°	5863.8389∠-33.8161°	6978.9445∠115.1263°	326.4288∠-42.8579°	163.2542∠98.0706°	473.4967∠143.4556°
14	5915.1635∠-34.3869°	5860.3291∠-33.8809°	6958.5763∠114.5746°	337.2132∠-10.5325°	48.3563∠7.735°	318.8923∠138.9324°
15	5922.6298∠-35.4492°	5815.4594∠-34.0541°	6967.9408∠113.6811°	449.0656∠14.5876°	190.2895∠-51.4379°	412.2522∠161.9998°
16	5919.5255∠-35.9684°	5768.882∠-33.9119°	6957.1599∠113.2783°	239.2256∠3.3134°	222.8298∠-94.5461°	209.9743∠147.6178°
17	5907.8305∠-36.0045°	5758.5554∠-33.983°	6944.2875∠113.2042°	94.121∠-58.1733°	97.8466∠-41.3099°	100.6052∠97.1419°
18	5886.2901∠-35.838°	5767.904∠-34.2891°	6951.496∠112.984°	178.3806∠-121.982°	182.0419∠28.0504°	179.8174∠175.3235°

Analysis of Double-Line (LL) Fault

For double line fault, case 2 is simulated with the assumption of fault resistance to be 10 Ω. The initial voltage at node 19 for phases a and b is enforced as the average of the initial source voltage for the first iteration and due to this the final voltages on phases a and b of node 19 are equal in magnitude and angle. The final voltages and currents at each nodes are depicted in Table 4.10.

Table 4.10
Node Voltages and Currents in Double Line Fault for Case 2

Node No.	Voltage			Load Current		
	Phase A	Phase B	Phase C	Phase A	Phase B	Phase C
1	7199.6∠0°	7199.6∠-120°	7199.6∠120°	1368.5965∠-33.1001°	1919.6845∠-29.199°	791.3249∠147.0299°
2	6953.452∠-0.3972°	7475.2529∠-122.0054°	7131.8815∠118.1408°	1368.5965∠-33.1001°	1919.6845∠-29.199°	791.3249∠147.0299°
19	**5849.91∠-33.6712°**	**5849.91∠-33.6712°**	**7107.6367∠117.6843°**	**1417.6526∠-28.1718°**	**1859.8018∠-33.7165°**	**871.9769∠135.7365°**
3	5829.6838∠-33.9892°	5795.8246∠-34.1698°	7076.3959∠117.1163°	542.2557∠ -19.1612°	973.6348∠-33.7578°	871.9769∠135.7365°
4	5777.0356∠-34.082°	5764.5602∠-34.4915°	7038.653∠116.8146°	325.4175∠-65.5929°	283.8831∠-34.0155°	254.4257∠113.068°
5	5738.4166∠-34.0446°	5759.762∠-34.8541°	7001.6765∠116.7378°	174.2641∠-74.6783°	190.9801∠2.6565°	171.3875∠76.1042°
6	5809.6929∠-34.5537°	5698.4706∠-34.7745°	7020.8118∠116.3273°	520.4211∠-8.7478°	900.8744∠-44.549°	758.928∠128.449°
7	5746.7368∠-34.6786°	5664.3214∠-35.1644°	6983.895∠115.9882°	396.1449∠-65.284°	330.9403∠-33.1125°	256.6039∠116.2726°
8	5705.7414∠-34.8278°	5660.2246∠-35.6454°	6978.1226∠115.6248°	210.3145∠-56.165°	229.6729∠1.8652°	171.966∠153.1354°
9	5839.5043∠-34.8123°	5654.8507∠-35.1205°	7016.4695∠115.8329°	314.4746∠59.4924°	397.9985∠-38.4344°	447.1183∠153.6225°
10	5865.3613∠-34.8411°	5554.3908∠-34.7928°	7016.7632∠115.8543°	50.3366∠105.7534°	433.6187∠-97.6407°	50.1027∠-89.0057°
11	5868.6403∠-35.1838°	5518.3435∠-34.5834°	7025.9493∠116.0873°	204.4767∠ 2.3268°	235.5779∠-97.545°	199.2613∠-39.5068°
12	5825.9615∠-34.9806°	5666.3972∠-35.3584°	6984.3923∠115.4017°	145.5461∠-6.1298°	234.2648∠47.7897°	498.3046∠124.6865°
13	5774.2984∠-35.3355°	5691.022∠-35.3968°	6963.2132∠114.7893°	336.7246∠-44.5248°	167.9623∠96.4824°	474.6061∠143.11°
14	5743.865∠-35.9952°	5687.6525∠-35.4653°	6942.6914∠114.2339°	347.4411∠-12.2391°	49.8488∠5.8677°	319.6579∠138.5832°
15	5751.9323∠-37.1125°	5642.0579∠-35.6469°	6951.8846∠113.3343°	462.3603∠12.9034°	196.2902∠-53.0531°	413.2099∠161.6511°
16	5749.0027∠-37.659°	5594.5323∠-35.4967°	6940.8995∠112.9295°	246.3265∠1.6102°	229.8421∠-96.127°	210.468∠147.2678°
17	5737.0871∠-37.6975°	5583.9868∠-35.5721°	6927.9308∠112.8549°	96.963∠-59.8765°	100.9492∠-42.9201°	100.8453∠96.7923°
18	5715.1229∠-37.5219°	5593.6378∠-35.8946°	6935.1171∠112.6338°	183.7231∠-123.6659°	187.7133∠26.4449°	180.2421∠174.9733°

Analysis of Single-Line-to-Ground (SLG) Fault

In this case, the system in case 2 is simulated for single line to ground phase fault. As explained previously, a fictitious node 19 is created between nodes 2 and 3 respectively.

The fault resistance is assumed to be 40 Ω. For the first iteration, voltages at node 19 is not enforced as carried out for the previous cases. The final voltages and currents at each node obtained in the final iteration are depicted in Table 4.11.

Table 4.11
Node Voltages and Currents for Single Line to Ground Fault for Case 2

Node No.	Voltage			Load Current		
	Phase A	Phase B	Phase C	Phase A	Phase B	Phase C
1	7199.6∠0°	7199.6∠-120°	7199.6∠120°	508.6357∠3.6163°	633.0838∠-115.0575°	785.1556∠148.1194°
2	7126.2574∠-0.7946°	7128.4301∠-120.9024°	7158.4656∠118.6735°	508.6357∠3.6163°	633.0838∠-115.0575°	785.1556∠148.1194°
19	**7107.4455∠-1.0383°**	**7102.9849∠-121.1599°**	**7140.055∠118.3464°**	**618.2931∠10.0208°**	**786.6003∠-120.6679°**	**864.067∠136.7229°**
3	7088.7046∠-1.3279°	7066.6586∠-121.5527°	7112.4023∠117.8651°	440.7255∠14.5727°	786.6003∠-120.6679°	864.067∠136.7229°
4	7043.7626∠-1.4406°	7038.7222∠-121.7858°	7077.062∠117.6035°	266.4889∠-32.9656°	232.3497∠-121.2535°	253.0886∠113.8535°
5	7015.8748∠-1.4551°	7031.9415∠-122.0498°	7038.0703∠117.5315°	142.5339∠-42.0888°	156.4291∠-84.5392°	170.5013∠76.8979°
6	7066.5331∠-1.8127°	6998.2596∠-122.0745°	7064.3156∠117.2224°	425.1009∠25.0203°	726.4847∠-131.6444°	751.1669∠129.4222°
7	7013.4734∠-1.9627°	6967.3769∠-122.3452°	7030.619∠116.9305°	324.1387∠-32.5856°	268.6817∠-120.1995°	254.8579∠117.2364°
8	6982.3473∠-2.1204°	6964.0856∠-122.6513°	7023.789∠116.6009°	171.862∠-23.4576°	186.672∠-85.1407°	170.848∠154.1115°
9	7088.8292∠-2.0319°	6977.05∠-122.3545°	7062.3202∠116.8083°	263.9174∠93.1108°	318.2131∠-125.2999°	441.9559∠154.7634°
10	7093.1538∠-2.0848°	6898.4935∠-122.166°	7071.4992∠116.9345°	41.8343∠138.2597°	348.9379∠174.9204°	49.5111∠-87.8711°
11	7091.7092∠-2.3438°	6860.7789∠-122.0775°	7084.2134∠117.2212°	169.2117∠35.1668°	189.4829∠174.9609°	197.6225∠-38.3729°
12	7082.9754∠-2.1392°	6994.3024∠-122.5531°	7032.974∠116.3676°	118.4593∠29.3518°	190.2768∠-38.8293°	492.3271∠125.6951°
13	7044.7798∠-2.3527°	7017.5∠-122.5885°	7021.2557∠115.7379°	272.515∠-10.9648°	137.8292∠9.6629°	469.0396∠144.2163°
14	7022.9063∠-2.7933°	7016.803∠-122.7072°	7009.8917∠115.2171°	283.3231∠21.5909°	39.5463∠-79.0005°	315.2759∠139.7421°
15	7026.9081∠-3.5718°	6988.8383∠-122.9428°	7030.0035∠114.4602°	378.7095∠46.5858°	157.244∠-140.2659°	408.4164∠162.8316°
16	7018.0983∠-3.9461°	6952.7335∠-122.9199°	7029.3089∠114.1342°	201.6864∠35.4251°	184.5042∠176.3701°	207.8373∠148.4837°
17	7007.9638∠-3.9879°	6944.0332∠-122.9824°	7017.6614∠114.0674°	79.0671∠-26.1009°	80.7608∠-130.2031°	99.556∠98.0192°
18	6991.329∠-3.9037°	6955.029∠-123.1329°	7023.9735∠113.8479°	150.186∠-90.0478°	150.9699∠-60.7934°	177.9619∠176.1874°

Analysis of Exact Fault Location

For the analysis purpose,first, a bisection search algorithm has been employed. Second, an incremental adjustment to match the simulated current of fault with the measurements is conducted. Finally, the sensitivity analysis of a search can be improved with the proposed algorithm that leads to matching of telemetered and calculated values as depicted in Table 4.12.

Table 4.12
Determination of Exact Location of Fault for Case 2

Fault No.	Fault Type	Reference Current Value	Actual Value of Current	Actual Distance of Fault
1	LLLG	1034.4848∠-63.0371°	1034.5056∠-63.038°	0.4004
		1592.2776∠-60.5388°	1592.2956∠-60.5396°	
		1866.5983∠-56.7464°	1866.6247∠-56.7469°	
2	LLL	2134.7033∠-68.6997°	2134.6756∠-68.6991°	0.3999
		2743.0912∠-67.7464°	2743.0605∠-67.7458°	
		3046.3189∠-64.4586°	3046.2838∠-64.4581°	
3	LLG	679.5504∠-30.9606°	679.5318∠-30.9594°	0.3984
		1225.4896∠-25.0207°	1225.4809∠-25.0199°	
		789.71∠147.3844°	789.7097∠147.3845°	
4	LL	1368.5965∠-33.1001°	1368.6158∠-33.1008°	0.4004
		1919.6845∠-29.199°	1919.7024∠-29.1996°	
		791.3249∠147.0299°	791.3253∠147.0298°	
5	LG	508.6357∠3.6163°	508.6492∠3.6142°	0.4063
		633.0838∠-115.0575°	633.0857∠-115.0575°	
		785.1556∠148.1194°	785.1545∠148.1193°	

4.4.3 Case 3: Distance Branching from a Common Node

This topology consists of 12 nodes and 11 switches where the switches and the respective lines are connected topologically. Breakers and recloser are equipped with the relay. Under normal operating condition, the breaker is used to energized the feeder. The source is considered at node 1 and three phase loads are connected to all remaining 11 nodes. For analysis purpose, the distributed energy sources are considered at nodes 2,3,6,8,10 and 12 respectively.

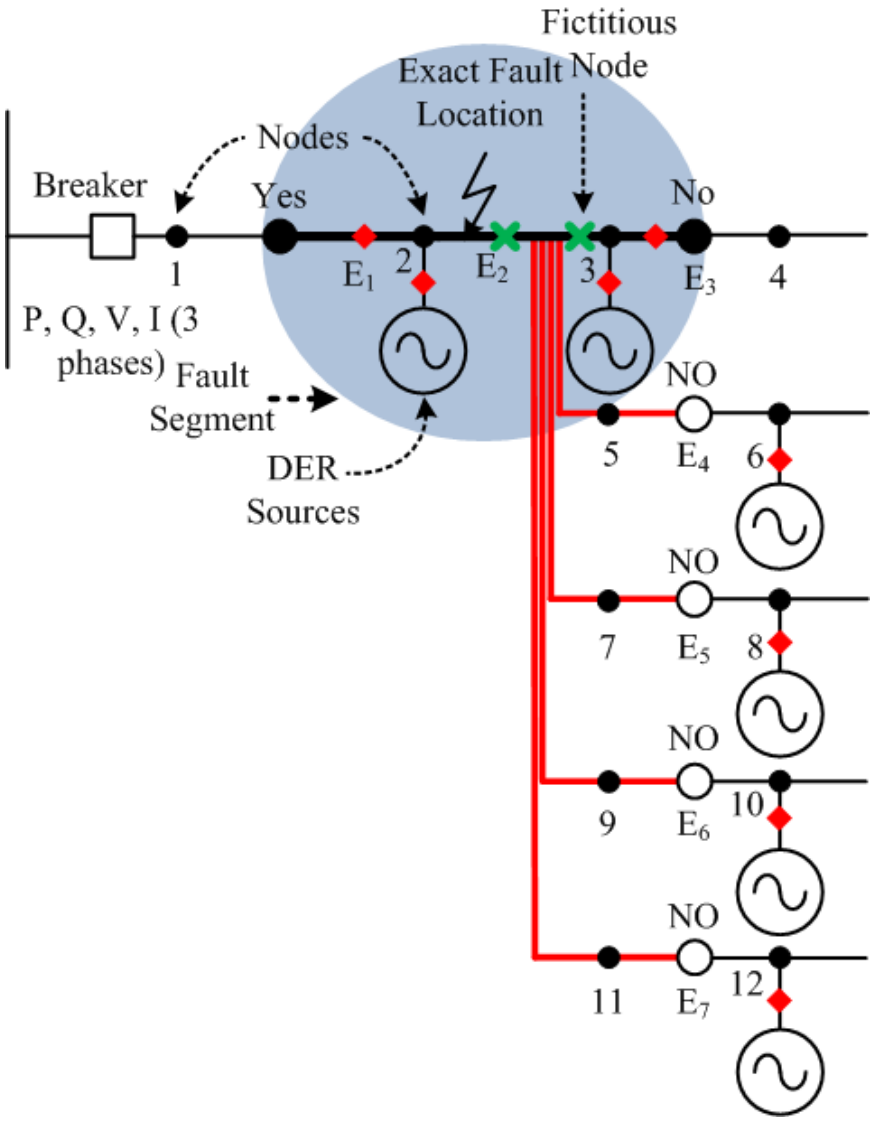

Figure 4.6: A case for determination of exact fault location with integration of DER's

Analysis of Three-Phase-to-Ground (LLLG) Fault

The system explained in case 3 is simulated for three phase to ground fault in which a fictitious node (node 13) is created between nodes 2 and 3 which is assumed to be at a distance of 40% from node 2 and 60% from node 3 of the total distance between

these nodes. The fault resistance of 40 Ω is presumed. The initial voltage at node 13 is enforced as the average of the initial source voltage for the first iteration and due to this the final voltages on each phase of node 13 are equal in magnitude and angle which are shown in Table 4.13. The backward-forward sweep method continues until the mismatch occurs between the new and the previous iterations in the load voltages is within the specified tolerance. The final iteration results of voltages and load currents at each nodes are depicted in Table 4.13.

Table 4.13
Node Voltages and Currents in Three Phase to Ground Fault for Case 3

Node No.	Voltage			Load Current		
	Phase A	Phase B	Phase C	Phase A	Phase B	Phase C
1	7199.6∠0°	7199.6∠-120°	7199.6∠120°	707.7733∠-67.8773°	266.1932∠-16.8659°	389.5014∠102.4517°
2	7067.0012∠0.4467°	7246.7905∠-120.1307°	7112.023∠119.5455°	707.7733∠-67.8773°	266.1932∠-16.8659°	389.5014∠102.4517°
13	**4707.6048∠-61.7656°**	**4707.6048∠-61.7656°**	**4707.6048∠-61.7656°**	**684.0849∠-57.5599°**	**219.5824∠-55.235°**	**561.8423∠94.9858°**
3	4685.1933∠-62.1092°	4709.1951∠-61.753°	4762.7915∠-61.3613°	410.0244∠-54.7375°	62.3609∠94.6263°	822.0018∠102.5824°
4	4661.858∠-62.2131°	4678.8035∠-61.7226°	4766.4∠-61.7899°	193.0561∠-83.5502°	213.7299∠-102.3563°	230.7821∠-24.2792°
5	4641.4684∠-61.5259°	4760.6189∠-62.3152°	4761.7587∠-61.3625°	287.0887∠-156.2558°	303.834∠28.9507°	1.6874∠-100.5356°
6	4636.2054∠-61.1184°	4792.7157∠-62.3187°	4793.8463∠-61.3724°	237.263∠156.3922°	250.38∠77.0476°	250.3209∠77.9939°
7	4696.7142∠-62.0289°	4665.8453∠-61.12°	4719.1179∠-60.8017°	84.2754∠164.099°	327.649∠-158.2366°	309.1179∠-155.1817°
8	4736.5776∠-61.9281°	4665.9038∠-60.6144°	4718.874∠-60.353°	253.3475∠96.7347°	278.617∠156.8962°	254.298∠157.1577°
9	4704.4118∠-62.6486°	4728.2952∠-62.252°	4799.5879∠-60.9456°	392.0561∠10.4303°	373.1689∠12.7182°	349.2889∠101.7979°
10	4686.937∠-63.1866°	4764.1115∠-62.3673°	4801.846∠-60.4076°	277.3666∠-38.7807°	230.893∠54.6711°	249.9039∠157.103°
11	4623.7298∠-63.0586°	4661.9498∠-61.0306°	4838.6263∠-60.8577°	466.8803∠-63.6268°	382.9269∠-157.2764°	373.6851∠106.6325°
12	4552.4491∠-63.3508°	4669.4229∠-60.3954°	4896.5438∠-61.0843°	307.5268∠-94.9919°	214.1592∠157.1153°	224.6483∠55.9541°

Analysis of Three-Phase(LLL) Fault

In this case, the system in case 3 is simulated for three phase fault. As explained previously, a fictitious node 13 is created between nodes 2 and 3 respectively. The fault resistance is assumed to be 10 Ω. The final voltages and currents at each node obtained in the final iteration are shown in Table 4.14.

Table 4.14
Node Voltages and Currents in Three Phase Fault for Case 3

Node No.	Voltage			Load Current		
	Phase A	Phase B	Phase C	Phase A	Phase B	Phase C
1	7199.6∠0°	7199.6∠-120°	7199.6∠120°	1658.3801∠-67.7896°	1105.3224∠-55.5278°	501.4412∠-50.0261°
2	6930.7978∠1.0278°	7266.1861∠-121.2533°	7208.4595∠120.301°	1658.3801∠-67.7896°	1105.3224∠-55.5278°	501.4412∠-50.0261°
13	**4382.3858∠-65.1791°**	**4382.3858∠-65.1791°**	**4382.3858∠-65.1791°**	**1626.6536∠-63.3959°**	**1125.9306∠-63.951°**	**410.4308∠-30.2645°**
3	4355.2715∠-65.5635°	4382.4618∠-65.1644°	4440.430∠-64.7334°	445.8313∠-58.6599°	62.1236∠91.9635°	878.3576∠99.3086°
4	4329.5162∠-65.6725°	4349.6857∠-65.1173°	4443.2691∠-65.2224°	207.8754∠-87.0097°	229.9017∠-105.751°	247.5655∠-27.7118°
5	4308.9687∠-64.8599°	4434.9808∠-65.8348°	4439.2381∠-64.7359°	309.4793∠-159.5451°	326.0542∠25.3887°	2.0466∠-102.4448°
6	4304.3581∠-64.3767°	4468.8617∠-65.8586°	4473.0595∠-64.7582°	255.5549∠153.1339°	268.5248∠73.5078°	268.2728∠74.6082°
7	4367.803∠-65.4751°	4335.9714∠-64.4087°	4393.8597∠-64.0802°	90.4518∠160.8653°	352.8687∠-161.4665°	332.2394∠-158.4197°
8	4410.9488∠-65.3803°	4336.7224∠-63.8146°	4393.8375∠-63.5612°	272.0503∠93.2826°	299.7656∠153.696°	273.1098∠153.9494°
9	4373.5478∠-66.2011°	4401.1568∠-65.7481°	4479.7716∠-64.266°	421.6476∠6.8102°	400.8188∠9.1819°	373.9168∠98.4995°
10	4352.4635∠-66.8113°	4439.027∠-65.8981°	4482.8386∠-63.6563°	298.6814∠-42.4054°	247.802∠51.1402°	267.6875∠153.8543°
11	4283.4291∠-66.6283°	4332.7416∠-64.3083°	4520.8071∠-64.1874°	504.9098∠-67.2606°	412.2193∠-160.5028°	399.6118∠103.3214°
12	4203.5325∠-66.9195°	4342.061∠-63.5738°	4580.9803∠-64.4578°	333.0532∠-98.5606°	230.3054∠153.9368°	240.1233∠52.5805°

Analysis of Double-Line-to-Ground (LLG) Fault

In this case, the system in case 3 is simulated for three phase fault. As explained previously, a fictitious node 13 is created between nodes 2 and 3 respectively. The fault resistance is assumed to be 40 Ω. The final voltages and currents at each node obtained in the final iteration are shown in Table 4.15.

Table 4.15
Node Voltages and Currents in Double Line to Ground Fault for Case 3

Node No.	Voltage			Load Current		
	Phase A	Phase B	Phase C	Phase A	Phase B	Phase C
1	7199.6∠0°	7199.6∠-120°	7199.6∠120°	469.6708∠-39.6631°	282.8182∠8.6833°	701.8074∠-82.0615°
2	7124.8306∠-0.14°	7253.4969∠-119.8113°	7337.4588∠120.3145°	469.6708∠-39.6631°	282.8182∠8.6833°	701.8074∠-82.0615°
13	**6180.6551∠-30.9296°**	**6180.6551∠-30.9296°**	**7361.4407∠120.3844°**	**513.0019∠-25.7792°**	**162.6437∠-22.0587°**	**536.4333∠-76.1222°**
3	6173.1089∠-31.1028°	6191.9483∠-30.8973°	7398.4303∠120.5163°	304.7439∠-22.2379°	55.0355∠121.959°	536.4333∠-76.1222°
4	6152.8427∠-31.2158°	6166.366∠-30.9315°	7390.5926∠120.2909°	146.2739∠-52.553°	162.1701∠-71.5652°	148.8379∠157.8015°
5	6140.0197∠-30.7579°	6230.9237∠-31.2333°	7399.0939∠120.5198°	216.4236∠-125.5347°	232.3938∠60.089°	0.5941∠66.0701°
6	6142.4173∠-30.5295°	6261.7809∠-31.2479°	7425.5051∠120.5701°	179.0826∠-173.0189°	191.6388∠108.1185°	161.6052∠-100.0636°
7	6176.2739∠-30.9541°	6153.4∠-30.4194°	7358.8883∠120.8501°	64.3739∠-165.2875°	247.9909∠-127.6061°	197.817∠26.4106°
8	6209.7387∠-30.8345°	6156.5365∠-30.0584°	7364.2403∠121.1424°	193.2448∠127.8283°	211.1577∠-172.5478°	162.9496∠-21.347°
9	6195.211∠-31.401°	6214.1029∠-31.1724°	7436.14∠120.5922°	298.2578∠41.8634°	284.1031∠43.9095°	226.2349∠-76.8309°
10	6183.1712∠-31.6549°	6243.7928∠-31.1883°	7443.7302∠120.7666°	210.2481∠-7.249°	176.175∠85.85°	161.2095∠-21.7228°
11	6136.377∠-31.6064°	6168.0534∠-30.4334°	7432.5372∠120.6782°	350.467∠-31.9693°	288.731∠-126.7863°	244.316∠-71.9979°
12	6088.7249∠-31.8035°	6181.6719∠-30.1074°	7459.7608∠120.5908°	229.9332∠-63.4446°	161.7685∠-172.5968°	147.4578∠-122.3708°

Analysis of Double-Line (LL) Fault

For double line fault, case 3 is simulated with the assumption of fault resistance to be 10 Ω. The initial voltage at node 13 for phases a and b is enforced as the average of the initial source voltage for the first iteration and due to this the final voltages on phases a and b of node 13 are equal in magnitude and angle. The final voltages and currents at each nodes are depicted in Table 4.16.

Table 4.16
Node Voltages and Currents in Double Line Fault for Case 3

Node No.	Voltage			Load Current		
	Phase A	Phase B	Phase C	Phase A	Phase B	Phase C
1	7199.6∠0°	7199.6∠-120°	7199.6∠120°	1124.6859∠-36.1128°	881.5276∠-20.6157°	702.7863∠-82.3322°
2	7015.5839∠-0.3816°	7333.7452∠-120.4389°	7329.315∠120.0802°	1124.6859∠-36.1128°	881.5276∠-20.6157°	702.7863∠-82.3322°
13	**6036.0535∠-32.3662°**	**6036.0535∠-32.3662°**	**7351.315∠120.0949°**	**1168.1515∠-30.0766°**	**809.0692∠-30.5816°**	**537.1812∠-76.4061°**
3	6028.9789∠-32.5453°	6047.2559∠-32.3305°	7388.2185∠120.2285°	311.8907∠-23.7609°	56.1349∠120.9639°	537.1812∠-76.4061°
4	6009.0259∠-32.6658°	6021.774∠-32.3715°	7380.5272∠120.0024°	149.7747∠-54.003°	166.064∠-73.0052°	149.0408∠157.513°
5	5994.9672∠-32.2001°	6087.1298∠-32.6652°	7388.8799∠120.2319°	221.6859∠-126.9769°	237.8501∠58.6567°	0.5957∠65.4956°
6	5996.7492∠-31.9657°	6118.0169∠-32.6728°	7415.2582∠120.2833°	183.4327∠-174.4551°	196.142∠106.6935°	161.8285∠-100.3503°
7	6031.74∠-32.3923°	6007.433∠-31.8504°	7348.4607∠120.5611°	65.9448∠-166.7014°	254.0644∠-129.0365°	198.1017∠26.1211°
8	6064.871∠-32.262°	6009.6031∠-31.4799°	7353.6234∠120.8541°	197.8608∠126.4008°	216.3204∠-173.9693°	163.1849∠-21.6353°
9	6051.8847∠-32.8452°	6070.1489∠-32.6068°	7425.8785∠120.3059°	305.2866∠40.4173°	290.8108∠42.4753°	226.5475∠-77.1165°
10	6040.5422∠-33.108°	6099.8728∠-32.6161°	7433.3556∠120.4809°	215.2125∠-8.702°	180.3316∠84.4222°	161.4345∠-22.0085°
11	5993.6304∠-33.0696°	6022.1192∠-31.8612°	7422.2201∠120.3919°	358.7974∠-33.4435°	295.7613∠-128.2119°	244.6563∠-72.2835°
12	5946.534∠-33.2831°	6034.8617∠-31.5242°	7449.5∠120.3054°	235.4313∠-64.9242°	165.7039∠-174.0136°	147.6609∠-122.6562°

Analysis of Single-Line-to-Ground (SLG) Fault

In this case, the system in case 3 is simulated for single line to ground phase fault. As explained previously, a fictitious node 13 is created between nodes 2 and 3 respectively. The fault resistance is assumed to be 40 Ω. For the first iteration, voltages at node 13

is not enforced as carried out for the previous cases. The final voltages and currents at each node obtained in the final iteration are depicted in Table 4.17

Table 4.17
Node Voltages and Currents for Single Line to Ground Fault for Case 3

Node No.	Voltage			Load Current		
	Phase A	Phase B	Phase C	Phase A	Phase B	Phase C
1	7199.6∠0°	7199.6∠-120°	7199.6∠120°	342.5996∠-6.3922°	215.3873∠37.5728°	700.7155∠-82.0436°
2	7162.462∠-0.4003°	7237.5345∠-119.702°	7344.4676∠120.3536°	342.5996∠-6.3922°	215.3873∠37.5728°	700.7155∠-82.0436°
13	**7152.1313∠-0.547°**	**7237.9162∠-119.6668°**	**7370.1397∠120.4327°**	**442.2838∠4.8861°**	**49.7959∠32.9466°**	**535.4745∠-76.1061°**
3	7146.0651∠-0.6911°	7240.0504∠-119.6173°	7408.2713∠120.5625°	262.4545∠8.6343°	49.7959∠32.9466°	535.4745∠-76.1061°
4	7123.2957∠-0.7895°	7217.5662∠-119.6329°	7402.9394∠120.3677°	126.346∠-22.1266°	138.5509∠-160.2666°	148.5896∠157.8783°
5	7126.0912∠-0.4476°	7271.6987∠-119.8108°	7402.5291∠120.5189°	186.3421∠-95.235°	199.1206∠-28.4205°	0.5293∠77.8415°
6	7131.8913∠-0.2645°	7300.2542∠-119.7673°	7426.7615∠120.5256°	154.2368∠-142.7539°	164.3778∠19.599°	161.5778∠-100.1081°
7	7141.7111∠-0.5428°	7204.0326∠-119.2875°	7377.4636∠120.9123°	55.7984∠-135.1033°	211.5762∠143.4695°	197.2273∠26.477°
8	7169.5544∠-0.4131°	7208.8320∠-119.0289°	7386.1136∠121.1842°	167.3744∠158.2497°	180.3343∠98.4817°	162.467∠-21.3052°
9	7171.2483∠-0.9592°	7255.1635∠-119.8516°	7439.8331∠120.6485°	257.6656∠72.3762°	243.6668∠-44.7265°	226.1772∠-76.7766°
10	7166.7739∠-1.1468°	7272.0848∠-119.8994°	7446.2751∠120.8054°	181.3926∠23.2592°	151.2634∠-2.8611°	161.1544∠-21.684°
11	7104.4564∠-1.061°	7202.9342∠-119.2475°	7454.9314∠120.7539°	302.6487∠-1.3465°	247.3709∠144.3549°	243.425∠-71.904°
12	7058.7583∠-1.1669°	7207.1732∠-118.9406°	7490.3928∠120.6385°	198.3352∠-32.808°	138.7507∠98.57°	146.8548∠-122.3231°

Analysis of Exact Fault Location

For the analysis purpose,first, a bisection search algorithm has been employed. Second, an incremental adjustment to match the simulated current of fault with the measurements is conducted. Finally, the sensitivity analysis of a search can be improved with the proposed algorithm that leads to matching of telemetered and calculated values as depicted in Table 4.18.

Table 4.18
Determination of Exact Location of Fault for Case 3

Fault No.	Fault Type	Reference Current Value	Actual Value of Current	Actual Distance of Fault
1	LLLG	707.7733∠-67.8773°	707.7734∠-67.8773°	0.4000
		266.1932∠-16.8659°	266.1931∠-16.8659°	
		389.5014∠102.4517°	389.5018∠102.4516°	
2	LLL	1658.3801∠-67.7896°	1658.3796∠-67.7896°	0.4000
		1105.3224∠-55.5278°	1105.3221∠-55.5278°	
		501.4412∠-50.0261°	501.4411∠-50.0261°	
3	LLG	469.6708∠-39.6631°	469.6716∠-39.6633°	0.4004
		282.8182∠8.6833°	282.8181∠8.6832°	
		701.8074∠-82.0615°	701.8075∠-82.0615°	
4	LL	1124.6859∠-36.1128°	1124.6864∠-36.1128°	0.4000
		881.5276∠-20.6157°	881.5279∠-20.6157°	
		702.7863∠-82.3322°	702.7864∠-82.3322°	
5	LG	342.5996∠-6.3922°	342.6002∠-6.3923°	0.4004
		215.3873∠37.5728°	215.3873∠37.5728°	
		700.7155∠-82.0436°	700.7155∠-82.0436°	

4.5 Conclusion

This chapter provides a groundwork on reversal from a presumed location and different types of faults to determine the exact location of fault in bidirectional flow of power in distribution feeders. This chapter explores a modern algorithm called the bisection method and incremental distance to detect the exact location of the fault. The advantage of this method is that reduces the time for fault detection and increases the overall reliability of the system. Also this method gives more accurate results in bidirectional power flow rather than in unidirectional power flow. Exact location of fault was carried out on radial distribution system as well as on distribution

system consisting of laterals and sub laterals.

Chapter 5

Concluding Remarks and Future Work

This thesis has demonstrated the candidatures of exact fault locations established from the existing analytical methods as well as in creating the applications on distribution management system (DMS). Determination of exact fault location is critical for the utility crew to restore the supply in a timely matter. Reliability of the distribution grid relies on reducing outage time and affected customers connected to the distribution feeder. This thesis attempts to provide a groundwork on reversal from a presumed location and fault types in determining candidate locations of a distribution feeders. Unlike in transmission grid, research has been carried out for the exact fault location in transmission systems which includes methods such as travelling wave

based scheme and harmonics based scheme. This thesis advances the procedure to determine the exact fault location in distribution feeder with radial system as well as with laterals and sub laterals. A systematic approach to determine the exact fault location is proposed based on the status of the fault indicators and the tripping condition of the recloser of the circuit breaker. A bisection search algorithm has been employed with the incremental distance adjustment to compare the fault currents with the actual currents in unidirectional and bidirectional flow of power. Several ideas can be explored as future work based on the work from this thesis:

1. Analysis of different types of fault at different location with parallel feeders.
2. Effectiveness of this method with another existing methods for determination of exact fault location in distribution feeders.
3. Incorporation of utility data to study the behaviour of the system.
4. Determination of exact location of fault using geographical information system (GIS) which includes latitude and longitudes and the shortest distance to reach to the fault location.

There could be a great potential of research thrusts intersecting with transportation engineering where the geographical locations of roads and electrical distribution grid would overlap for optimizing the locations of search by utilizing the time search based on traffic conditions and strategies that may expedite the search and pinpoint the true

location of fault, resulting in saving search time.

The notion of resilience has been widely promoted in recent years. The foundation of this work would provide a more robust way to search topologically and can be extended to multiple events that may occur within a distribution network. Coordination among all sensing information can be challenging because communication may be not available during the time of extreme events. This work can be further investigated by introducing drones in helping to find out the physical structure in the aftermath of extreme events. It is believed that transportation and power engineering network paradigms may converge.

References

[1] B. Stott, "Review of load flow calculation methods," *Proceedings of the IEEE*, vol. 62, no. 7, pp. 916–929, Jul. 1974.

[2] B. Stott, J. Jardim, and O. Alsac, "DC power flow revisited," *IEEE Trans. Power Syst.*, vol. 24, no. 3, pp. 1290–1300, Aug. 2009.

[3] A. Garces, "A linear three-phase load flow for power distribution systems," *IEEE Trans. Power Syst.*, vol. 31, no. 1, pp. 827–828, Jan. 2016.

[4] F. Ding and K. A. Loparo, "Feeder reconfiguration for unbalanced distribution systems with distributed generation: A hierarchical decentralized approach," *IEEE Trans. Power Syst.*, vol. 31, no. 2, pp. 1633–1642, Mar. 2016.

[5] S.Civanlar, J. Grainger, H.Yin, and S.S.H.Lee, "Distribution feeder reconfiguration for loss reduction," *IEEE Trans. Power Del.*, vol. 3, no. 3, pp. 1217–1223, Jul. 1988.

[6] R. Lee and C. Brooks, "A method and its application to evaluate automated

distribution control," *IEEE Trans. Power Del.*, vol. 3, no. 3, pp. 1232–1240, Jul. 1988.

[7] M. E. Baran and F. F. Wu, "Network reconfiguration in distribution systems for loss reduction and load balancing," *IEEE Trans. Power Del.*, vol. 4, no. 2, pp. 1401–1407, April 1989.

[8] T. Taylor and D. Lubkeman, "Implementation of heuristic search strategies for distribution and feeder reconfiguration," *IEEE Trans. Power Syst.*, vol. 3, no. 2, pp. 619–626, May. 1988.

[9] T. Wagner, A. Chikhani, and R. Hackam, "Feeder reconfiguration for loss reduction: An application of distribution automation," *IEEE Trans. Power Del.*, vol. 6, no. 4, pp. 1922–1933, Oct. 1991.

[10] T. Chen and S. Wang, "Simplified bidirectional-feeder models for distribution-system calculations," *IET Generation, Transmission & Distribution Journal*, vol. 142, no. 5, pp. 459–467, Sept. 1995.

[11] A. G. Fonseca, O. L.Tortelli, and E. M. Lourenco, "Extended fast decoupled power flow for reconfiguration networks in distribution systems," *IET Generation, Transmission & Distribution Journal*, vol. 12, no. 22, pp. 6033–6040, Dec. 2018.

[12] J. Liu and P. Srikantha, "Decentralized topology reconfiguration in multiphase

distribution networks," *IEEE Trans. Signal Process.*, vol. 5, no. 3, pp. 598–610, Sep. 2019.

[13] J. Zhu, D. L. Lubkeman, and A. A. Girgis, "Automated fault location and diagnosis on electric power distribution feeders," *IEEE Trans. Power Del.*, vol. 12, no. 2, pp. 801–809, Apr. 1997.

[14] C. H. Castro, J. B. Bunch, and T. M.Topka, "Generalized algorithms for distribution feeder deployment and sectionalizing," *IEEE Trans. Power App. Syst.*, vol. 99, no. 2, pp. 549–557, Mar/Apr. 1980.

[15] M. S. Choi, S. J. Lee, D. S. Lee, and B. G. Jin, "A new fault location algorithm using direct circuit analysis for distribution systems," *IEEE Trans. Power Del.*, vol. 19, no. 1, pp. 35–41, Jan. 2004.

[16] M. Kezunovic, "Smart fault location for smart grids," *IEEE Trans. Smart Grid*, vol. 2, no. 1, pp. 11–22, Mar. 2011.

[17] Y. Gong and A. Guzman, "Integrated fault location system for power distribution feeders," *IEEE Trans. Ind. Appl.*, vol. 49, no. 3, pp. 1071–1078, May/Jun 2013.

[18] J. H. Teng, W. H. Huang, and S. W. Luan, "Automatic and fast faulted line-section location method for distribution systems based on fault indicators," *IEEE Trans. Power Syst.*, vol. 29, no. 4, pp. 1653–1662, Jul. 2014.

[19] F. C. Trindade, W. Freitas, and J. C. Vieira, "Fault location in distribution

systems based on smart feeder meters," *IEEE Trans. Power Del.*, vol. 29, no. 1, pp. 251–260, Feb. 2014.

[20] F. C. T. amd Walmir Freitas, "Low voltage zones to support fault location in distribution systems with smart meters," *IEEE Trans. Smart Grid*, vol. 8, no. 6, pp. 2765–2774, Nov. 2017.

[21] S. Bhela, V. Kekatos, and S. Veeramachaneni, "Enhancing observability in distribution grids using smart meter data," *IEEE Trans. Smart Grid*, vol. 9, no. 6, pp. 5953–5961, Nov. 2018.

[22] Q. Zhou, D. Shirmohammadi, and W. E. Liu, "Distribution feeder reconfiguration for service restoration and load balancing," *IEEE Trans. Power Syst.*, vol. 12, no. 2, pp. 724–729, May. 1997.

[23] ——, "Distribution feeder reconfiguration for operation cost reduction," *IEEE Trans. Power Syst.*, vol. 12, no. 2, pp. 730–735, May. 1997.

[24] K. N. Miu, H. D. Chiang, and R. McNulty, "Multi-tier service restoration through network reconfiguration and capacitor control for large scale radial distribution networks," *IEEE Trans. Power Syst.*, vol. 15, no. 3, pp. 1001–1007, Aug. 2000.

[25] M. W.Siti, D. V. Nicolae, A. A. Jimoh, and A. Ukil, "Reconfiguration and load balancing in the LV and MV distribution networks for optimal performance," *IEEE Trans. Power Del.*, vol. 22, no. 4, pp. 2534–2540, Oct. 2007.

[26] A. S. Meliopoulos, E. Polymeneas, Z. Tan, R. Huang, and D. Zhao, "Advanced distribution management system," *IEEE Trans. Smart Grid*, vol. 4, no. 4, pp. 2109–2117, Dec. 2013.

[27] T. Fawzi, K.F.Ali, and S. El-Sobki, "A new planning model for distribution systems," *IEEE Trans. Power App. Syst.*, vol. 102, no. 9, pp. 3010–3017, Sept. 1983.

[28] B. K. Ghazani, H. Seyedi, B. M. Ivatloo, K. Zare, and S. Shargh, "Reconfiguration of distribution networks considering coordination of the protective devices," *IET Generation, Transmission & Distribution Journal*, vol. 11, no. 1, pp. 82–92, Jan. 2017.

[29] Y. Y. Hsu and Y. J. Hwu, "Planning of distribution feeder reconfiguration with protective device coordination," *IEEE Trans. Power Del.*, vol. 8, no. 3, pp. 1340–1347, Jul. 1993.

[30] I. Lim, T.S.Sidhu, M.S.Choi, S.J.Lee, and B. Ha, "An optimal composition and placement of automatic switches in das," *IEEE Trans. Power Del.*, vol. 28, no. 3, pp. 1474–1482, Jul. 2013.

[31] K. Sridharan and N. N. Schulz, "Outage management through amr systems using an intelligent data filter," *IEEE Trans. Power Del.*, vol. 16, no. 4, pp. 669–675, Oct. 2001.

[32] C. Chen and S. Duan, "Optimal integration of plug-in hybrid electric vehicles

in microgrids," *IEEE Trans. Ind. Informat.*, vol. 10, no. 3, pp. 1917–1926, Aug 2014.

[33] M.N.Kabir, Y.Mishra, G.Ledwich, Z.Y.Dong, and K. Wong, "Coordinated control of grid-connected photovoltaic reactive power and battery energy storage systems to improve the voltage profile of a residential distribution feeder," *IEEE Trans. Ind. Informat.*, vol. 10, no. 2, pp. 967–977, May 2014.

[34] M.-A. Rostami, A. Kavousi-Frad, and T. Niknam, "Expected cost minimization of smart grids with plug-in hybrid electric vehicles using optimal distribution feeder reconfiguration," *IEEE Trans. Ind. Informat.*, vol. 11, no. 2, pp. 388–397, Apr. 2015.

[35] W. Su, H. R. Eichi, W. Zeng, and M. Y. Chow, "A survey on the electrification of transportation in a smart grid environment," *IEEE Trans. Ind. Informat.*, vol. 8, no. 1, pp. 1–10, Feb 2012.

[36] C.-M. Chan, C.-N. Lu, and Y. L. Lo, "Optimal use of existing distribution feeders to accommodate transportation electrification," *IEEE Trans. Intell. Transp. Syst.*, vol. 16, no. 4, pp. 1941–1950, Aug. 2015.

[37] A. Kavousi-Fard, M. A. Rostami, and T. Niknam, "Reliability-oriented reconfiguration of vehicle to grid networks," *IEEE Trans. Ind. Informat.*, vol. 11, no. 3, pp. 682–691, Jun. 2015.

[38] S. Chanda and A. K.Srivastava, "Defining and enabling resiliency of electric

distribution systems with multiple microgrids," *IEEE Trans. Smart Grid*, vol. 7, no. 6, pp. 2859–2868, Nov. 2016.

[39] C. Chen, J. Wang, F. Qiu, and D. Zhao, "Resilient distribution system by microgrids formation after natural disasters," *IEEE Trans. Smart Grid*, vol. 7, no. 2, pp. 958–966, Mar. 2016.

[40] B. D. Russell and C. L. Benner, "Intelligent systems for improved reliability and failure diagnosis in distribution systems," *IEEE Trans. Smart Grid*, vol. 1, no. 1, pp. 48–56, Jun. 2010.

[41] H. Gao, Y. Chen, Y. Xu, and C. C. Liu, "Resilence-oriented critical load restoration using microgrids in distribution systems," *IEEE Trans. Smart Grid*, vol. 7, no. 6, pp. 2837–2848, Nov. 2016.

[42] T. Ding, Y. Lin, G. Li, and Z. Bie, "A new model for resilient distribution systems by microgrids formation," *IEEE Trans. Power Syst.*, vol. 32, no. 5, pp. 4145–4147, Sept. 2017.

[43] W. Yuan, J. Wang, F. Qiu, C. K. Chen Chen, and B. Zeng, "Robust optimization based resilient distribution network planning against natural disasters," *IEEE Trans. Smart Grid*, vol. 7, no. 6, pp. 2817–2826, Nov. 2016.

[44] Y. Jiang, C. C. Liu, M. Diedesch, E. Lee, and A. K.Srivastava, "Outage management of distribution systems incorporating information from smart meters," *IEEE Trans. Power Syst.*, vol. 31, no. 5, pp. 4144–4154, Sept. 2016.

[45] T. Sakaguchi and K. Matsumoto, "Development of a knowledge based system for power system restoration," *IEEE Trans. Power App. Syst.*, vol. 102, no. 2, pp. 320–329, Feb. 1983.

[46] Y. Liu and N. N. Schulz, "Knowledge-based system for distribution system outage locating using comprehensive information," *IEEE Trans. Power Syst.*, vol. 17, no. 2, pp. 451–456, May. 2002.

[47] W. H.Kersting, *Distribution System Modeling and Analysis*, 4th ed. CRC Press., 2018.

[48] C. Trevino, "Cases of diffiult covergence in load-flow problems," in *IEEE Summer Power Meeting, Los Angeles, USA*, Feb. 1970.